https://doi.org/10.15388/vu.thesis.91
https://orcid.org/0000-0002-4147-9375

VILNIUS UNIVERSITY
CENTER FOR PHYSICAL SCIENCES AND TECHNOLOGY

Pranas
UŠINSKAS

Target Design of Calcium Hydroxyapatite Thin Films

DOCTORAL DISSERTATION

Natural Sciences
Chemistry N 003

VILNIUS 2020

This dissertation was written between 2014 and 2018 at Vilnius University.
Academic supervisor – Dr. Živilė Stankevičiūtė (Vilnius University, Natural Sciences, Chemistry – N 003).

Academic consultant – Prof. Habil. Dr. Aivaras Kareiva (Vilnius University, Natural Sciences, Chemistry – N 003).

This doctoral dissertation will be defended in a public meeting of the Dissertation Defence Panel:

Chairman – **Prof. Dr. Henrikas Cesiulis** (Vilnius University, Natural Sciences, Chemistry – N 003).
Members:
Dr. Audronė Gefenienė (Centre for Physical Sciences and Technology, Natural Sciences, Chemistry – N 003);
Assoc. Prof. Dr. Remigijus Ivanauskas (Kaunas University of Technology, Natural Sciences, Chemistry – N 003);
Prof. Dr. Jiri Pinkas (Masaryk University Brno, Natural Sciences, Chemistry – N 003);
Prof. Habil. Dr. Arūnas Ramanavičius (Vilnius University, Natural Sciences, Chemistry – N 003).

The dissertation shall be defended at a public/closed meeting of the Dissertation Defence Panel at 14 h on 30 October 2020 in Inorganic Chemistry auditorium 141 of the Institute of Chemistry, Faculty of Chemistry and Geoscience, Vilnius University. Address: Naugarduko g. 24, LT-03225 Vilnius, Lithuania. Tel.: +370 5 2193108. Fax: +370 5 2330987.

The text of this dissertation can be accessed at the libraries of (name of the institutions granted the right to conduct doctoral studies in alphabetical order), as well as on the website of Vilnius University: www.vu.lt/lt/naujienos/ivykiu-kalendorius

https://doi.org/10.15388/vu.thesis.91
https://orcid.org/0000-0002-4147-9375

VILNIAUS UNIVERSITETAS
FIZINIŲ IR TECHNOLOGIJOS MOKSLŲ CENTRAS

Pranas
UŠINSKAS

Kalcio hidroksiapatito plonų sluoksnių tikslinis dizainas

DAKTARO DISERTACIJA

Gamtos mokslai
Chemija N 003

VILNIUS 2020

Disertacija rengta 2014-2018 metais Vilniaus universitete.

Mokslinis vadovas - dr. Živilė Stankevičiūtė (Vilniaus universitetas, gamtos mokslai, chemija – N 003).
Mokslinis konsultantas - prof. habil. dr. Aivaras Kareiva (Vilniaus universitetas, gamtos mokslai, chemija – N 003).

Gynimo taryba:
Pirmininkas: prof. dr. Henrikas Cesiulis (Vilniaus universitetas, gamtos mokslai, chemija – N 003).
Nariai:
dr. Audronė Gefenienė (Fizinių ir technologijos mokslų centras, gamtos mokslai, chemija – N 003).
doc. dr. Remigijus Ivanauskas (Kauno technologijos universitetas, gamtos mokslai, chemija – N 003);
prof. dr. Jiri Pinkas (Brno Masaryko universitetas, gamtos mokslai, chemija – N 003);
prof. habil. dr. Arūnas Ramanavičius (Vilniaus universitetas, gamtos mokslai, chemija – N 003).

Disertacija bus ginama viešame Chemijos mokslo krypties gynimo tarybos posėdyje 2020 m. spalio 30 d. 14 val. Vilniaus universiteto Chemijos ir geomokslų fakulteto Chemijos instituto Neorganinės chemijos auditorijoje.
Adresas: Naugarduko g. 24, LT-03225 Vilnius, Lietuva. Tel.: 2193108. Faksas: 2330987.

Disertaciją galima peržiūrėti Vilniaus universiteto, Fizinių ir technologijos mokslų centro bibliotekose ir VU interneto svetainėje adresu: https://www.vu.lt/naujienos/ivykiu-kalendorius

CONTENTS

LIST OF ABBREVIATIONS

AFM - atomic force microscopy
ASTM - cobalt alloys
BCP – biphasic calcium phosphate
BG – bioactive glass
CAM – contact angle measurement
CHAp – calcium hydroxyapatite
CP – calcium phosphate
DTA - differential thermal analysis
FDA - Food and Drug Administration
FTIR - Fourier transform infrared spectroscopy
GC – glass ceramics
HA, HAP - hydroxyapatite
HDPE - high density polyethylene
PEEK – polyetheretherketone
PGA - poly(glycolic acid)
PLA - polylactide
PLGA - poly(lactic-co-glycolic) acid
PMMA - poly(methyl methacrylate)
PVA - poly(vinyl alcohol)
SBF - simulated body fluid
SD – standard deviation
SEM - scanning electron microscopy
TCP - tricalcium phosphate
TEA – triethylamine
TG – thermogravimetric analysis
THA - total hip arthroplasty
TiIPro - titanium isopropoxide
UHMWPE - ultra-high molecular weight polyethylene
XRD – X – ray diffraction

INTRODUCTION

As the population age is increasing, the demand for hard tissue repair and replacement is expanding as the bones lose their physical properties during the years, requiring techniques and materials for implant preparation. The research in this field is directed to engineering biomaterials and coatings with appropriate chemical and mechanical properties, suface chemistry and surface topography. This is being achieved by mimicking the natural organization of bone on the implant surface, which allows to accelerate bone healing through enhanced cell attachment and tissue formation [1], [2].

Calcium hydroxyapatite, $Ca_{10}(PO_4)_6(OH)_2$, (CHAp), commonly referred as hydroxyapatite (HA, HAP or CHAp) is a bioceramic material, extremely similar to the inorganic part of bones and the dentine of teeth and it is non-toxic within any quantity and osteoconductive [3], [4]. As it's mechanical strenght is low, for implant production it is usually combined with biocompatible materials with higher mechanical strenght. It has been used commercially as a coating on metallic implants since the 1980's and it is still the most widely used coating matelial for load bearing applications up to day [2], [5]–[7]. CHAp has excellent biocompatibility (which means that it is accepted by surrounding tissues without adverse effects and *vice versa* [8]) due to its compositional similarity to natural bone and exhibits a surface chemistry that supports bone in-growth [9]–[12]. To fully achieve this, right conditions like the composition of CHAp, coating technique and the substrate itself must be applied.

In the early stages of implant development the main criteria for the first implant development was appropirate physical properties and non-toxicity [13], so that titanium and titanium alloys, stainless steel and cobalt-chromium alloys were extensively used. It was noted, that metal implants have tendency to oxidize, are biologically inert thus do not induce regeneration after implantation and have mechanical mismatch with the natural bone [8], [14], [15]. Poor implant fit and incomplete osseointegration lead to micromotion, stress shielding and cause osteolysis - all of which ultimately contribute to implant loosening and failure in 10-25 years, requiring an arduous, painful, and expensive revision surgery [16].

Calcium phosphate coatings provide the necessary interlayer for the bone ingrowth, while the substrate bears the load [17]. Coating substrates with osteoconductive biomaterials is one of various surface modification methods used to improve the mechanical, chemical and biological properties for biomedical applications opening new opportunities for implants and prosthetic devices [7], [17], [18]. The CHAp thin films have been synthesized using many preparation methods [19]. Although, plasma spray technique is only method approved by FDA for biomedical applications and gained commercial success [20] the method has some disadvantages.

The main aim of this doctoral thesis was target design of calcium hydroxyapatite thin films on different substrates. The results obtained on the specific modifications of surfaces of substrates and design of sub-layers for the fabrication of CHAp coatings and characterization of obtained thin films shows novelty and originality of this PhD thesis. For this reason, the tasks to achieve the main goal were formulated as follows:

1. To modify the surface of titanium (Ti) substrate for the sol-gel synthesis of porous and hydrophilic calcium hydroxyapatite coating.
2. To synthesize and characterize calcium hydroxyapatite coatings on novel silicon nitride (Si_3N_4) substrate.
3. To develop an accelerated synthesis approach for the rapid fabrication of calcium hydroxyapatite thin films.

1. LITERATURE REVIEW

1.1 Use of the implants in medicine

A medical device is defined as implantable if it is either partly or totally introduced, surgically or medically, into the human body and is intended to remain there after the procedure [21]. Usually implantable medical devices are used to replace or support missing or damaged biological structure and in ideal scenario it should become a part of the host's body. Besides there functions, implants and bioactive materials have become indispensable tool in medicine and are also used to deliver medication, monitor body functions and etc. Some of the implants stay in the host's body permanently – like hip implants, and others are removed, after they are no longer needed – like chemotherapy ports. In general, many implants are prosthetics and the earliest example of this could be a toe, belonging to a noblewoman, found in Egypt dated 950-710 B.C.

Fig. 1. Ancient implant [22], [23]

Even through prothetics, were used since ancient times, a significant breakthrough in this field was after the introduction of the first generation of biomaterials in 1960-1970, as the production of biomedical implants became possible [23]. Biomaterials are natural or synthetic materials used to function in bio-environment [24]. They can made from skin, bone or other body tissues, metal, plastics, ceramics or other materials. Despite huge variety of implants by many criteria, this literature review focuses on on load bearing dental and orthopaedic implants, as these types are most relatable to the research made. The possible applications of implants are listed in Table 1.

Table 1.Uses of biomaterials [25]

No.	Uses of Biomaterials	Example
1	Replacement of damaged or diseased part	Artificial hip/knee joint replacement
2	Improving functionality or abnormality	Cardiac pacemaker
3	Assist in healing	Sutures, bone plates and screws
4	Improving cosmetic abnormality	Mastectomy augmentation, chin augmentation
5	Aid to diagnosis	Probes and Catheres

In the early period of implants, material was considered fit for implantation if it had minimal to zero toxicity. Later, both for dental and orthopaedic implants structural and functional integration to the living bone became a common requirement for the term success. This sets two main goals for proper implants: to achieve the matching of mechanical properties mimicking the characteristics of bone or tissue, and achieving biocompatibility and osteoconductivity. The term for this was offered by Branemark, naming the process “osteointegration” [23]. This could also be called bio-integration, even though it is sometimes used with a slighly different meaning – “stimulate bone growth with bioactive surface, that encourages the bond between the implants and the surrounding bone” [26]. The success of osteointegration depends on many factors like implant design, surface, topography and chemical factors like composition and structure. To summarize, material should not be cytotoxic, surface should be rough and porous. To achieve this, main development is focused on the surface of the materials and one of the main techniques used for that is applying coatings [27].

1.1.1. Ortophedic implants

Orthopedics is a branch of surgery intended to restore the function of load-bearing joints which are subjected to high level of mechanical stresses, wear, and fatigue in the course of normal activity. These devices include prostheses for hip (Fig. 2(a)), knee (Fig. 2(b)), ankle, shoulder (Fig. 2(c)), and elbow joints (Fig. 2(d)) [2].

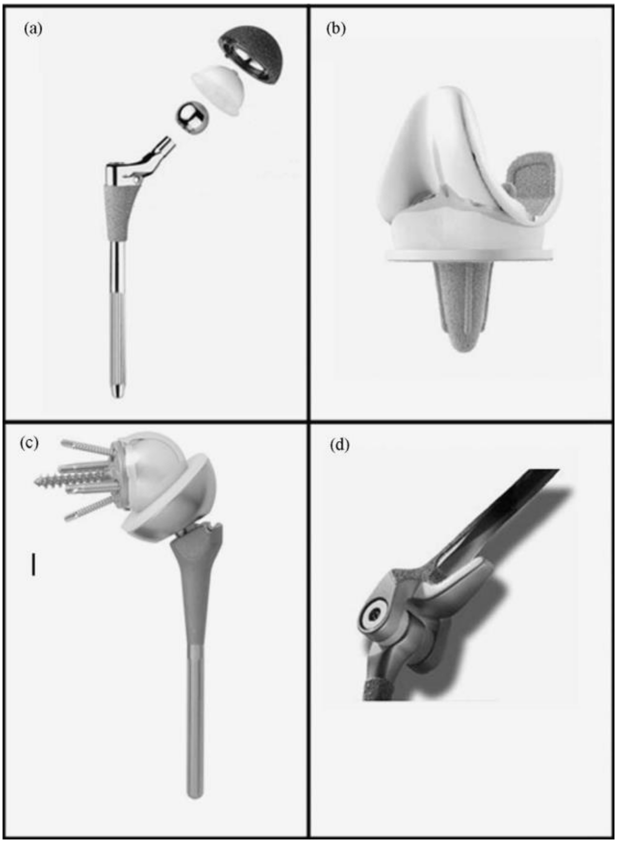

Fig. 2. Orthopedic Implant devices used for load bearing applications: (a) hip implant, (b) knee implant, (c) shoulder implant, (d) elbow implant [2].

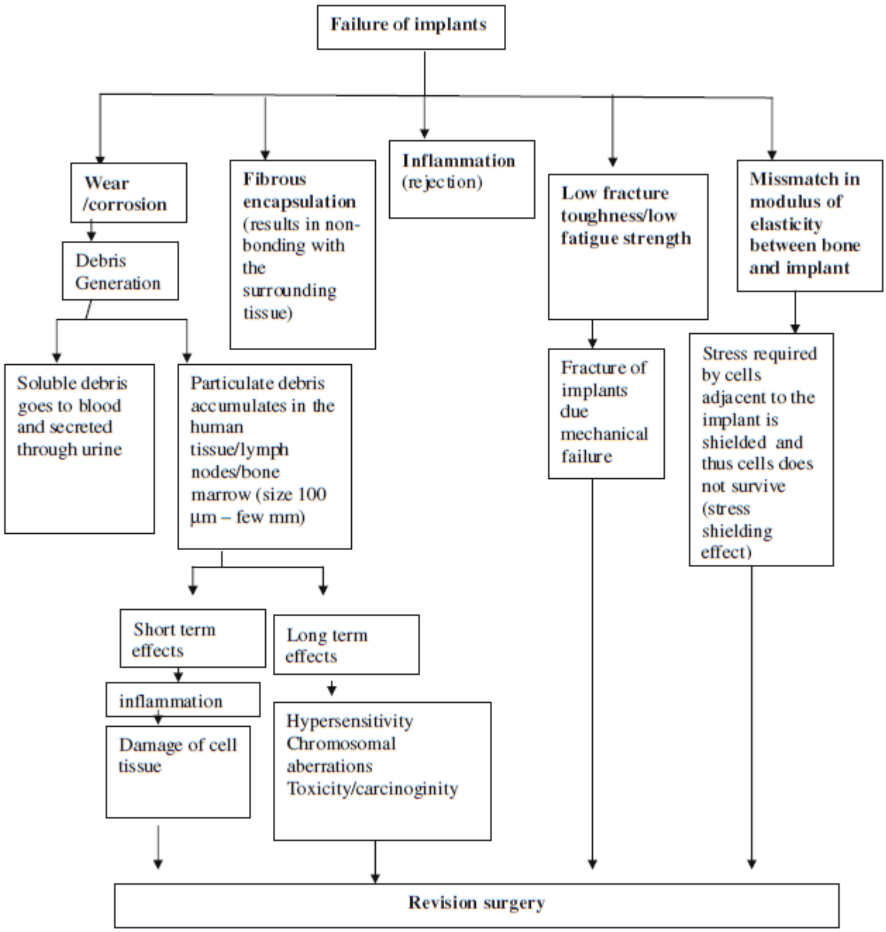

Fig. 3. Various causes for failure of implants that leads to revision surgery [34].

They also include the fracture fixation devices such as wires, pins, plates, screws, etc. [2]. With an ageing population, trauma, diseases, war, and sports related injuries there is an ever-expanding requirement for hard tissue repair and development of implants for orthopedic applications [2], [19], [28]–[30]. It was estimated, that in 2011, 460,000 hip and 712 knee replacements procedures performed in the US and double this number worldwide. It is expected that this number will double till 2025 as a result growing demand for a higher quality of life [25]. Although total hip arthroplasty has been called the main surgical procedure in orthopedics, there is a significant amount of research on-going in order to increase the longevity of the implants, because unfortunatelly now most joint replacemens fail after 10-25 years because of incomplete osseointegration and implant failure requiring a painful and expencive revision surgery [16], [31], [32]. Implants may fail due to many factors, one of them being host's biological response to the accumulation of microscopic wear debris, particularly PE. As today, THA commonly has a metal-on polymer bearing contact, with a cobalt chromium alloy (CoCr) head and an ultra-high molecular weight polyethylene (UHMWPE) acetabular cup [31]. Accumulation of wear debris leads to bone loss, inflamation and aseptic implant loosening causing an infection [25], [33].

Another important reason of failure is the fact, that almost all metal and alloys in body environment release metal ions which lead to loosening. Reaction between metallic implant and body fluids may be minimized by coating them with bioactive material like HA [35].

1.1.2. Dental implants

Dental implants are used to restore teeth by replacing both tooth and its root. Metallic implant is inserted into the gum so that bone cells grow around it and fix it. Titanium is the first choice for this purpose, as it osseointegrates rapidly to the surrounding tissue and forms a tight seal against bacterial invasion. Then abutment is placed on the anchor and then artificial tooth – crown [2].

The first traces of dental implants could be dated back to 2500 BC in ancient Egypt, where golden wire was used to stabilize teeth. Significant experiment was performed by Dr. Hunter in 1700,s when he transplanted incompletely developed tooth into the comb of a rooster and observed the blood vessels of the rooster grew straight into the pulp of the tooth [23]. Another significant breakthrough was made by Dr. P. Brånemark in 1952. While studying blood flow in rabbit femurs by placing titanium chambers in their bone, he noticed, that over time titanium became attached to the bone. That is where the concept of osseointegration was proposed meaning "a direct structural and functional connection between ordered, living bone, and the surface of a load carrying implant" [23].

As was already mentioned, metallic biomaterials, such as stainless steel, cobalt-based alloys, titanium and its alloys are widely used as artificial hip joints, bone plates and dental implants due to their excellent mechanical properties. However, there are some problems with metallic implants due to corrosion and release of ions in biological fluids after implantation, which leads poor implant fixation or even rejection of implant due to a lack of properties, such as osteoconductivity and osteoinductivity, and infections due to bacterial adhesion and colonization at the implantation site. To overcome these surface problems, surface modification was established, including chemical treatment, physical and biological methods. In the 1987, de Groot et al. [36] published their work on the development of plasma-sprayed hydroxyapatite implants. Further improvements were developed by several other authors which introduced the Screw-Vent implant which had a hydroxyapatite coating on it. This coating allowed more rapid adaptation of the bone to the implant surface and osseointegration. What is more, increased implant functional surface allows better stress transfer. Schematic illustration of the approach for electrochemical deposition of pure CHAp for coating dental implants is presented in Fig. 4 [37].

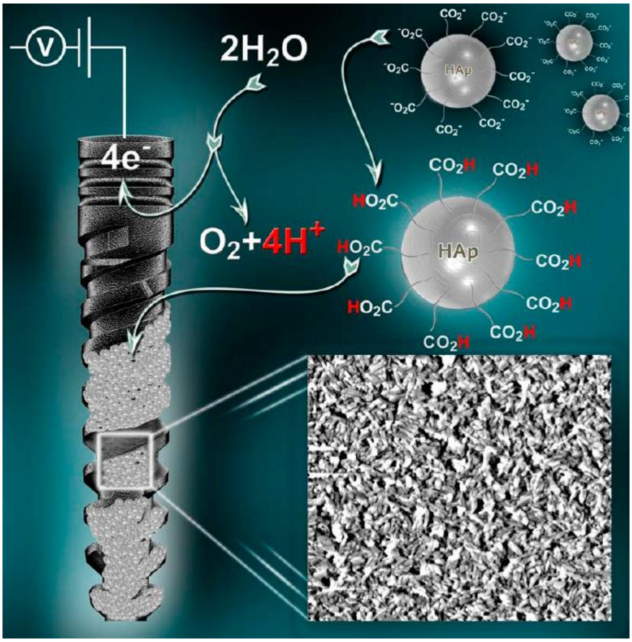

Fig. 4. Schematic illustration of the approach for electrochemical deposition of pure CHAp for coating dental implants [37].

Even though plasma spay coated titanium with hydroxyapatite layer is already used in the field of dentistry, there are some concerns related to this. One these is that hydroxyapatite may undergo resorbtion and degradation, finally loosening titanium particles. The long – term adherence of coating particles is poor, the thickness and composition is uneven. Other coatings considered for this purpose are titanium nitride, carbon, glass, titatnium dioxide [23]. Plasma sprayed CHAp-coated dental implants have also been related with some clinical risks such as the delamination of the coating from the titanium implant surface and failure at the implant–coating interface, despite the fact that the coating is well attached to the bone tissue [39] .

1.1.3. Materials used for dental and orthopedic implants

1.1.3.1. Metals

In general, materials used for implants could be devided in metals, polymers and ceramics [2]. Historically metals and alloys were the first materials used for modern implants and are used up to day, with titanium, cobalt-based alloys and stainless steel being the most popular. They have a wide range of applications – fracture fixation, partial and total joint replacement (see Fig. 5), external splints, braces and traction appratatus, dental amalgams.

The metallic implants usually have high strength and tougness, but are susceptible to chemical and electrochemical degradation – thus may corrode/wear, leading to generation of particulate debris, which may cause infection or other adverse biological reactions [17], [25], [40]. The mechanical properties of different implants and bone are compared in Table 2.

Stainless steel is iron-based alloy with a minimum of 10.5% Cr. Type 316L is one of the most widely used material for implant fabrication in orthopaedic applications up to day. As all metals, it possesses good mechanical properties, reasonable corrosion resistance, biocompatibility and density [17], [40].

Besides Cr for the corrosion resistance, Co alloys usually have small parts of iron, molybdenum or tungsten to alter the properties. For the implant application the most common types are Co–Cr–Mo (ASTM F75), Co–Cr–Mo (ASTM F799), Co–Cr–W–Ni (ASTM F90) and Co–Ni–Cr–Mo–Ti (ASTM F562) [2].

The ongoing use of titanium and its alloys (like Ti_6Al_4V, Ti_6Al_7Nb) for dental and orthopaedic applications can be attributed to it’s low density, and biocompatibility [7], [20]. Titanium also tends to develop stable oxide film, mainly consisting of TiO_2, which provides the excellent corrosion resitance [17], [41].

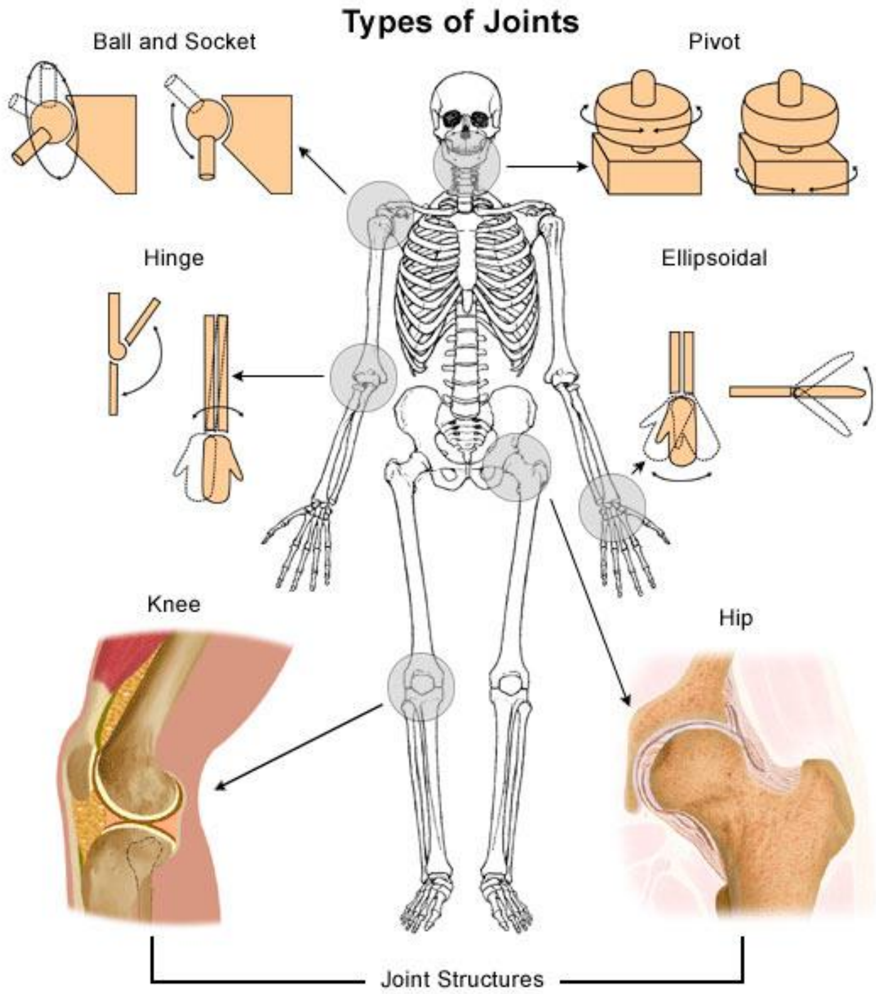

Fig. 5. Types of joints.

Magnesium is an emerging low density metal for orthopaedic applications, as it is biodegradable and biocompatible. While degrading it provides room for ingrowing bone. Compared to other metals, it’s elastic modulus is closer to bone than other metals [42]. That removes the requirement for second surgery for implant removal. As the degradation needs to be controlled, calcium phosphate coatings have been suggested as a mean to control corrosion rate [30], [43].

Table 2. Comparison of Mechanical Properties between Implant Materials and Bone [11]

Material	Young's Modulus (GPa)	Tensile Strength (MPa)
Alumina	365	6–55
Sintered HA	70–90	50–110
HA coating	0.5–5.3[34]	>51[87,88]
316L stainless steel	193	540
Co-Cr alloys	230	900–1540
Ti-6Al-4V, wt %	106	900
PMMA bone cement	3.5	70
HDPE	1	30
Cortical bone	7–30	50–150
Cancellous bone	0.1–1	1.5–3

1.1.3.2. Polymers

Polymers are huge class of materials which differ from each other in chemical composition, molecular weight, polydispersity, crystallinity, hydrophobicity, solubility and thermal transitions. Besides, their properties can be fine-tuned and they can be fabricated into complex structures as opposite to ceramics, as they are viscoelastic. The main drawback for the most of the polymers is the lack of rigidity, ductility and ultimate mechanical properties required in load bearing applications. Also, most of them are unable to meet the strict demands of the *in vivo* physiological environment [30], that is why only some of the most potential and interesting for the research according author are described below.

Polyetheretherketone (PEEK) is a polymer biomaterial, used for orthopaedic applications since 1980's [38]. It is an alternative to metal implants because of it's mechanical properties, biocompatibility, low modulus of elasticity and translucency to X-rays [44]. It can be processed through injection molding, extrusion or mashining allowing medical device manufacturers broad design and manufacturing flexibility [45]. It is unreactive and resistant to chemical and thermal degradation.

High density polyethylene (HDPE) was used for biological application, but was replaced by ultra high molecular weight polyethylene (UHMWPE).

UHMWPE compared to HDPE has almost the same chemical structure, comparable mechanical properties, relatively low cost, excellent creep resistance, good processability and biocompatibility, but higher rigidity and impact resistance [46]. It is usually used as bearing surface and artificial bones. Like with the most polymers, the main concern is that wear debris may cause osteolysis and loosening. One of the methods to solve this is the use of hydroxyapatite to improve biological fixation between the implant and the human cells [47].

Various apatite-containing formulations based on PMMA are used in orthopedics, as a bone cement for implant fixation, as well as to repair certain fractures and bone defects. PMMA is obtained by polymerization of toxic monomers, what may cause thermal and chemical necrosis [37], [48]. Moreover, it is neither degradable nor bioactive, does not bond chemically to bones and might generate particulate debris leading to an inflammatory foreign body response [30].

The most popular synthetic polymers PLA, PGA and their copolymers—PLGA. They are biocompatible, mostly non-inflammatory and break down gradually in the physiological environment of the body into biocompatible products [25]. They have been investigated as scaffolds for replacement and regeneration of a variety of tissues, cell carriers, controlled delivery devices for drugs, membranes or films, screws, pins and plates for orthopedic applications [30], [49]. One of the problems of PLGA is that it's degradation rate is un-matched with the growth of new bone, although it adjusted by varying component monomers [30], [37]. Furthermore, PLGA is known to support osteoblast migration and proliferation, which is a necessity for bone tissue regeneration. Unfortunately, such polymers on their own are too weak to be used in load bearing situations. In addition, they exhibit bulk degradation, leading to both a loss in mechanical properties and lowering of the local solution pH that accelerates further degradation in an autocatalytic manner. As the body is unable to cope with the vast amounts of implant degradation products, this might lead to an inflammatory foreign body response [30].

1.1.3.3. Ceramics

Ceramics are inorganic compounds of metallic or nonmetallic materials, with bonding which is usually formed at elevated temperatures. A class of such materials used for orthopaedic applications are commonly referred to bioceramics. These bioceramics may be bioinert (alumina, zirconia), bioresorbable (tricalcium phosphate), bioactive (hydroxyapatite, bioactive glasses, and glass ceramics), or porous for tissue in growth (hydroxyapatite coating, and bioglass coating on metallic materials). Their success depends on their ability to induce bone regeneration and bone in growth at the tissue–implant interface without the intermediate fibrous tissue layer [2].

Synthetic calcium phosphates (CP) are very important biomaterials due to their high bioactivity in human bones and dental biomineralized tissues. These CP bio-ceramics are widely used to treat bone defects due to their chemical similarity to bone minerals with well biocompatibility [50], [51]. Interestingly, the mineral component in bones and teeth is a highly carbonate-substituted, hydroxyl-deficient form of calcium hydroxyapatite [52]. The nanodimensional and nanocrystalline forms of calcium phosphates can be utilized in biomineralization and as biomaterials due to the excellent biocompatibility [53], [54]. Nanoscience is indeed revolutionized every single human craft and discipline, including medicine. Among nanomaterials, nanocalcium hydroxyapatite (n-CHAp) has been widely used in scaffolds for bone tissue engineering as well as implant coating material.

Many bioactive glass (BG)/glass ceramics (GC) have been prepared by various techniques during last decades [55]. Bioactive glasses are a group of synthetic silica-based biomaterials which are developed and used as a filler material or bone graft substitute in order to bone repair and regeneration applications by formation of apatite layer on their surfaces [56], [57]. In contact with simulated body fluid (SBF), BGs are capable to form an apatite-like surface layer. Usually, the BGs are surgically implanted into fracture or bone defect for enhancing the healing rate due to their bioactivity [58], [59]. It is known that different composites and nanocomposite scaffolds cause the better biological behaviour of the scaffolds. For example, the graphene-based CHAp composites showed better mechanical and enhanced antibacterial properties. In addition, these composites show their improved cell behaviour compared to the individual components [60]. Up to now, there are enormous efforts to develop different coatings that can enhance the biocompatibility properties of metallic implant materials and provide antimicrobial effects [61]–[65]. In the field of bone regeneration, has pushed towards an extensive use of CHAp coated implants as a bone substitute, in view of its similarity to the inorganic phase of mineralized tissues.

The quality of synthetic biomaterials, however, is highly dependent on the overall characteristics and features of the synthesized powders. Such attributes include density, purity, phase composition, crystallinity, particle size, particle-size distribution, particle morphology, and specific surface area. Thus, all mentioned properties of bioceramics are highly sensitive to the processing conditions, which are very much responsible for the crystallinity, crystal shape, crystal size, crystal size distribution and phase purity of the resulting powders. Metal-substituted $Ca_{10}(PO_4)_6(OH)_2$ nanocrystallites were also synthesized and investigated [66]–[70]. In most of the cases cationic substitution of calcium did not changed the surface morphology of the end product.

Biphasic calcium phosphate (BCP) ceramic comprises a mixture of CHAp and β-TCP. This material was regarded as suitable for synthetic bone applications and has been extensively used as substitution materials for artificial bone grafts [71], [72]. Nano-sized particles of BCP have been successfully prepared via sol-gel method after calcination of gel precursors at 900 °C. However, as the calcination temperature was increased up to 1200 °C, the increase of CHAp phase with reduction in β-TCP phase in BCP was observed [73].

The results are promising with respect to the application of sol-gel derived calcium phosphosilicate glasses containing sodium or magnesium as bioresorbable materials. It is evident that such implanted materials could be successfully applied for new bone formation and have utility for cell-tracking applications in regenerative medicine. Due to their high amount of amorphous glassy phase and their enhanced apatite forming ability even after sintering at high temperatures, these novel glass–ceramics can be suggested for the synthesis of scaffolds for bone tissue repair or engineering [74]–[77].

1.2. Natural human bone

1.2.1. Composition and stucture of human bone

Humans are born with 270 bones and this number decreases to 206 by adulthood. All this internal framework of bones performs six major functions: support, movement, protection, production of blood cells, storage of minerals, and endocrine regulation. These properties are mainly attributed to the remarkable hierarchical architecture - the mineralized fibrils, which is assembled by collagen molecules and mineralized by apatite crystals (looking like needles or thin plates, about 40–60 nm long, 20 nm wide, and 1.5–5 nm thick [1]) during the formation of the bone, still acts as the bone's universal elementary building block, as shown in Fig. 6 [78].

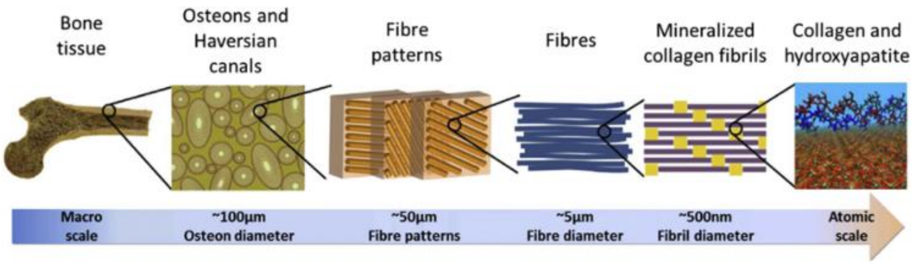

Fig. 6. The hierarchical structure of bone ranging from microscale skeleton to nanoscale collagen and hydroxyapatite [78].

The main inorganic phase of human bone is calcium hydroxyapatite ($Ca_{10}(PO_4)_6(OH)_2$, HA) – up to 65%, with other being 25% organic material and 5% water by weight [7], [79]. Besides that, there is a significant amount of other ions, like magnesium, sodium and potassium, so while producing HA coatings, the goal is to achieve them as similar as posible to natural bone in composition, crystal structure, crystallinity, crystal size, and morphology [80] even though it may be debated [81]. HA has a Ca:P ratio of 1.67 (5:3), however the Ca:P ratio in bone minerals actually varies between 1.37 and 1.87, indicating that these varied compositions of bone minerals may contain other additional ions, such as strontium, zinc and carbonate [1].

Table 3. Chemical composition of bone (wt %) [37].

Inorganic Phase	Organic Phase
HAp ≈ 60	Collagen ≈ 20
H_2O ≈ 9	Non-collagenous proteins (osteocalcin, osteonectin, osteopontin, thrombospondin, morphogenetic proteins, sialoprotein, serum proteins) ≈ 3
Carbonate ≈ 4	Traces: Polysaccharides, lipids, cytokines
Citrate ≈ 0.9	Primary bone cells: osteoblasts, osteocytes, osteoclasts
Na^+ ≈ 0.7	-
Mg^{2+} ≈ 0.5	
Cl^- ≈ 0.13	
Others: K^+, F^-, Zn^{2+}, Fe^{2+}, Cu^{2+}, Sr^{2+}, Pb^{2+}	

The organic matrix is composed 90% of two types of collagen and non – collagenous organic material. Type I collagen is dominating and is being secreted by osteoblasts. Non - collagenous organic materials are endogenous proteins which play an important role in biological activity and are being produced by the bone cells [79].

Bone cells are called osteoblasts, osteoclasts, osteocytes and bone – lining cells. Osteoblasts, bone lining cells and osteoclasts are present on bone surfaces and are derived from local mesenchymal cells called progenitor cells. Osteocytes are found in the interior of the bone and are produced from the fusion of mononuclear bloodborne precursor cells. Main function of osteoblasts is to synthesize the components that constitute the extracellular matrix of bone [74]. Osteoclasts are involved in bone resorption which is needed for bone remodelling in response to growth or changing mechanical stresses upon the skeleton. When bone surfaces are neither in the formative nor resorptive phase, they are covered by bone lining cells, who protect it from osteoblast resorbtive activity. Once the osteoblast is finished working it is trapped inside of the bone. When the osteoblast becomes trapped, it becomes known as an osteocyte. Osteocytes are main mechanoreceptors of bone and may secrete growth factors in response to mechanical stress [37], [79].

1.2.2. Properties of human bone

To discuss or design the biomimetic artificial scaffolds, understanding of the structures and biomechanical properties of natural bone is required. Bone is a multifunctional composite which among its other functions serves as a support for other tissues in the body. As a structural material it is stiff, strong, tough, lightweight and is adaptable. It's excellent mechanical properties are due to its complex, composite and hierarchical structure [82]. Human bone's density distribution from inside to outside spans a significant range: the spongy low-density bone in the middle is called trabecular or cancellous bone and the high-density outside is called cortical bone as shown in Fig. 7 [83]. Mechanical properties of the bone are determined by the chemical compostion and structure [78], [84].

Cortical bone makes 80% of the bone mass, whereas cancellous with honeycomb structure accounts for roughly 20% of the total mass of the skeleton. The cortical bone has a higher Young's modulus value in order to provide sufficient mechanical strength to bear weight. Fracture toughness values in the range reported for cortical bone (2–12 MPa·m1/2) are required for load-bearing applications [56]. The special alignment of the cancellous bone structure, however, is able to dampen the sudden stress [1]. This unique hierarchical structure of bone enables its self-repairing properties; bone can alter its geometry and material properties in response to changing external load stimuli, and it undergoes a continuous remodeling process [56].

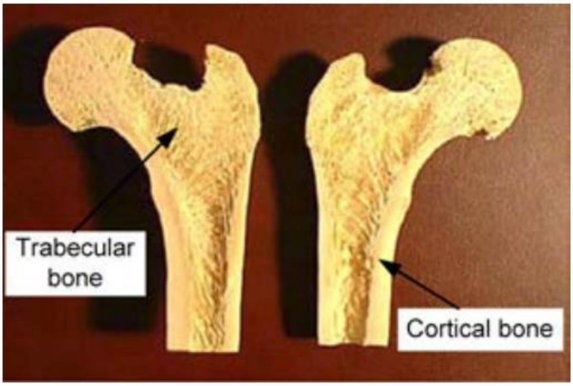

Fig. 7. A cross-sectional view of femur bone [83]

Table 4. Mechanical properties of human bones [1]

	Test direction related to bone axis	
	Parallel	Normal
Tensile strength (MPa)	124–174	49
Compressive strength (MPa)	170–193	133
Bending strength (MPa)	160	
Shear strength (MPa)	54	
Young's modulus (GPa)	7.0–18.9	11.5
	20–27 (random)	
Ultimate tensile strain	0.014–0.031	0.007
Ultimate compressive strain	0.0185–0.026	0.028
Yield tensile strain	0.007	0.004
Yield compressive strain	0.010	0.011

One of the main properties of describing mechanical properties of bone is elastic modulus (usially of Young's modulus). Given the complexity of the bone structure, it is not surprising that values reported in the literature vary a lot. A change in mineral content due to ageing of other reasons affects the elastic, post-yield and ultimate properties of bone [82], [85].

A general trend is the elastic modulus increases with mineral volume fraction in a roughly linear correlation. Human enamel has a very high degree of mineralization, and corresponding elastic modulus is about 80 GPa.

1.3. Synthetic calcium phosphates

Calcium phosphate (CaP) is the common name of a family of minerals containing calcium cations together with phosphate anions, and sometimes hydrogen or hydroxide ions. Synthetic calcium phosphate bioceramics are widely used in the field of bone regeneration, both in orthopedics and in dentistry, due to their good biocompatibility, osseointegration and osteoconduction [37]. Among these calcium phosphate bioceramics, the most used materials are calcium hydroxyapatite, tricalcium phosphate, octacalcium phosphate, amorphous calcium phosphate, dicalcium phosphate and other.

1.3.1. Composition and stucture of calcium hydroxyapatite

Calcium phosphates with a Ca/P atomic ratio between 1.5 and 1.67 are called apatites (e.g., hydroxyapatite or fluorapatite). The term apatite was coined in 1786 by German geologist Abraham Gottlob Werner based on the ancient Greek word “apatao”, which means “to mislead” [37]. Calcium hydroxyapatite $Ca_{10}(PO_4)_6(OH)_2$ (HA) is an inorganic mineral exhibiting a typical apatite lattice structure namely ($A_{10}(BO_4)_6X_2$) where A, B and X are represented by Ca^{2+}, PO_4^{3-}, and OH^-, respectively. Early X-ray diffraction studies have shown HA having a crystalline hexagonal arrangement of Ca^{2+}, PO_4^{3-} ions around columns of OH^-ions. The crystal structure of HA belongs to the six fold space group (P63/m) with unit cell dimensions of a=b=9.421 nm and c=6.884 nm [86]. Fig. 8 represents a prospective view of a HA crystal unit cell [87].

Pure HA contains 39.68 wt % calcium and 18 wt % phosphorus giving rise to a Ca:P mole ratio of 1.67.

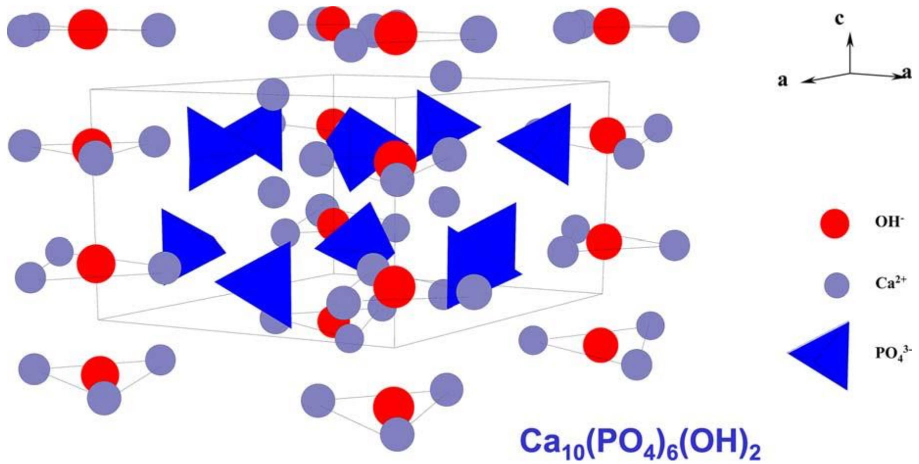

Fig. 8. Structure of calcium hydroxyapatite.

1.3.2. Properties of calcium hydroxyapatite

Physical properties, such as surface morphological features, stoichiometry, solubility of HA and other are very important for the biological properties (bioactivity, osteoconductivity, osteoinductivity) of final implants. Due to its poor mechanical properties (brittleness and inflexibility), the use of hydroxyapatite as a substitute bone material is unfortunately limited to places that are not subject to great tension [88]. On the other hand, a hydroxylapatite material is a perfect component of composite implants with synthetic polymers and biopolymers. Dense hydroxyapatite bioceramics, formed into suitable shapes, may be used in the creation of implants for the middle ear and eye (orbital implant), and are included in inner dialysis systems [89]. Hydroxyapatite is widely used as a coating of metallic implants for bones in order to improve and accelerate the process of osseointegration [90]. Hydroxyapatite powder plays an important role in dentistry (e.g., in the treatment of dental pulp and dentine hypersensitivity). Hydroxyapatite,present in toothpastes and dental gels, reduces the deposition of accretions on teeth. It can also be used as a component of dental cements and fillings. It is also worth mentioning that microporous structures of hydroxyapatite can serve as carriers of drugs supplying medicinal substances directly to a destination. Properties of calcium phosphates, which influence biological processes including protein adsorption, cell adhesion and cell differentiation are also important for biological processes [87].

Lager pore size and lower macroporosity show greater ingrowth of biomaterial compared to bioceramics with smaller pore size and higher macroporosity [91]. It was demonstrated that HA with pores ranging from 20 nm to 500 μm enhanced protein adsorption significantly. In addition, a larger number of micropores also enhance the adsorption of proteins, such as fibrinogen and insulin [87]. Besides, protein adsorption also depends on surface charge and solubility of calcium phosphate bioceramics. Moreover, the dissolution process also is affected by microporosity and macroporosity of bioceramics. The dissolution increases with decreasing crystal size and increasing microporosity and macroporosity [91].

One of the primary features of hydroxyapatite is its capacity for ion substitution (i.e., ion exchange). This means that the locations for hydroxyl ions may be occupied by ions of a similar size and charge, such as Cl^- or F^-. In turn, the locations for calcium cations may be occupied by the ions Mg^{2+}, Mn^{2+}, Sr^{2+} or other [86], [88], [92]. An important aspect is also the possibility of the substitution of ions with different charges. For example,it is possible to exchange phosphate ions (−3) with carbonate ions (−2). Such a situation leads to the creation of a positively charged vacancy, which is compensated for by the simultaneous release of one cation of calcium (Ca^{2+}) and one hydroxyl ion (OH^-) [93]. This capacity for the ion exchange of hydroxyapatites has been used recently in biomaterials engineering. One also uses the fact that the introduction of even small quantities of some ions may cause changes/improvements in biological, physicochemical, or mechanical properties [94]–[96].

It should be emphasized that infections around bone implants comprise the key problem for modern reconstruction surgery [60]–[63], [65], [97]–[100]. Therefore, implantation surgery seeks additional factors that increase the antibacterial activity around introduced biomaterials. At present, a fairly common tendency is to use the antibacterial properties of certain ions, including silver (Ag^+) [98], [99], [101] and copper (Cu^{2+}) [102]–[105]. In addition, one tries to look for the possibility of using other ions, such as cerium Ce^{3+} [106]–[109], titanium Ti^{4+} [110], [111], manganese (Mn^{2+}) [112], [113] and strontium Sr^{2+} [114], among others. The mechanisms of the antibacterial activity of ions are not fully explained yet.

1.3.3. Synthesis methods

The sol-gel synthesis route in combination with the dip-coating process, represents an easy low cost and efficient route to coat large surfaces, permitting also the tailoring of the microstructure from the chemistry of the sol-gel synthesis [90]. In 1998 Gross et al. [115] demonstrated that calcium hydroxyapatite (CHAp) coatings could be successfully synthesized through the sol-gel technique, using calcium diethoxide and triethyl phosphite dissolved in ethanol as starting materials. 1,2-ethanediol was used as complexing agent in the sol-gel processing. It was concluded that the production of thin homogeneous hydroxyapatite coatings by sol-gel method on titanium substrates using alkoxide precursors required control of the aging time and annealing temperature. Worth mentioning, that CHAp powders were first time obtained through the sol-gel technique using alkoxides as starting materials in 1990 [116]. The sol-gel method offers a molecular-level mixing of the calcium and phosphorus precursors, which capable of improving extent, in comparison with conventional methods. Besides, the sol-gel approach provides significantly milder conditions for the synthesis of HA powders or films. In the sol-gel synthesis of HA, calcium alkoxides or salts are frequently using as calcium precursors. In most cases, phosphorus compounds – oxide, triethylphosphate and triethylphosphite are employing as phosphorus precursors in water or organic solvents phase. However a long period of the sol-gel preparation time, 24 h or longer is commonly reported in literature as required to form desirable product. This is because of slow reaction between calcium and phosphorus precursors in the sol phase.

A number of methods have been used for HA powder synthesis. One of the most widely used methods is wet precipitation, where chemical reactions take place between calcium and phosphorus ions under a controlled pH and temperature of the solution. The precipitated powder is typically calcined at 400-1000 ^{o}C in order to obtain a stoichiometric, apatitic structure. However, fast precipitation during phosphate solution titration (to calcium solution) leads to chemical inhomogeneity in the final product. Slow titration and diluted solutions must be used to improve chemical homogeneity and stoichiometry of the resulting HA. Careful control of the solution condition is critical in the wet precipitation. Otherwise, a decrease of solution pH below about 9 could lead to the formation of Ca-deficient HA structure [4].

The synthesis of HA requires a correct molar ratio of 1.67 between Ca and P in the final product. A number of combinations between calcium and phosphorus precursors were employed for sol-gel HA synthesis.

1.4. Coating techniques

So far, a number of commercial techniques have been developed to create the HAp coating on metallic implants, such as sol–gel dip and/or spin coating (Figs. 9 and 10, respectively) [15], [96], [117]–[126], electrochemical deposition (see Fig. 4) [17], [127]–[130], electrophoretic deposition (Fig. 11) [119], [131]–[134], plasma spraying process (Fig. 12) [135]–[137], magnetron sputtering technique (Fig. 13) [138]–[140], hot isostatic pressing (Fig. 14) [141]–[143], pulsed laser deposition (Fig. 15) [143], [144] and biomimetic deposition (Fig. 16) [145]. Amongst the techniques listed, only plasma spraying due to its very good coating properties is commercially approved by the Food and Drug Administration (FDA), USA for biomedical coatings on implants [146]. However, HAp coating by plasma spray technique is also limited. It is due to poor uniformity in coating thickness and its adherence to substrate, phase impurity, and low crystallinity. Moreover, plasma spray deposition is not able to produce a uniform HAp coating with complex geometry.

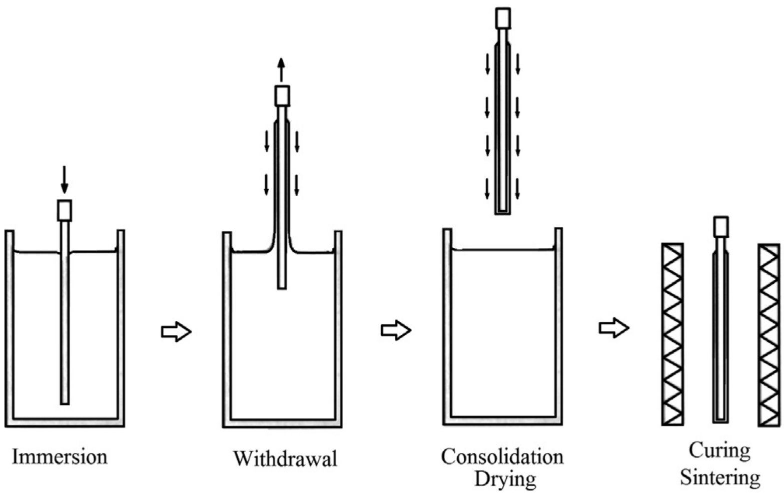

Fig. 9. Sol-gel dip-coating technique.

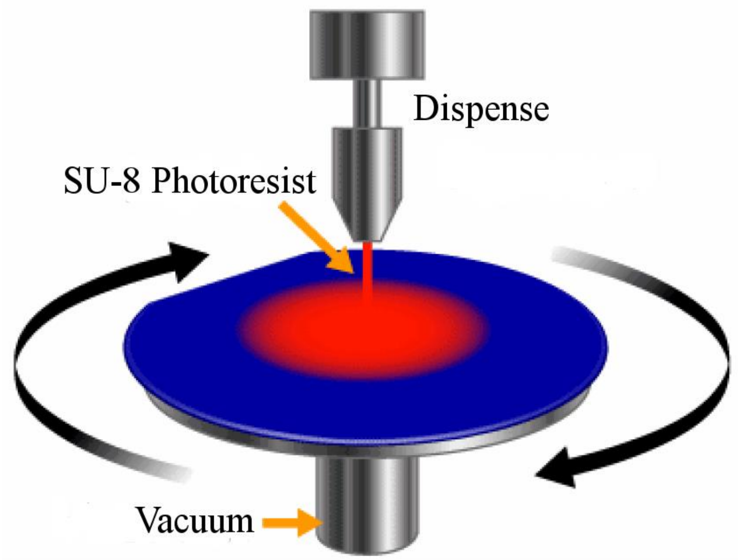

Fig. 10. Sol-gel spin-coating technique.

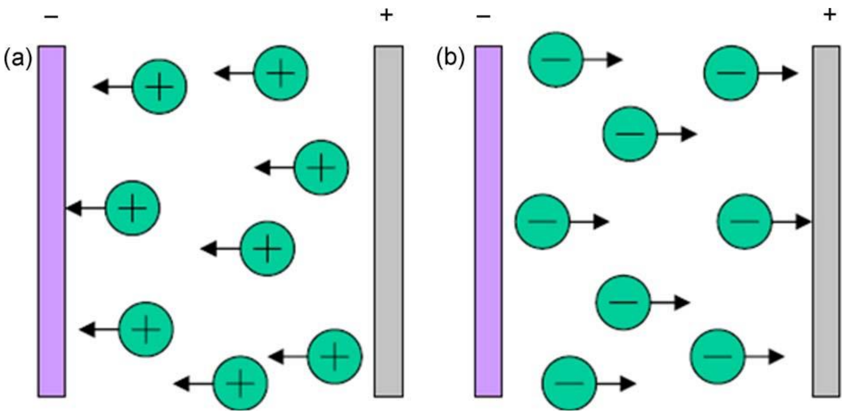

Fig. 11. Electrophoretic deposition technique.

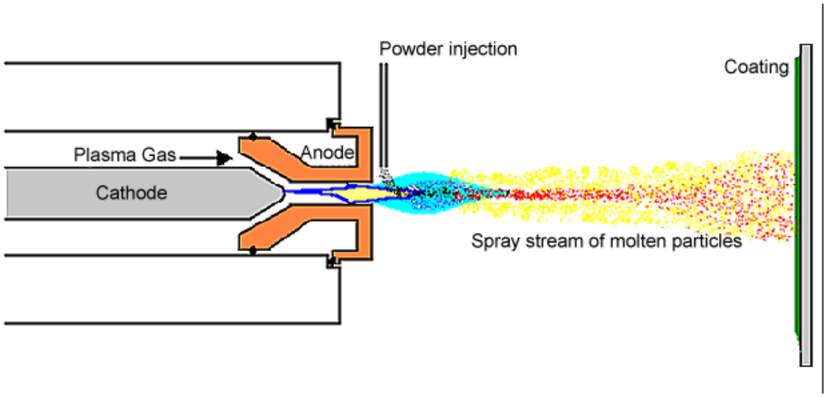

Fig. 12. Plasma spraying technique.

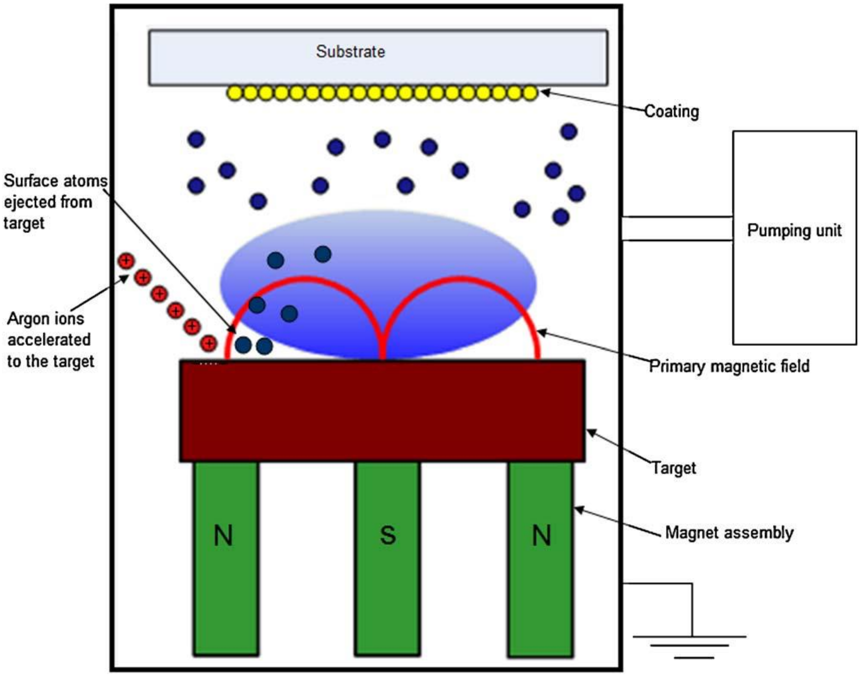

Fig. 13. Magnetron sputtering technique.

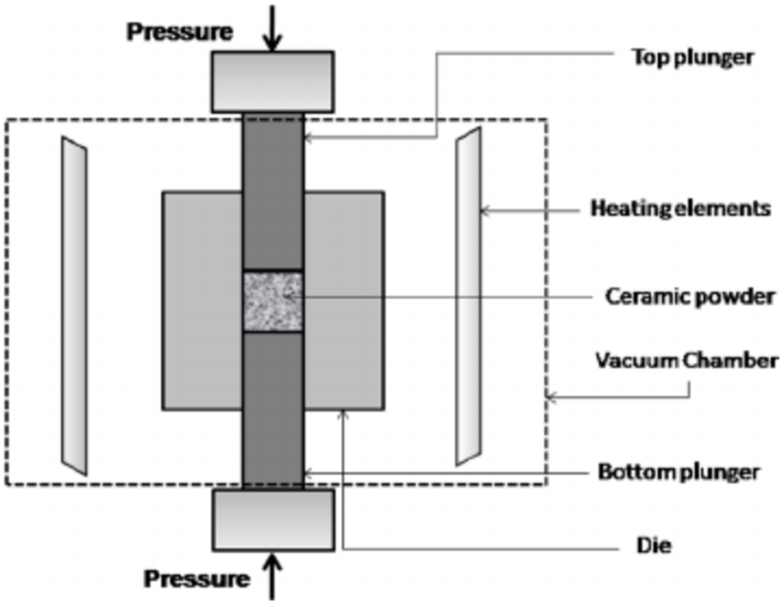

Fig. 14. Hot isostatic pressing technique.

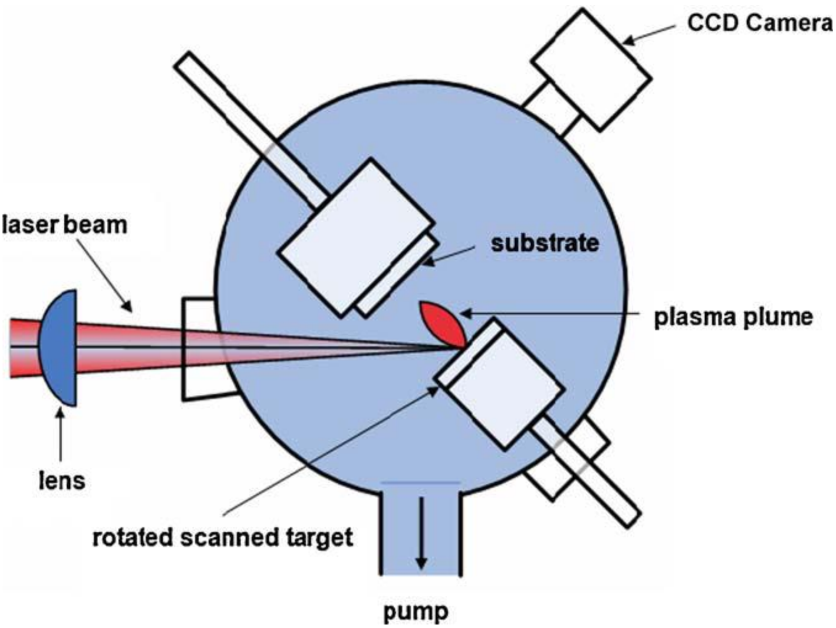

Fig. 15. Pulsed laser deposition technique.

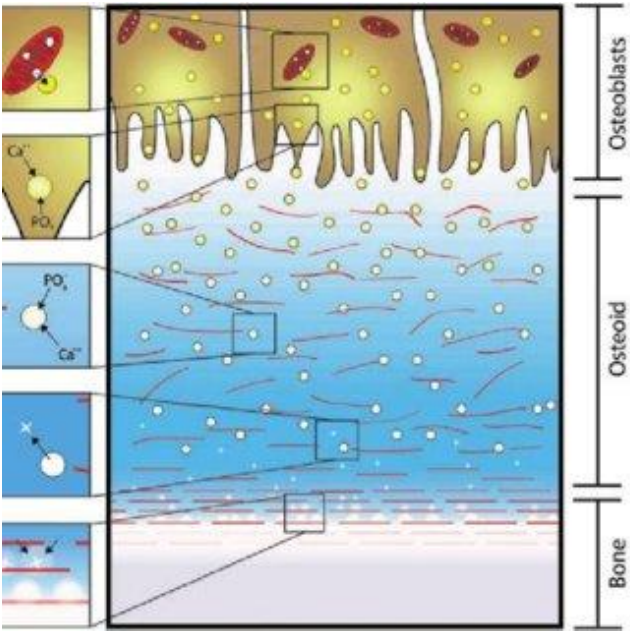

Fig. 16. Biomimetic deposition.

The summarized techniques used for the preparation of Hap coatings demonstrate some advantages such as high deposition rates, formation of uniform coating thickness on flat substrates, possibility to obtain dense and porous coatings, a high reproducibility and reliability and high adhesion properties. However, the sol-gel synthesis method is relatively cheap, provides very thin and homogeneous coatings, the method is suitable to fabricate thin films at low processing temperatures and can be used to coat complex shapes and different substrates.

2. EXPERIMENTAL

2.1 Materials and methods

2.1.1. Materials

Materials used for calcium hydroxyapatite coatings preparation are listed in Table 5.

Table 5. List of reagents.

Reagent	Chemical formula	Purity	Producer
Calcium acetate monohydrate	$Ca(CH_3COO)_2 \cdot H_2O$	99.9 %	Fluka
1,2- ethandiol	$C_2H_6O_2$	99.0 %	Alfa Aesar
Ethylenediamine tetra acetic acid (EDTA	$(HO_2CCH_2)_2NCH_2CH_2N(CH_2CO_2H)_2$	99.0 %	Alfa Aesar
Triethylamine (TEA)	$(HOCH_2CH_2)_3N$	99.0 %	Merck
Phosphoric acid	H_3PO_4	85.0 % (concentration)	Reachem
Calcium hydroxide	$Ca(OH)_2$	≥ 95%	Roth
Poly(vinyl alcohol) (PVA 70000)	$[-CH_2CHOH-]_n$	99.5 %	Aldrich

2.1.2. Methods

2.1.2.1. Synthesis of calcium hydroxyapatite thin films

The calcium hydroxyapatite coating solution was prepared using calcium acetate monohydrate was as starting material. To the aqueous solution of $Ca(CH_3COO)_2$ the 1,2-ethandiol was added. The obtained mixture was stirred for 30 min at 65 °C. Then ethylenediaminetetraacetic acid was added, and after 15 min triethanolamine (TEA) was slowly added. The solution was stirred for 10 h. Then diluted phosphoric acid was added (Ca/P ratio was 1.67). Finally, this solution was mixed by ratio 5:3 with PVA dissolved in distilled water. Composition - 0.003 mol $Ca(CH_3COO)_2{\cdot}H_2O$, 0.003 mol TiIPro, 0.009 mol citric acid, 2.22 mol H_2O and 0.00004 mol PVA 70000, 5.39 mol H_2O.

For the fabrication of calcium titanate sublayers by sol-gel route the citric acid was dissolved in distilled water and mixed with titanium (IV) isopropoxide. The solution was stirred at 90 °C until titanium isopropoxide was completely dissolved. In the next step, either calcium acetate monohydrate ($Ca(CH_3COO)_2{\cdot}H_2O$ or calcium hydroxide $Ca(OH)_2$ as the Ca source were added to the above solution. Therefore, two separate solutions were prepared. Next, 1,2-ethandiol was added to the both solutions under the stirring for 1 h at room temperature. Finally, these solutions were mixed with PVA dissolved in distilled water.

A schematical diagrams of sol-gel preparation of calcium titanate sublayers are shown in Fig. 17.

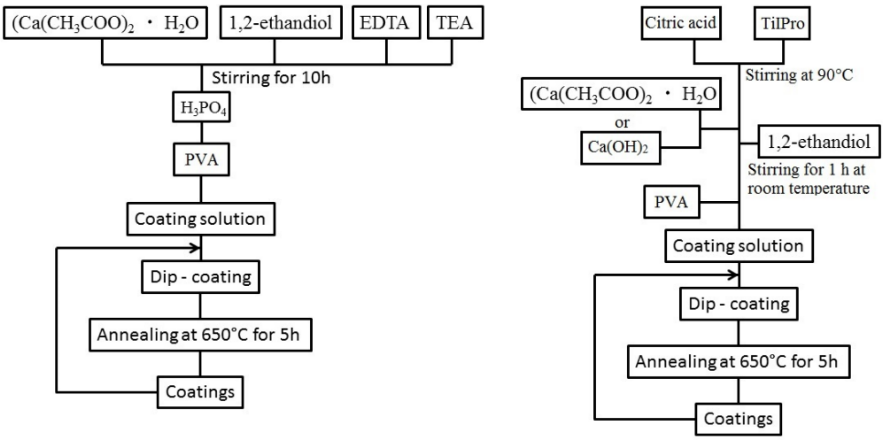

Fig. 17. Schematical diagrams of sol-gel preparation of calcium titanate sublayers (right) and calcium hydroxyapatite thin films (left).

2.1.2.1. Substrate cleaning and coating

All substrates were cleaned in an ultrasonic bath with acetone, ethanol and distilled water sequentially.

For the accelerated route to obtain coatings, one dip-coating cycle consisted of dipping the substrate and retrieving it, drying for 10 minutes in 200°C in dip-coater dryer and leaving for 110 minutes to reach temperature equilibrium with the room repeated 5 times. After that, samples were heated to 650 °C with temperature ramp of 1 °C/min and annealed for 5 h. The samples were left to cool to the room temperature within the furnace. The formation of coatings on silica substrate was performed using a dip-coater (Holmarc HO-TH-02B). The dipping rate of substrate was 85 mm/min and lifting rate was 40 mm/min. The substrate was left in the gel solution for 20 s.

The standard route contained of immersing (85 mm/min) and withdrawal (40 mm/min) for all the samples. The dipping procedure was repeatedly performed 10, 20 and 30 times unless stated differently. Substrates were annealed at 650°C for 5 h using the same temperature ramp of 1°C/min after each dip-coating procedure. The samples were cooled to the room temperature within the furnace.

Additionally, in some experiments the Ti substrates were heat-treated at 650°C for 5 h with temperature ramp of 1°C/min.

2.1.2.2. Instrumentation and characterisation techniques

The synthesis products were analyzed by X-ray diffraction (XRD, Rigaku MiniFlex II) analysis, scanning electron microscopy (SEM, Hitachi SU 70), AFM measurements (Veeco Bioscope 2 atomic force microscope) and contact angle measurements (KSV Instrument CAM 100).

FTIR spectra were recorded in transmission mode by using FTIR spectrometer ALPHA (Bruker, Inc.), equipped with a room temperature detector DLATGS. Spectra were acquired from 100 interferogram scans with 2 cm^{-1} resolution.

Raman spectra were recorded using inVia Raman (Renishaw, United Kingdom) spectrometer equipped with thermoelectrically cooled (−70 °C) CCD camera and microscope. Raman spectra were excited with 442 nm radiation from He–Cd laser. The 50×/0.75 NA objective lens and 2400 lines/mm grating were used to record the Raman spectra. The accumulation time was 400 s. To avoid damage of the sample, the laser power at the sample was restricted to 0.8 mW. The Raman frequencies were calibrated using the silicon standard according to the line at 520.7 cm^{-1} and air O_2 (1555.0 cm^{-1}) and N_2 (2330.1 cm^{-1}) bands. The high resolution Raman spectra were excited with 632.8 nm He–Ne laser (1 mW power at the sample) and dispersed with 2400 lines/ mm grating. Spectral slit width near 1500 cm^{-1} determined by analysis of air O_2 band was 3.4 cm^{-1}. Parameters of the bands were determined by fitting the experimental spectra with Gaussian-Lorentzian shape components using GRAMS/A1 8.0 (Thermo Scientific) software [147].

Thermogravimetric analysis of precursor gels was performed using Perkin Elmer Pyris 1 TGA instrument.

3. RESULTS AND DISCUSSION

3.1 Sol-gel derived porous and hydrophilic calcium hydroxyapatite coating on modified titanium substrate

The results of thermogravimetric (TG) analysis of synthesized Ca-Ti-O precursor gels are presented in Fig. 18. Three weight loss mechanisms in the temperature ranges of 50–250 °C, 250–430 °C and 430–650 °C can be distinguished in the TG curves. In the first step, the weight loss (approximately 15%) is associated with evaporation of the adsorbed and structural water. In the second stage the main decomposition of the gel occurs (45%) due to thermal degradation of organic parts (ethylene glycol, PVA, citrates) present in the gels. Finally, pyrolysis of the remaining constituents (about 20%) of the gels between 430 and 650 °C takes place. No further weight loss could be observed above 650 °C.

Interestingly, the TG curves Ca-Ti-O precursor gels obtained using calcium acetate and calcium hydroxide as starting material are almost identical. The TG/DTA curves of the Ca-P-O precursor gel are shown in Fig. 18. Again, in the first mass loss stage (about 15%) in the temperature range of 160–200 °C evaporation of moisture from the gel takes place. The main decomposition of the gel with the mass loss of about 65% could be observed up to 650 °C, similarly to the Ca-Ti-O gel.

Fig. 19. represents XRD patterns of HAp coatings fabricated on the Ti substrate which was heat-treated before dip-coating procedure. The pre-heating of Ti substrate was performed to create an initial titanium oxide layer that would prevent further development of oxide layer during the formation of the coatings.

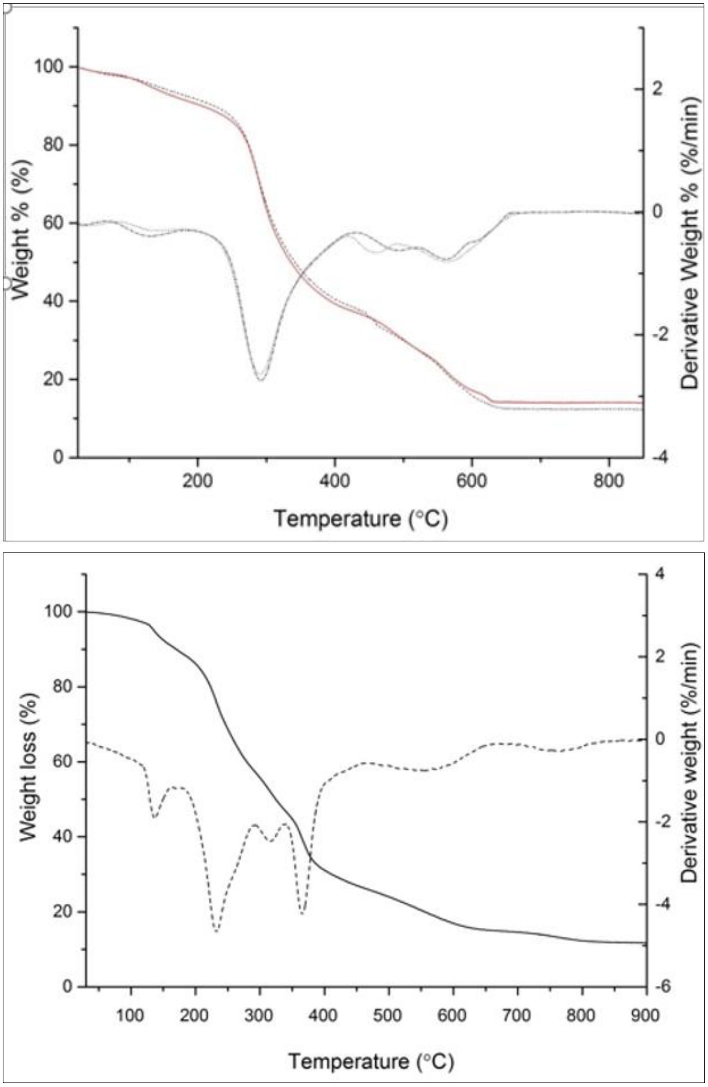

Fig. 18. TG/DTA curves of Ca-Ti-O precursor gels obtained using calcium acetate (dotted line) and calcium hydroxide (solid line) as starting material (top) and TG/DTA curves of Ca-P-O precursor gels (bottom).

The intensity of reflections attributable to the HAp phase increases with increasing number of coating layers. Consequently, the intensity of the diffraction peaks related to the Ti substrate monotonically decreases. Evidently, the formation of TiO_2 is suspended by the initial pre-heating process of substrate at 650 °C for 5 h in air. The intensity of characteristic diffraction peaks of titanium oxide remains unchanged upon increasing the number of dip-coating and annealing procedures.

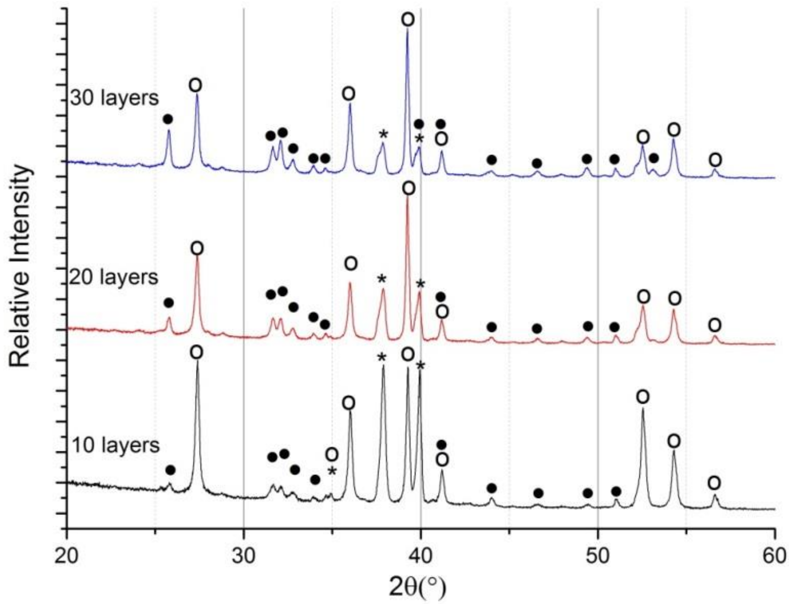

Fig. 19. XRD patterns of HAp films on the pre-heated Ti at 650 °C for 5 h in air. Diffraction peaks: • - ($Ca_{10}(PO_4)_6(OH)_2$ (PDF: 74-0566); o – TiO_2 (PDF: 73-2224); * - Ti (PDF: 44-1294).

For example, Fig. 20. represents XRD patterns of HAp coatings obtained directly on cleaned titanium substrate without preliminary heating at elevated temperatures. In this case, the HAp diffraction peaks are visible already after 10 coating procedures. Their intensity monotonically increases with increasing number of layers up to 30 layers. Again, the intensity of diffraction peak attributable to Ti decreased with increasing number of HAp layers. However, the intensity of the peaks associated with TiO_2 phase evidently increases, indicating the continuous growth of titanium oxide. These results confirm the effect of pre-annealing procedure of Ti substrate to prevent further development of titanium oxide layer during fabrication of the HAp coatings (see Fig. 21) [148].

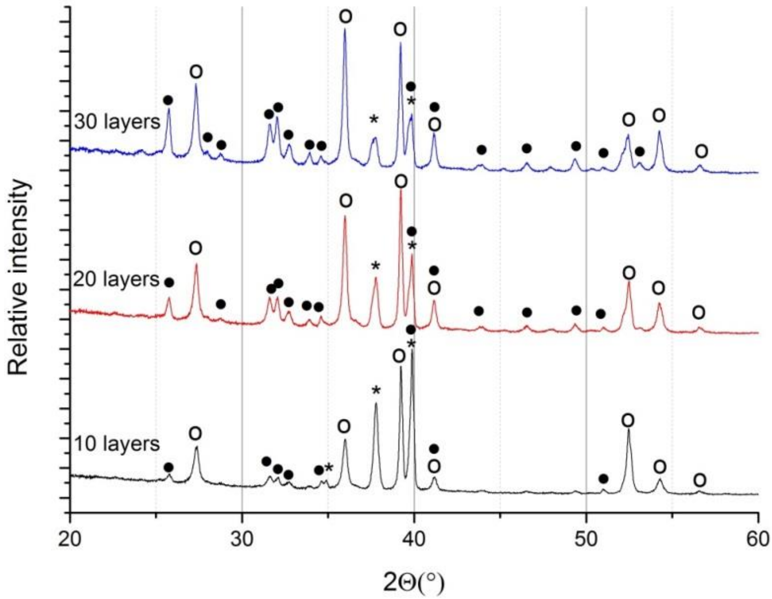

Fig. 20. XRD patterns of HAp films on the Ti.
Diffraction peaks: • - ($Ca_{10}(PO_4)_6(OH)_2$ (PDF: 74-0566);
o – TiO_2 (PDF: 73-2224); * - Ti (PDF: 44-1294).

Figs. 22 and 23 represent XRD patterns of HAp coatings obtained on the Ti substrates prepared with 10 sublayers of $CaTiO_3$ (calcium acetate was used as Ca source). As evident, the peaks attributable to $CaTiO_3$ are clearly visible after 10 coating cycles, however, along with $CaTiO_3$, TiO_2 is present at the Ti surface . The formation of HAp is visible after 10 dipping procedures. After additional 10 coating cycles, the intensity of HAp diffraction peaks evidently increased. The diffraction peaks attributable to $CaTiO_3$ are not visible anymore, as the sublayer of $CaTiO_3$ was fully covered by HAp. Moreover, it appears that TiO_2 is also forming in the sol-gel processing when the Ti substrate was not preheated before the formation of the $CaTiO_3$ sublayer (see Fig. 22). The intensity of TiO_2 reflections increases with each step of dipping in the HAp gel procedure. Thus, the initial formation of a sublayer of calcium titanate on the Ti substrate did not prevent the formation of titanium oxide.

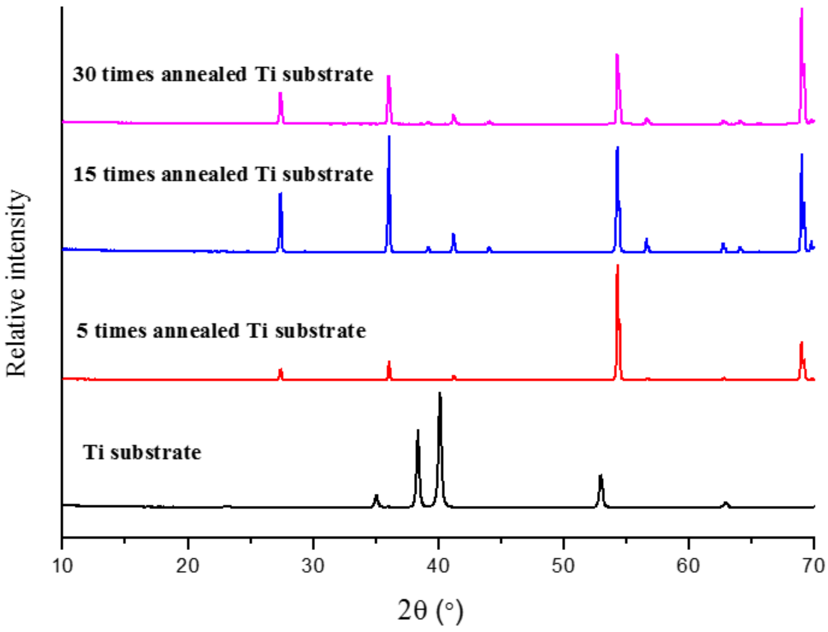

Fig. 21. XRD patterns of Ti substrates repeatedly heated at 1000 ºC for 5 h with temperature ramp of 1 ºC/min [148].

The situation is different, when the Ti substrate was pre-heated before the formation of a calcium titanate sublayer. Apparently, the intensities of diffraction peaks of TiO_2 remain unchanged with increasing number of HAp layers up to 20 (see Fig. 23).

The same set of experiments was performed when calcium hydroxide was used as Ca source to form a $CaTiO_3$ sublayer on the Ti substrate. XRD patterns of HAp coatings obtained on sublayers of $CaTiO_3$ (calcium hydroxide was used as Ca source), which were fabricated on heat-treated and just cleaned titanium substrate indicated that the formation of HAp proceeds independently on the nature of the calcium starting material (see Figs. 24 and 25). The intensity of reflections attributable to TiO_2 remains unchanged with increasing the number of HAp coatings on the heat-treated Ti substrate (with $CaTiO_3$ sublayer). However, the amount of TiO_2 increased monotonically when Ti without initial pre-heating was used.

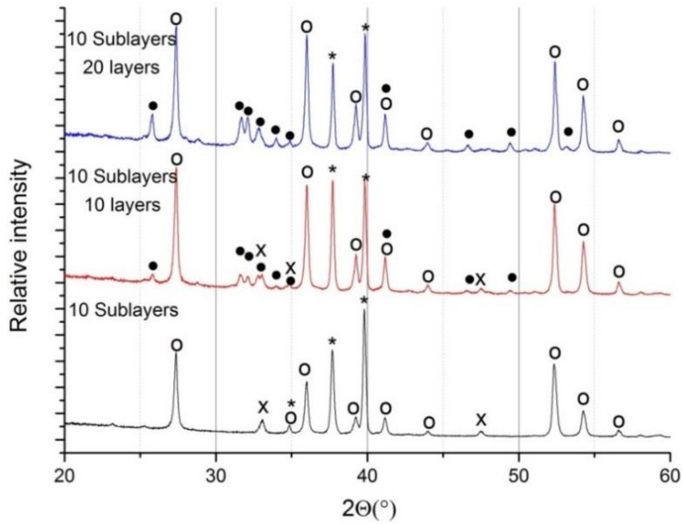

Fig. 22. XRD patterns of HAp films on Ti (without initial pre-heating). Diffraction peaks are marked: • - ($Ca_{10}(PO_4)_6(OH)_2$ (PDF: 74-0566); o – TiO_2 (PDF: 73-2224); * - Ti (PDF: 44-1294); x – $CaTiO_3$ (PDF: 22-0153).

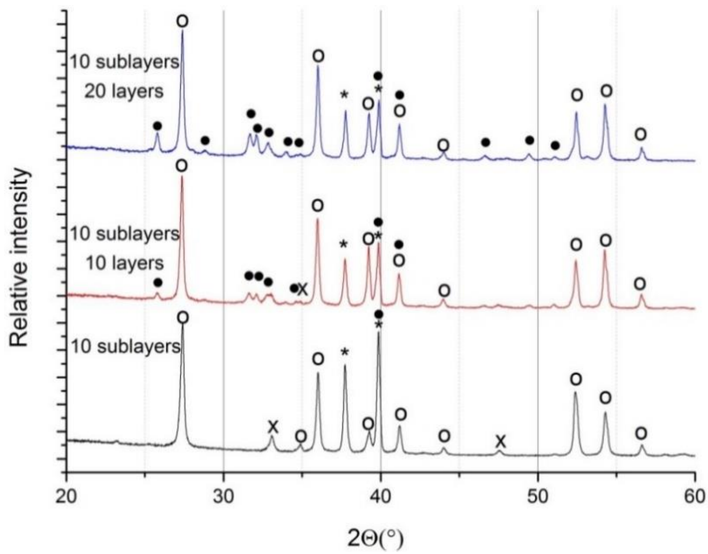

Fig. 23. XRD patterns of HAp films on the pre-heated at 650 °C for 5 h in air. Diffraction peaks: • - ($Ca_{10}(PO_4)_6(OH)_2$ (PDF: 74-0566); o – TiO_2 (PDF: 73-2224); * - Ti (PDF: 44-1294).

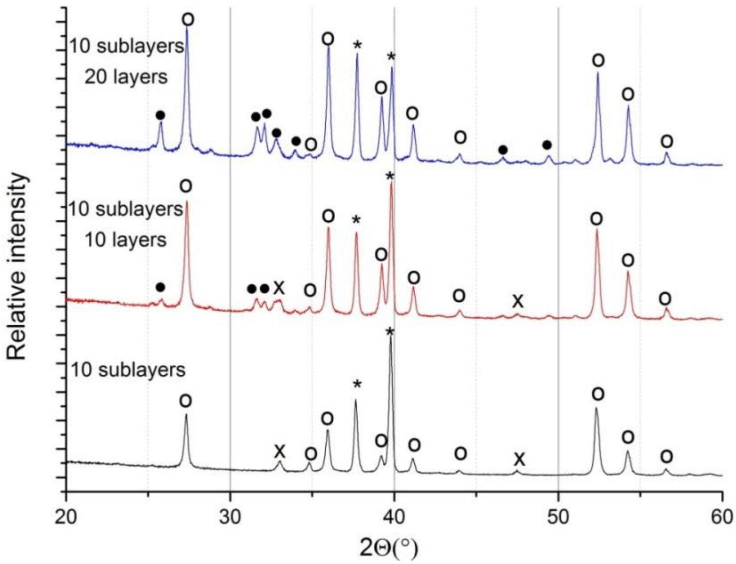

Fig. 24. XRD patterns of CHAp films on Ti (without initial pre-heating) with $CaTiO_3$ sublayer (derived from calcium hydroxide) annealed at 650 °C for 5 h in air. Diffraction peaks are marked: • - ($Ca_{10}(PO_4)_6(OH)_2$ (PDF: 74-0566); o – TiO_2 (PDF: 73-2224); * - Ti (PDF: 44-1294); x – $CaTiO_3$ (PDF: 22-0153).

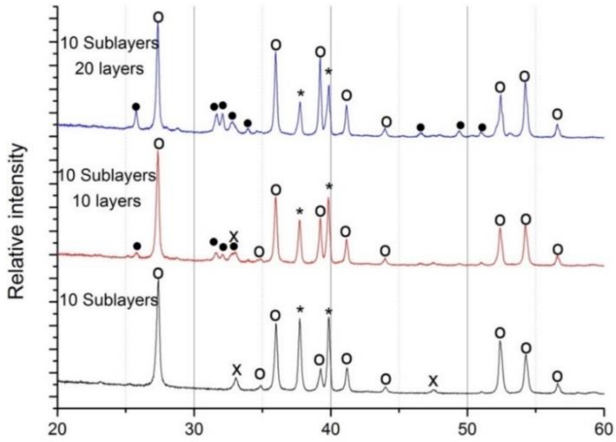

Fig. 25. XRD patterns of CHAp films on processed Ti (initially pre-heated) with $CaTiO_3$ sublayer (derived from calcium hydroxide) annealed at 650 °C for 5 h in air. Diffraction peaks are marked: • - CHAP ($Ca_{10}(PO_4)_6(OH)_2$ (PDF: 74-0566); o – TiO_2 (PDF: 73-2224); * - Ti (PDF: 44-1294); x – $CaTiO_3$ (PDF: 22-0153).

The morphology of coatings was investigated using scanning electron microscopy (SEM). Fig. 26 shows the SEM micrographs of HAp obtained on as-prepared for coating and thermally processed Ti substrates.

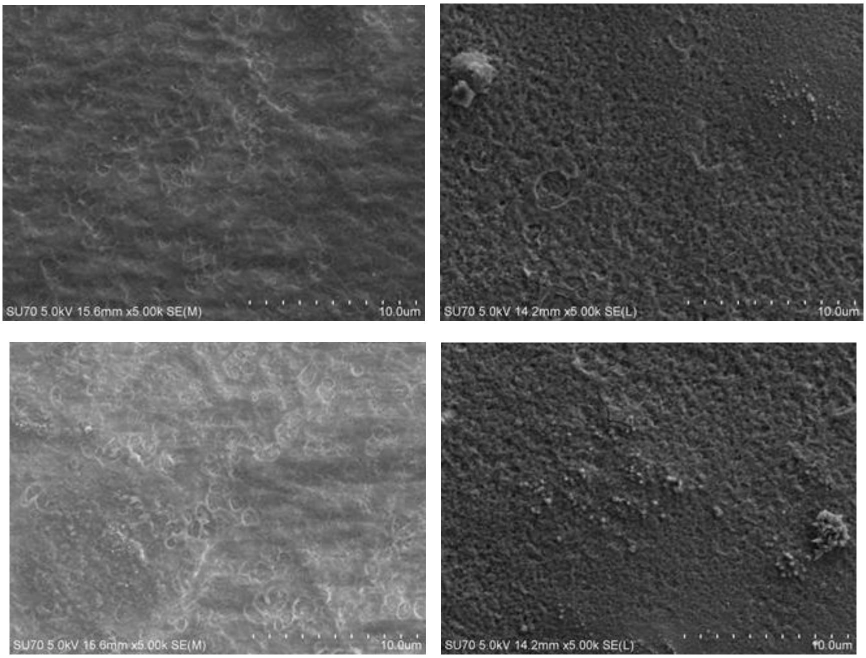

Fig. 26. SEM micrographs of CHAp coatings obtained on Ti without initial pre-heating (bottom) and on initially pre-heated (top): 10 (left) and 30 layers (right).

Obviously, the influence of pre-annealing of the substrate on the morphology of HAp thin films is negligible. However, the formation of a more porous surface with increasing number of layers is evident. On the other hand, the surface morphology of coated Ti substrates with CHAp is quite different in comparison with pure Ti substrate (see Fig. 27 [148]. As seen from Fig. 27, the surface of titanium substrate consisted of the regular shaped crystallites with a size of 3–10 µm. The size of TiO_2 crystallites increases with increasing the duration of annealing.

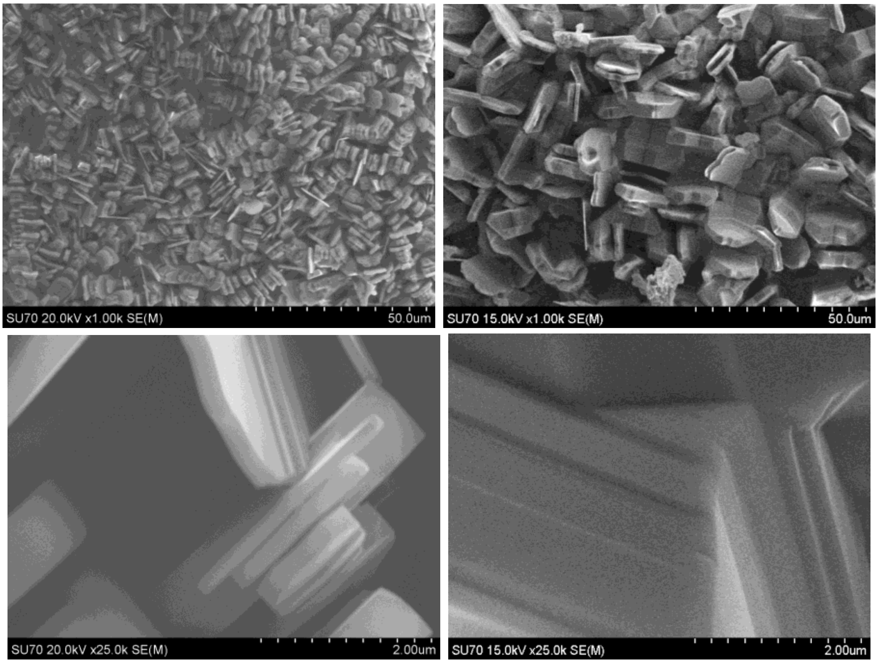

Fig. 27. SEM micrographs of Ti substrates repeatedly heated at 1000 ºC for 5 h with temperature ramp of 1 ºC/min: 5 times (at left) and 15 times (at right) [148].

As mentioned before, the $CaTiO_3$ sublayer was synthesized using calcium acetate and calcium hydroxide, respectively as starting materials on both pre-heated and as-received Ti substrates. The SEM micrographs of the $CaTiO_3$ sublayer and CHAp layer on $CaTiO_3$ sublayer obtained from calcium acetate on heat-treated Ti substrates are shown in Fig. 28. The main morphological features of calcium titanate are quite different compared to HAp.

The $CaTiO_3$ islands 2-3 µm in size composed of spherical nanoparticles have formed on the pre-heated Ti substrate. This type of surface morphology disappeared after dipping this substrate 10 times to the Ca-P-O sol-gel solution. Again, the formation of a porous HAp surface is observed. With increasing number of HAp layers, however, the surface morphology of thin films remains almost unchanged. The SEM micrographs of $CaTiO_3$ sublayer and HAp on $CaTiO_3$ sublayer obtained from calcium hydroxide on just cleaned Ti substrates are shown in Fig. 29. Apparently, after formation of the HAp films the surface became flatter and more porous. The microstructure of fabricated HAp is very similar to that observed for the HAp coating on Ti substrate without initial pre-heating and without additional $CaTiO_3$ sublayer.

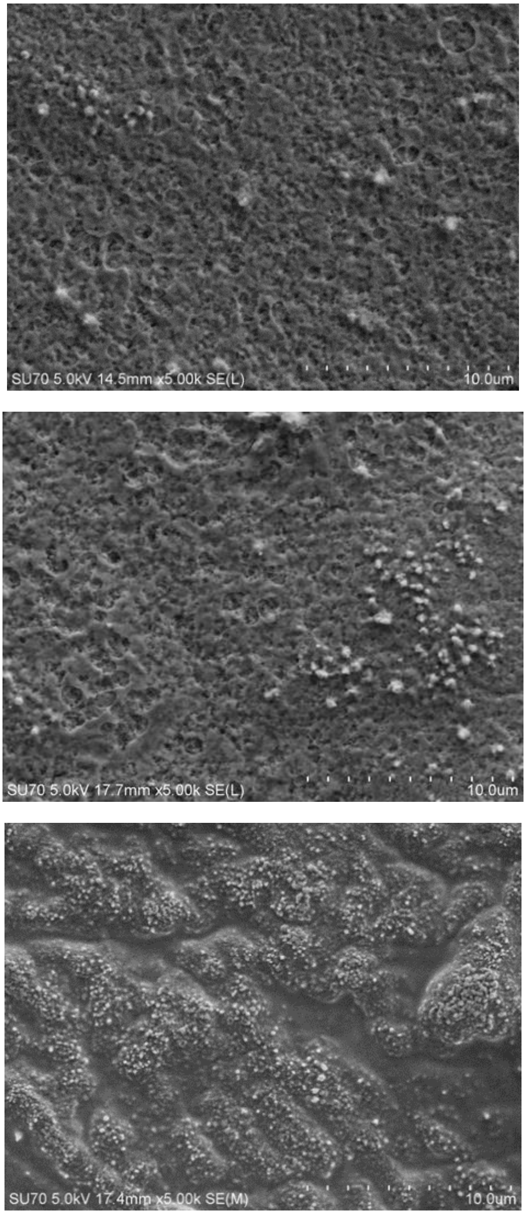

Fig. 28. SEM micrographs of $CaTiO_3$ obtained from calcium acetate on heat-treated Ti substrate (bottom) and CHAp coatings prepared on $CaTiO_3$ sublayer: 10 layers (middle) and 20 layers (top).

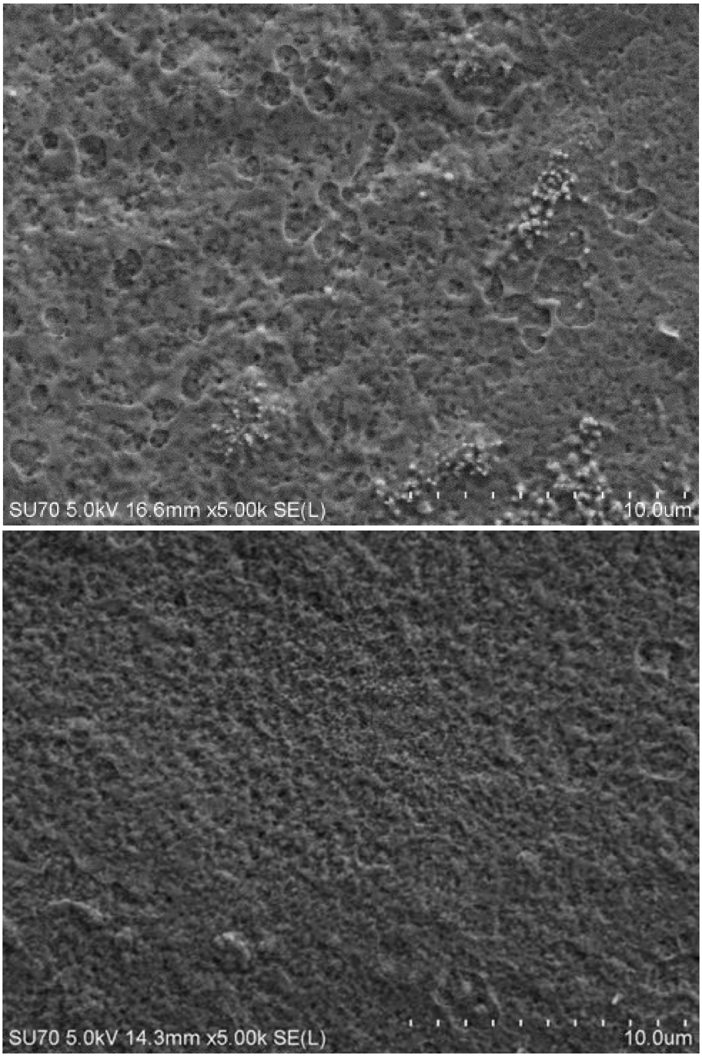

Fig. 29. SEM micrographs of $CaTiO_3$ obtained from calcium hydroxide on Ti substrate without initial pre-heating (top) and 20 layers of CHAp coatings prepared on $CaTiO_3$ sublayer (bottom).

To estimate the wettability of the coatings obtained, contact angle measurements (CAM) were performed. The results of these measurements are summarized in Table 6.

Table 6. Results of contact angle measurements (CA – contact angle).

Number of layers on modified substrate	CA without sublayer	CA with $CaTiO_3$ sublayer from $Ca(Ac)_2$	CA with $CaTiO_3$ sublayer from $Ca(OH)_2$
10	75.96±1.22	62.90±1.88	83.44±0.41
20	76.42±2.54	76.18±5.87	71.57±6.14
30	66.22±8.05	72.50±1.53	80.55±3.84
Number of layers on not modified substrate			
10	68.93±3.17	67.24±0.85	71.96±1.00
20	49.42±0.67	58.53±5.46	51.36±3.15
30	52.07±1.46	53.35±5.59	51.26±2.18

Interestingly, the hydrophobic properties are not dependent on a number of CHAp layers up to 20. The contact angle of dip-coated samples on unheated and pre-heated Ti substrates with and without $CaTiO_3$ sublayers remains around 70 degrees. However, increasing the number of HAp layers to 30, the contact angle decreased monotonically from ~70 down to 49.4-58.5 degrees. This very interesting tendency could be related to the phase composition of the CHAp films [149]. As evident from the XRD patterns, the crystallinity of CHAp also increases significantly after obtaining 30 layers on the substrates. So, the decrease of hydrophobicity is associated with formation of CHAp crystallites with hydrophilic OH groups. The surfaces remained hydrophilic after 30 immersing, withdrawal and annealing steps independent of the Ti surface pre-treatment conditions. The increased hydrophilicity of CHAp-coated Ti enhances a wettability of the coatings. Consequently, such coatings can accelerate osteointegration, i. e. structural and functional connection between living bone and the surface of a load-bearing artificial implant [149].

3.2 Sol-gel processing of calcium hydroxyapatite thin films on silicon nitride (Si_3N_4) substrate

The results of XRD analysis of CHAp coatings are presented in Fig. 30. The XRD patterns of CHAp films on silicon nitride substrate without $CaTiO_3$ sublayer show the formation of CHAp phase already after ten coating procedures. The intensity of diffraction peaks attributable to the CHAp increases with increasing the number of coatings. Evidently, the $CaTiO_3$ sublayer formed on silicon nitride does not promote the formation of CHAp phase.

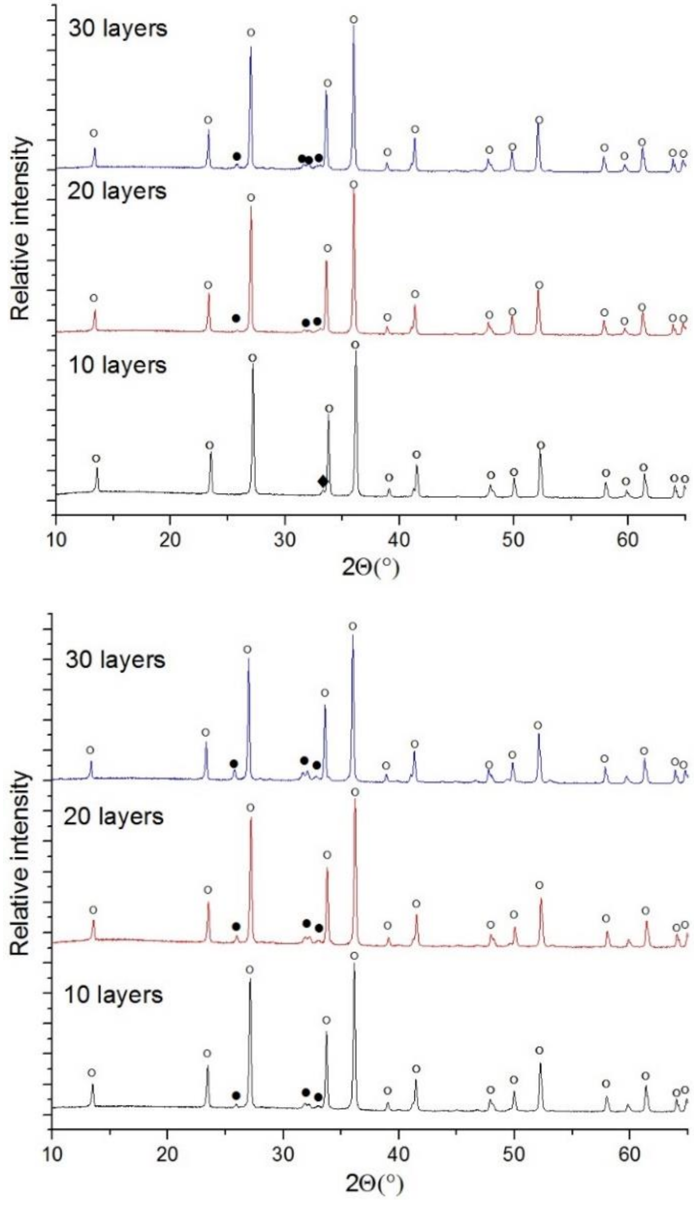

Fig. 30. XRD patterns of CHAp films (top) and CHAp films with sublayer (bottom) on silicon nitride substrate. Diffraction peaks: • - $(Ca_{10}(PO_4)_6(OH)_2$ (PDF: 74-0566); o – Si_3N_4; ♦ - $CaTiO_3$

SEM micrographs of the CHAp coatings are presented in Figs. 31 and 32. Evidently, the morphology of ten layers of CHAp and $CaTiO_3$ on silicon nitride is different.

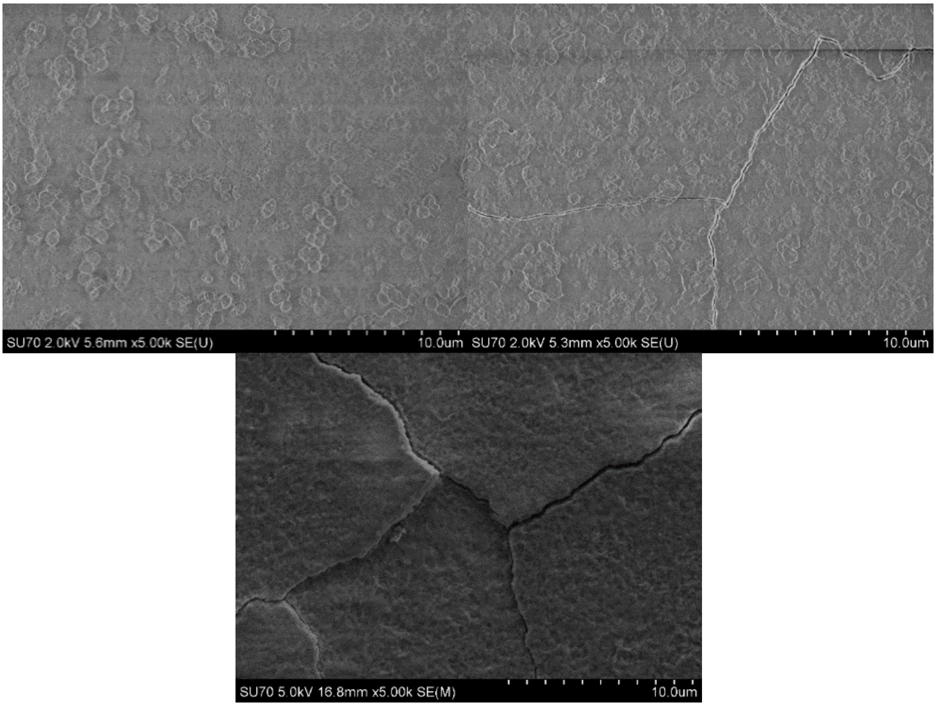

Fig. 31. SEM micrographs of CHAp coatings obtained on silicon nitride: 10 (left), 20 (right) and 30 (bottom) layers

The surface of $CaTiO_3$ sublayer (Fig. 32) totally flat and smooth, whereas the formation of islands of CHAp (Fig. 31) on the surface of substrate is clearly seen. In both cases (without and with sublayer) the surface morphology changes with increasing amount of CHAp layers. The island structure remains for the CHAp sample obtained after 20 coating procedures directly on the silicon nitride substrate. However, the good connectivity between CHAp grains is visible for the sample obtained on the substrate with calcium titanate sublayer. Besides, the cracks on the coatings have formed in both cases. The cracks become more visible for the CHAp coatings obtained after 30 dip-coating cycles. The differences of the surface morphology of thicker coatings disappeared, i.e., are not dependent on the sublayer structure. The both coatings are slightly cracked, having smoother surface without formation of islands.

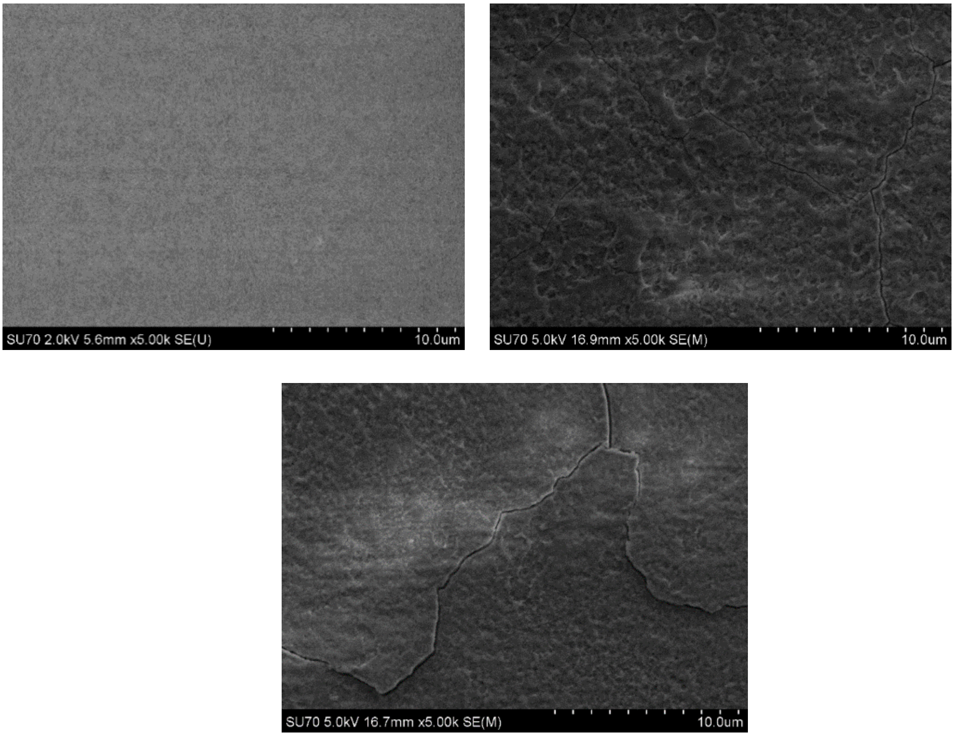

Fig. 32. SEM micrographs of coatings obtained on silicon nitride: 10 layers of sublayer (left), 20 (middle) and 30 layers (right) CHAp on top.

The cracking could have been caused by thermal expansion mismatch between the film and the susbtrate. As the films get more thicker they get more vulnerable to the expansion and contraction. As we left our samples to cool in furnace during procedure, this could potentially be avoided by controlled and slower cooling. The coating thickness determined by SEM for the sample obtained after 30 dip-coating cycles was about 2 μm.

The results obtained by SEM are in a good agreement with those obtained by AFM measurements (Fig. 33).

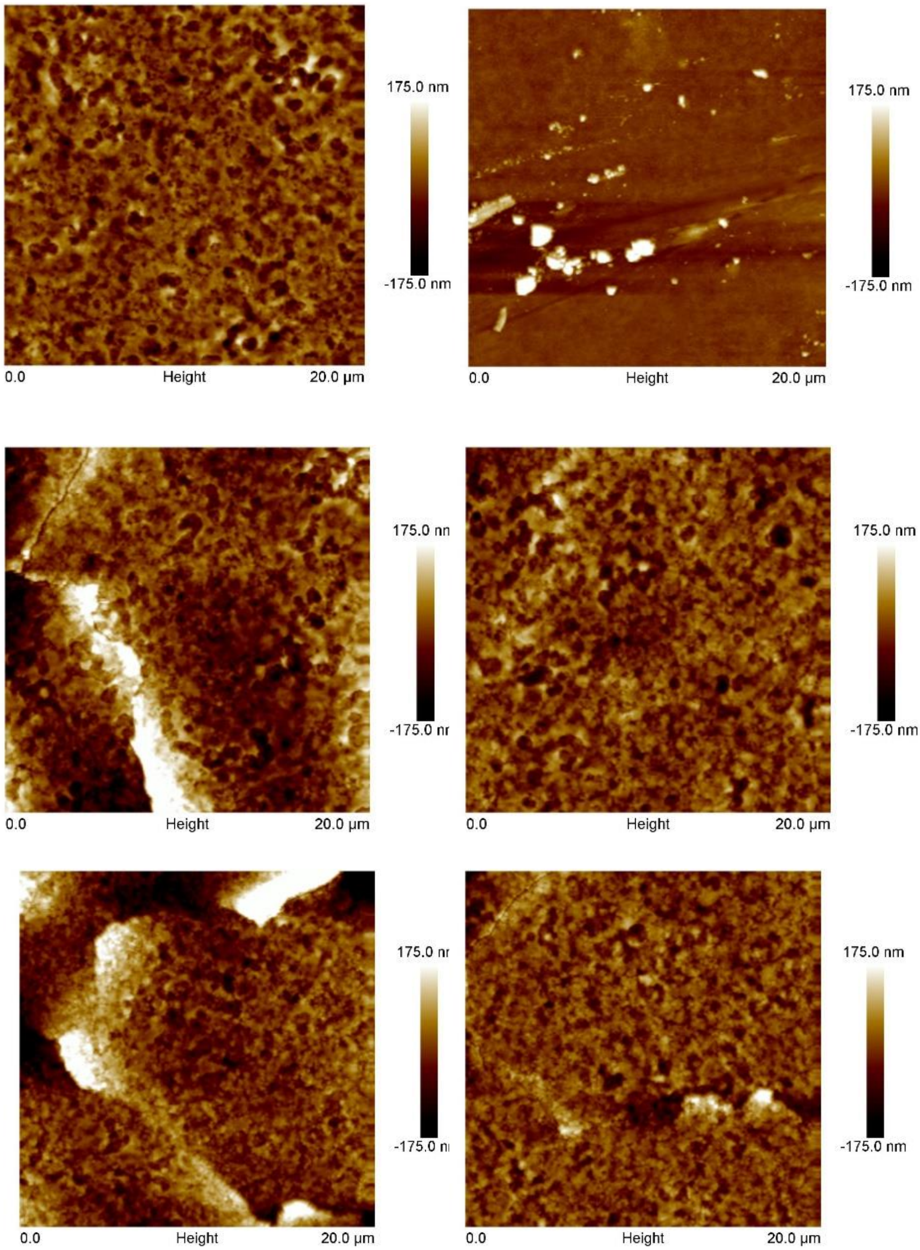

Fig. 33. AFM micrographs of CHAp films (left) and CHAp films with sublayer (right): 10, 20 and 30 layers (accordingly from top to bottom)

The edges of cracks are evident in the AFM images of CHAp coatings obtained after 20 and 30 dip-coating procedures. Moreover, the obtained CHAp coatings are porous. The coatings should be porous for the medical applications since the blood and related human fluids should have a possibility to circulate through the material. However, the pore size is not crucial feature.

Figure 34 shows Raman spectrum of 30-layer coating on Si_3N_4 substrate. The most intense band at 962 cm^{-1} belongs to ν_1 (A_1) symmetric stretching vibration of tetrahedral PO_4^{3-} group [150]–[152]. Peak position of this band indicates that studied compound is stoichiometric hydroxyapatite with molar Ca/P ratio of 1.667 [150], [153]. Lower intensity bands near at 587 and 631 cm^{-1} are associated with triple degenerate (F_2 symmetry) asymmetric bending modes ν_4 of phosphate group [151], [152]. The doubly degenerate (E symmetry) symmetric deformation vibrational modes ν_2 are visible near 432 cm^{-1}. Two bands located at 1045 and 1071 cm^{-1} are assignable to triply degenerate (F_2) asymmetric stretching vibrational mode of phosphate group ν_3 [151], [152]. The low frequency bands (below 350 cm^{-1}) might be associated with translations of Ca^{2+},PO_4^{3-}, and OH^- groups and vibrations of phosphate group [153], [154]. In the high frequency spectral region the relatively broad feature is visible at 3569 cm^{-1}. This band belongs to O–H stretching vibration of hydroxyl group and immediately confirms hydroxylation of the studied sample [153]–[156]. The width of the ν_1 band provides information on the degree of crystallinity of the studied compounds [153], [156]. For this purpose we recorded high resolution Raman spectra by using 632.8 nm excitation wavelength and 2400 lines/mm grating. The width of ν_1 band determined as full width at half maximum (FWHM) was found to be 11.5 cm^{-1}. Similar FWHM values were obtained for 10-layer (11.8 cm^{-1}) and 20-layer (11.7 cm^{-1}) deposited samples on Si_3N_4 substrate. Obtained FWHM values are relatively high comparing with well-ordered crystalline structure of hydroxyapatite (4–7cm^{-1}) [153], [156]. The FWHM value of O−H stretching vibration was also relatively high (70.3 cm^{-1}), comparing with previously reported values for hydroxyapatite (6–12 cm^{-1}) [156]. Thus, presented Raman data indicate that studied samples possess hydroxyapatite molecular structure; although the long range arrangement is relatively disordered with dominant nanocrystalline-like form. Interestingly, during sol–gel preparation of CHAp thin films on silicon substrate, the formation of oxyhydroxyapatite $Ca_{10}(PO_4)_6(OH)_{2-2x}O_x$ instead of CHAp was observed [87]. However, this was not the case during fabrication of CHAp films on silicon nitride substrate.

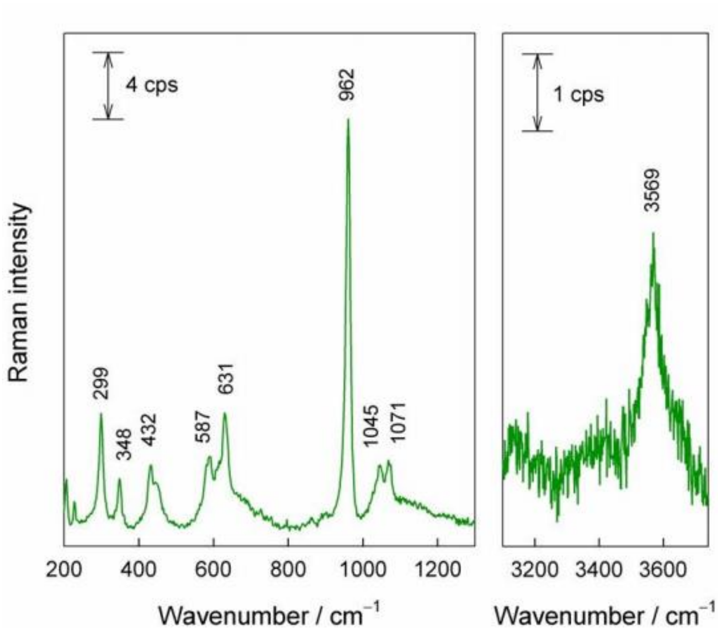

Fig. 34. Raman spectrum of sample containing 30 layers of Ca–P–O gel deposited on Si_3N_4 substrate in 200–1300 and 3100–3700 cm^{-1} spectral regions. Excitation wavelength is 442 nm (0.8 mW)

To estimate wettability of the coatings obtained, the contact angle measurements (CAM) were performed. The results of these measurements are summarized in Table 7.

Table 7. Contact angle results determined for CHAp coatings (n = 3).

Amount of CHAp layers	Without sublayer	$CaTiO_3$ sublayer from $Ca(Ac)_2$
10	97.2±0.1	93.1±3.5
20	100.3±3.5	94.1±0.6
30	93.4±1	92.2±1.3

No significant differences could be observed between the CHAp coatings fabricated without and with $CaTiO_3$ sublayer. The contact angles determined for the synthesized specimens using 10, 20 and 30 immersion and withdrawal procedures were found to be in the range of 92-100°. The obtained results of contact angle measurements show slight correlations between number of layers and contact angle values of CHAp surfaces. However, the contact angle slightly decreases for the CHAp films obtained after 30 coating procedures possibly due to the formation of cracks and higher porosity. As seen, with increasing number of layers up to 20, the hydrophobicity of surfaces increased. Finally, the results presented in this study demonstrated that suggested sol-gel process is perfectly suitable for the synthesis of calcium hydroxyapatite on the silicon nitride substrate allowing to control phase purity and morphological properties of CHAp. The obtained materials could be effectively used as multifunctional delivery systems for biotechnological applications [157], [158].

3.3 Accelerated fabrication of calcium hydroxyapatite thin films on silicon substrate

The XRD results of CHAp coatings obtained by accelerated procedure are presented in Fig. 35. The XRD patterns of CHAp films on silica substrate show the formation of CHAp phase already after 1 coating cycle (5 dips). However, using standard sol-gel procedure calcium hydroxyapatite phase on silicon substrate along with minor amount of tricalcium phosphate could be obtained only after 15 or 30 coating procedures [159].

SEM micrographs of the CHAp coatings are presented in Fig. 36. As seen, a smooth homogenous surface with small grains is obtained after 1 coating cycle. After 3 coating cycles, the surface is rougher, with bigger grains and few cracks. This might be caused by thermal expansion mismatch between the coating and the susbtrate. This more perfect microstructer could be obtained by controlling the cooling procedure. The final sample, obtained after 6 coating cycles contains the biggest grains due to the increased number of annealing procedures. The size of formed spherical particles (~100-200 nm) is independent on the amount of used coating cycles. However, the progressive changes in the surface morphology of CHAp films with increasing the spinning time were observed when standard sol-gel procedure was used for the fabrication of CHAp coatings [159]. Moreover, the silicon substrate was completely coated by calcium hydroxyapatite plate-like crystals or regular polygons with bigger particle size (300-400 nm) was determined from the SEM micrographs (Fig. 37).

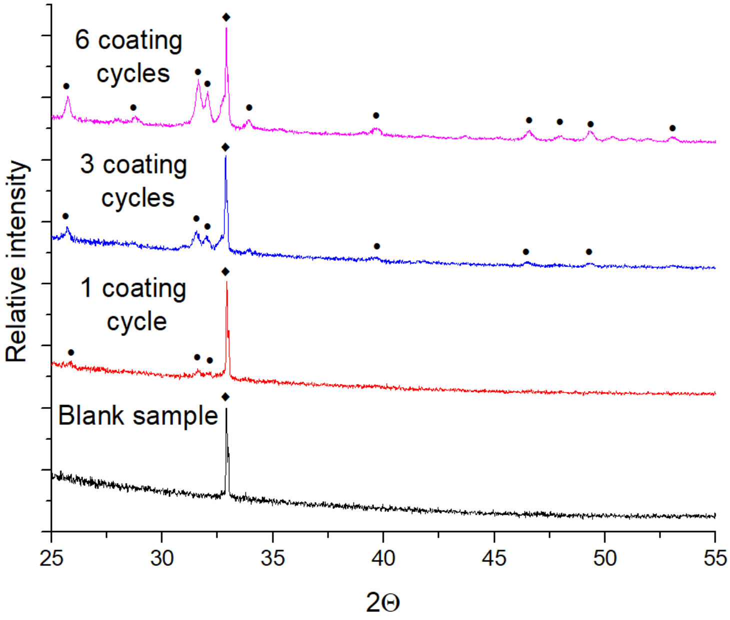

Fig. 35. XRD patterns of CHAp films on silica substrate.
Diffraction peaks: • - ($Ca_{10}(PO_4)_6(OH)_2$ (PDF: 74-0566); ♦ - Si.

The SEM results are in a good agreement with the results of contact angle measurements. After the initial coating, the contact angle increased from 67° (blank sample) to 85°. With the increasing number of coating cycles, the contact angle decreased due to the existance of cracks on the surface and higher porosity. Interestingly, in the sample prepared using standard sol-gel procedure and containing 5 layers of CHAp the contact angle determined was 90.8° [159]. However, again with further increasing number of layers of CHAp, the hydrophobic properties of films decreases or remain very similar. So, the hydrophobic-hydrophilic properties of CHAp coating synthesized on silicon substrate seem to be independent on the used synthesis method.

Fourier transform infrared (FTIR) spectroscopy in transmission mode revealed that free PO_4^{3-} ion belongs to tetrahedral (T_d) symmetry and its vibrational spectrum consists from four modes; Raman-active totally symmetric stretching ν_1 (A_1), Raman-active double degenerate symmetric deformation ν_2 (E), both infrared and Raman-active triply degenerate asymmetric stretching ν_3 (F_2), and both infrared and Raman-active triply

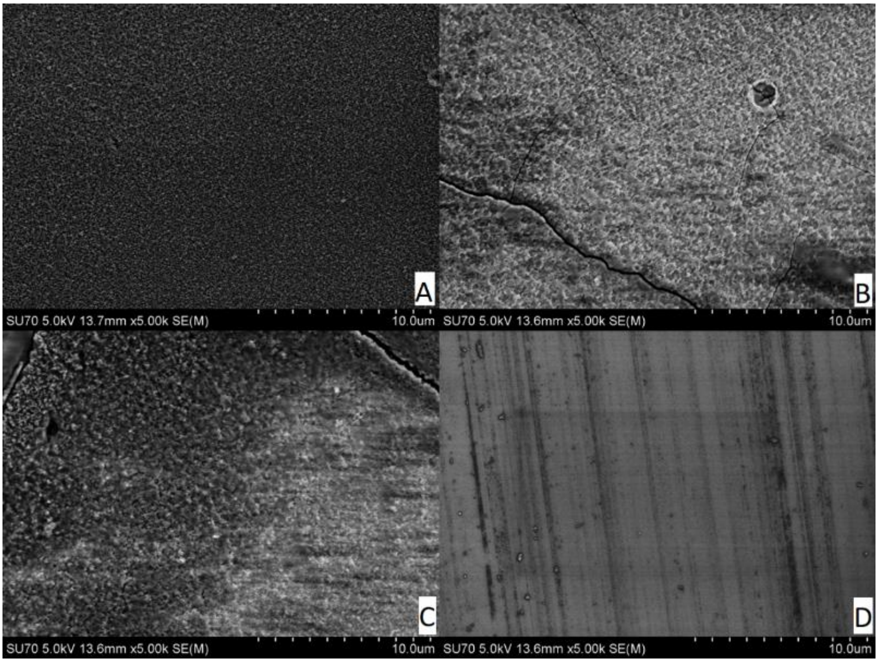

Fig. 36. SEM micrographs of CHAp coatings obtained on silica: 1 (A), 3 (B) 6 (C) coating cycles and blank sample (D).

degenerate asymmetric deformation ν_4 (F_2) vibrational modes [151], [160], [161]. Figure 38 compares FTIR spectra of different CHAp layers on Si substrate. Peak positions and assignments of the bands are listed in Table 8. Peak positions of the PO_4^{3-} coincide well with hydroxyapatite structure [150], [162], [163]. In the high frequency region the sharp band due to O−H stretching vibrations of OH^- ion is visible at 3571 cm^{-1}; thus confirming presence of the hydroxyapatite crystal lattice. The width of ν(OH) band determined as full width at half maximum (FWHM) was found to be 15.5 cm^{-1} for 6 cycles sample. This value is slightly large comparing with previously reported values for crystalline hydroxyapatite (6−12 cm^{-1}) [156]; however, is considerable lower comparing with calcium hydroxyapatite film on Si_3N_4 substrate (70.3 cm^{-1}).

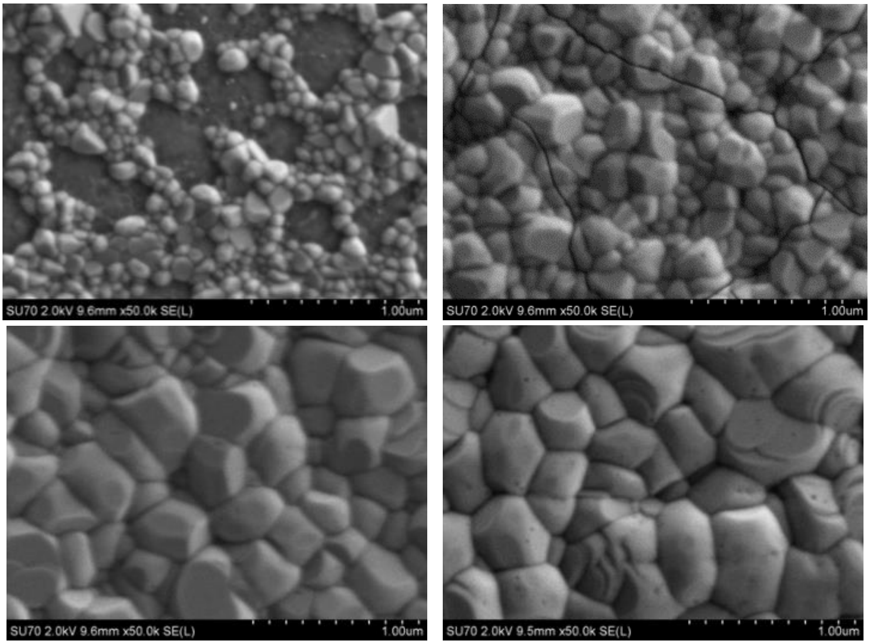

Fig. 37. SEM micrographs of CHAp coatings containing 1 layer (top, left), 5 layers (top, right), 15 layers (bottom, left) and 30 layers (bottom, right) of Ca-P-O gels and calcined at 1000 °C after each spin-coating procedure [159].

The relative amount of carbonate ions was evaluated by analysis of integrated intensity ratios $A(CO_3^{2-})/A(PO_4^{3-})$ (Table 8). One can see that relative amount of carbonate slightly increases with decreasing number of deposited layers. The relative amount of hydroxyl ion remains similar for all studied samples. Importantly, the hydroxyapatite structure is preserved even for very thin (1 cycle – 5 dips) coating on Si, as clearly visible from the presence of ν(OH) peak near 3570 cm^{-1} (Figure 38).

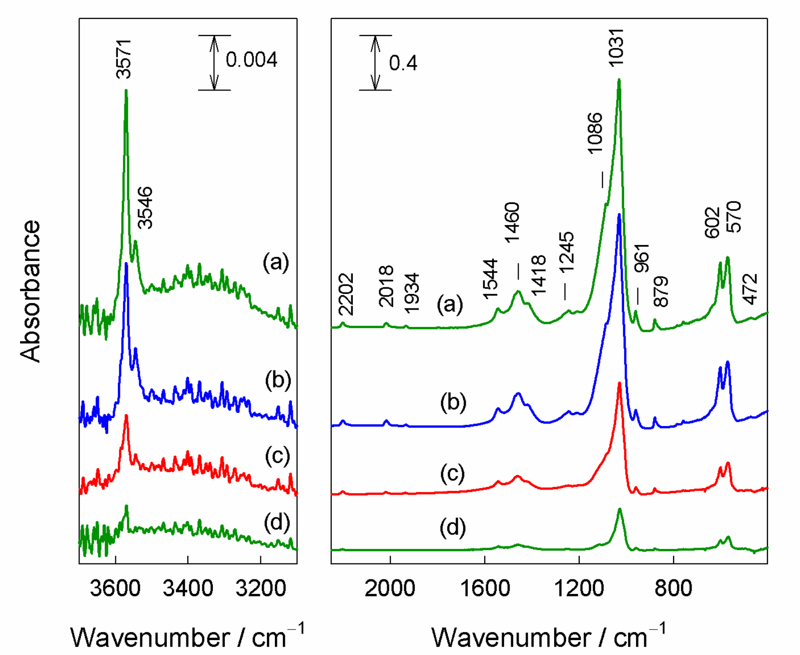

Fig. 38. FTIR absorbance spectra of annealed (650 °C, 5h) CHAp films on Si substrate: (a) 6 cycles, (b) 5 cycles; (c) 3 cycles, and (d) 1 cycle.

Table 8. Infrared wavenumbers [cm^{-1}] of CHAp films on Si substrate.

Mode, molecular group	6 cycles	5 cycles	3 cycles	1 cycle	Mode, molecular group
ν_1 (A_1), PO_4^{3-}	961.3 m	961.2 m	959.8 m	958.8 m	961.3 m
ν_2 (E), PO_4^{3-}	473 vw	473 vw	n.o.	n.o.	473 vw
ν_3 (F_2), PO_4^{3-}	1031.2 vs 1086 sh	1030.6 vs 1085 sh	1029.0 vs 1084 sh	1028.1 vs n.o.	1031.2 vs 1086 sh
ν_4 (F_2), PO_4^{3-}	570.4 s 601.8 s	570.8 s 602.2 s	569.2 s 601.1 s	567.8 s 600.6 s	570.4 s 601.8 s
$\nu_{as}(CO_3)$, CO_3^{2-}	1418 m, sh 1459.8 m 1544.3 m	1419 m, sh 1460.4 m 1543.9 m	1422 m, sh 1460.3 m 1543.1 m	1420 m, sh 1459.0 m 1541.1 m	1418 m, sh 1459.8 m 1544.3 m
$\gamma(CO_3)$, CO_3^{2-}	879.4 m	879.4 m	879.6 m	879.5 m	879.4 m

Mode, molecular group	6 cycles	5 cycles	3 cycles	1 cycle	Mode, molecular group
overtones/ combination modes, PO_4^{3-}, HPO_4^{2-}	1933.9 w 2017.5 w 2202.2 w	1934.2 w 2017.0 w 2202.0 w	1935.9 w 2018.2 w 2202.7 w	1936.7 w 2017.0 m 2202.3 m	1933.9 w 2017.5 w 2202.2 w
ν(OH) OH^-	3545.6 vw 3570.8 w	3545.1 vw 3570.4 w	3544.7 vw 3570.3 w	n.o. 3570.0 w	3545.6 vw 3570.8 w
ν_1 (A_1), PO_4^{3-}	961.3 m	961.2 m	959.8 m	958.8 m	961.3 m

Abbreviations: n.o. – not observed; ν – stretching; ν_{as} – asymmetric stretching; γ – out of plane deformation; vs – very strong; s – strong; m – middle; w – weak; vw – very weak; sh –shoulder.

CONCLUSIONS

1. Calcium hydroxyapatite ($Ca_{10}(PO_4)_6(OH)_2$; CHAp) coatings on Ti substrate were fabricated for the first time by modifying its surface by a calcium titanate sublayer and/or pre-heating the substrate at elevated temperatures before the coating procedure. The results of TG analysis of synthesized Ca-Ti-O precursor gels obtained using calcium acetate and calcium hydroxide as starting material were almost identical. The main decomposition of the Ca-P-O precursor gel with the mass loss of about 65% was observed up to 650 °C, similarly to the Ca-Ti-O gel.

2. It was determined that the intensity of reflections attributable to the CHAp phase in the XRD patterns of fabricated films increased with increasing number of coating layers. The formation of TiO_2 phase which reduces adhesion of CHAp films was arrested by initial pre-heating of the substrate at 650 °C for 5 h in air. Besides, the intensity of reflections attributable to TiO_2 remained unchanged with increasing the number of CHAp coatings on the heat-treated Ti substrates with $CaTiO_3$ sublayer.

3. It was also demonstrated that surface modification of Ti substrate did not have any influence on the morphology of the CHAp thin films. However, the formation of more porous surface with increasing amount of layers was evident. Contact angle measurements showed that with increasing the number of CHAp layers from 20 up to 30, the contact angle decreased monotonically from ~70 to 49.4-58.5 ^{o} indicating the formation of high quality of hydrophilic CHAp coatings.

4. Calcium hydroxyapatite coatings were fabricated from Ca–P–O sol–gel solution for the first time to the best our knowledge on silicon nitride (Si_3N_4) substrate. For comparison, the CHAp films were dip-coated also on a silicon nitride substrate modified with calcium titanate sublayer. From XRD results were observed that formation of CHAp as single phase occurs after annealing of coatings with or without calcium titanate sublayer in air atmosphere at 650 °C for 5 h. However, the amount of deposited CHAp was found to be lower in the presence of $CaTiO_3$ sublayer.

5. According to SEM micrographs and AFM images, it was found that the morphological features of CHAp coatings were dependent on number of layers of the end product. The formation of islands was observed for the CHAp sample obtained after 20 coating procedures directly on the silicon nitride substrate. However, the good connectivity between CHAp grains was determined for the sample obtained on the substrate with calcium titanate sublayer. The both CHAp coatings obtained after 30 dip-coating cycles were slightly cracked and porous, having smoother surface without formation of islands.

6. The Raman spectroscopy data indicated that studied coatings on Si_3N_4 substrate possess hydroxyapatite molecular structure and no formation of oxyhydroxyapatite $Ca_{10}(PO_4)_6\ (OH)_{2-2x}O_x$ on silicon nitride was observed. The contact angles determined for the synthesized specimens using 10, 20, and 30 immersion and withdrawal procedures were found to be in the range of 92–100° showing low level of hydrophobicity.

7. Calcium hydroxyapatite thin layers were fabricated from Ca-P-O sol-gel solution on silica (Si) substrate using improved dip-coating method. This suggested technique allowed to achieve desired results 4 times faster in comparison with previously suggested processing.

8. XRD results confirmed the formation of CHAp as single phase after annealing of coatings in air atmosphere at 650 °C for 5 h. SEM micrographs of the CHAp surfaces revealed the formation of smooth and homogenous coatings with small grains. The size of formed spherical particles (~100-200 nm) was independent on the amount of used coating cycles.

9. The spectroscopic data also indicated the presence of ordered crystalline structure of hydroxyapatite film. The SEM results were in a good agreement with the results of contact angle measurements. After the initial coating, the contact angle increased from 67° (blank sample) to 85°. With the increasing number of coating cycles, the contact angle decreased due to the existance of cracks on the surface and higher porosity.

REFERENCE LIST

[1] S. Wu, X. Liu, K. W. K. Yeung, C. Liu, and X. Yang, "Biomimetic porous scaffolds for bone tissue engineering," *Mater. Sci. Eng. R Reports*, vol. 80, no. 1, pp. 1–36, 2014.

[2] S. R. Paital and N. B. Dahotre, "Calcium phosphate coatings for bio-implant applications: Materials, performance factors, and methodologies," *Mater. Sci. Eng. R Reports*, vol. 66, no. 1–3, pp. 1–70, 2009.

[3] J. V Rau *et al.*, "Fe-doped hydroxyapatite coatings for orthopedic and dental implant applications," *Appl. Surf. Sci.*, vol. 307, pp. 301–305, 2014.

[4] D. M. Liu, T. Troczynski, and W. J. Tseng, "Water-based sol-gel synthesis of hydroxyapatite: Process development," *Biomaterials*, vol. 22, no. 13, pp. 1721–1730, 2001.

[5] E. Milella, "Preparation and characterisation of titania/hydroxyapatite composite coatings obtained by sol–gel process," *Biomaterials*, vol. 22, no. 11, pp. 1425–1431, 2001.

[6] T. S. Y. Fujishiro, N. Sato, S. Uchida, "Coating of Catio3 on Ti Substrates By Hydrothermal Reactions," *Journal of materials science: Materials in medicine*, vol. 9. pp. 363–367, 1998.

[7] B. Mavis and A. C. Taş, "Dip Coating of Calcium Hydroxyapatite on Ti-6Al-4V Substrates," *J. Am. Ceram. Soc.*, vol. 83, no. 4, pp. 989–991, 2004.

[8] C. M. Xie *et al.*, "Silver nanoparticles and growth factors incorporated hydroxyapatite coatings on metallic implant surfaces for enhancement of osteoinductivity and antibacterial properties," *ACS Appl. Mater. Interfaces*, vol. 6, no. 11, pp. 8580–8589, 2014.

[9] A. Belcarz *et al.*, "Covalent coating of hydroxyapatite by keratin stabilizes gentamicin release," *J. Biomed. Mater. Res. - Part B Appl. Biomater.*, vol. 89, no. 1, pp. 102–113, 2009.

[10] G. A. Fielding, M. Roy, A. Bandyopadhyay, and S. Bose, "Antibacterial and biological characteristics of silver containing and strontium doped plasma sprayed hydroxyapatite coatings," *Acta Biomater.*, vol. 8, no. 8, pp. 3144–3152, 2012.

[11] L. Sun, C. C. Berndt, K. a Gross, and A. Kucuk, "Material Fundamentals and Clinical Performance of Plasma- Sprayed Hydroxyapatite Coatings : A Review," *J. Biomed. Mater. Res.*, vol. 58, no. 5, pp. 570–592, 2001.

[12] O. Geuli, N. Metoki, N. Eliaz, and D. Mandler, "Electrochemically Driven Hydroxyapatite Nanoparticles Coating of Medical Implants," *Adv. Funct. Mater.*, vol. 26, no. 44, pp. 8003–8010, 2016.

[13] A. Arifin, A. Bakar, N. Muhamad, J. Syarif, and M. Ikram, “Material processing of hydroxyapatite and titanium alloy (HA / Ti) composite as implant materials using powder metallurgy : A review,” *J. Mater.*, vol. 55, pp. 165–175, 2014.
[14] A. Barbas, A. Bonnet, P. Lipinski, R. Pesci, and G. Dubois, “Development and mechanical characterization of porous titanium bone substitutes,” *J. Mech. Behav. Biomed. Mater.*, vol. 9, pp. 34–44, 2012.
[15] M. Catauro, F. Bollino, F. Papale, C. Ferrara, and P. Mustarelli, “Silica – polyethylene glycol hybrids synthesized by sol – gel : Biocompatibility improvement of titanium implants by coating,” *Mater. Sci. Eng. C*, vol. 55, pp. 118–125, 2015.
[16] E. Fournier, R. Devaney, M. Palmer, J. Kramer, R. El Khaja, and M. Fonte, “Superelastic Orthopedic Implant Coatings,” pp. 0–6, 2014.
[17] N. Eliaz, T. M. Sridhar, U. Kamachi Mudali, and B. Raj, “Electrochemical and electrophoretic deposition of hydroxyapatite for orthopaedic applications,” *Surf. Eng.*, vol. 21, no. 3, pp. 238–242, 2005.
[18] P. Usinskas, Z. Stankeviciute, A. Beganskiene, and A. Kareiva, “Sol-gel derived porous and hydrophilic calcium hydroxyapatite coating on modified titanium substrate,” *Surf. Coat. Technol.*, 2016.
[19] K. Balani, Y. Chen, S. P. Harimkar, and N. B. Dahotre, “Tribological behavior of plasma-sprayed carbon nanotube-reinforced hydroxyapatite coating in physiological solution,” vol. 3, pp. 944–951, 2007.
[20] W. Xu, W. Hu, M. Li, and C. Wen, “Sol–gel derived hydroxyapatite/titania biocoatings on titanium substrate,” *Mater. Lett.*, vol. 60, no. 13, pp. 1575–1578, 2006.
[21] Y. H. Joung, “Development of implantable medical devices: From an engineering perspective,” *Int. Neurourol. J.*, vol. 17, no. 3, pp. 98–106, 2013.
[22] N. Huebsch and D. J. Mooney, “Inspiration and application in the evolution of biomaterials,” vol. 462, no. November, 2009.
[23] C. M. Abraham, “A Brief Historical Perspective on Dental Implants , Their Surface Coatings and Treatments,” pp. 50–55, 2014.
[24] U. Tariq, Z. Haider, R. Hussain, and K. Tufail, “measurements LIBS Analysis of Hydroxyapatite Extracted from Bovine Bone for Ca / P Ratio Measurements,” vol. 030027, 2017.
[25] S. G. Ghalme, A. Mankar, and Y. Bhalerao, “Biomaterials in Hip Joint Replacement,” vol. 4, no. 2, pp. 113–125, 2016.
[26] E. Milella, F. Cosentino, A. Licciulli, and C. Massaro, “Preparation and characterisation of titania/hydroxyapatite composite coatings obtained by sol-gel process,” *Biomaterials*, vol. 22, no. 11, pp. 1425–1431, 2001.

[27] P. A. Ramires, A. Romito, F. Cosentino, and E. Milella, “The influence of titania/hydroxyapatite composite coatings on in vitro osteoblasts behaviour,” *Biomaterials*, vol. 22, no. 12, pp. 1467–1474, 2001.
[28] S. Wu, X. Liu, K. W. K. Yeung, C. Liu, and X. Yang, “Biomimetic porous scaffolds for bone tissue engineering,” *Mater. Sci. Eng. R Reports*, vol. 80, no. 1, pp. 1–36, 2014.
[29] A. Arifin, A. B. Sulong, N. Muhamad, J. Syarif, and M. I. Ramli, “Material processing of hydroxyapatite and titanium alloy (HA/Ti) composite as implant materials using powder metallurgy: A review,” *Mater. Des.*, vol. 55, pp. 165–175, 2014.
[30] S. Dorozhkin, “Calcium Orthophosphate-Containing Biocomposites and Hybrid Biomaterials for Biomedical Applications,” *J. Funct. Biomater.*, vol. 6, no. 3, pp. 708–832, 2015.
[31] M. Pettersson *et al.*, “Surface & Coatings Technology Structure and composition of silicon nitride and silicon carbon nitride coatings for joint replacements,” *Surf. Coat. Technol.*, vol. 235, pp. 827–834, 2013.
[32] W. E. Garrett, M. F. Swiontkowski, J. N. Weinstein, J. Callaghan, R. N. Rosier, and J. Daniel, “American Board of Orthopaedic,” 2006.
[33] B. S. Bal and M. N. Rahaman, “Orthopedic applications of silicon nitride ceramics,” *Acta Biomater.*, vol. 8, no. 8, pp. 2889–2898, 2012.
[34] M. Geetha, A. K. Singh, R. Asokamani, and A. K. Gogia, “Ti based biomaterials , the ultimate choice for orthopaedic implants – A review,” *Prog. Mater. Sci.*, vol. 54, no. 3, pp. 397–425, 2009.
[35] M. Mittal, S. K. Nath, and S. Prakash, “Improvement in mechanical properties of plasma sprayed hydroxyapatite coatings by Al2O3 reinforcement,” *Mater. Sci. Eng. C*, vol. 33, no. 5, pp. 2838–2845, 2013.
[36] K. De Groot, R. Geesink, C. P. A. T. Klein, and P. Serekian, “Plasma sprayed coatings of hydroxylapatite,” *J. Biomed. Mater. Res.*, vol. 21, no. 12, pp. 1375–1381, Dec. 1987.
[37] N. Eliaz and N. Metoki, “Calcium phosphate bioceramics: A review of their history, structure, properties, coating technologies and biomedical applications,” *Materials (Basel).*, vol. 10, no. 4, 2017.
[38] S. Barkarmo *et al.*, “Nano-hydroxyapatite-coated PEEK implants: A pilot study in rabbit bone,” *J. Biomed. Mater. Res. - Part A*, vol. 101 A, no. 2, pp. 465–471, 2013.
[39] S. fang Zhao, Q. hong Jiang, S. Peel, X. xiang Wang, and F. ming He, “Effects of magnesium-substituted nanohydroxyapatite coating on implant osseointegration,” *Clin. Oral Implants Res.*, vol. 24, no. A100, pp. 34–41, 2013.

[40] R. I. M. Asri, W. S. W. Harun, M. A. Hassan, S. A. C. Ghani, and Z. Buyong, “A review of hydroxyapatite-based coating techniques: Sol-gel and electrochemical depositions on biocompatible metals,” *J. Mech. Behav. Biomed. Mater.*, vol. 57, pp. 95–108, 2016.
[41] W. Xu, W. Hu, and M. Li, “Sol – gel derived hydroxyapatite / titania biocoatings on titanium substrate,” vol. 60, pp. 1575–1578, 2006.
[42] H. W. Kim, Y. H. Koh, L. H. Li, S. Lee, and H. E. Kim, “Hydroxyapatite coating on titanium substrate with titania buffer layer processed by sol-gel method,” *Biomaterials*, vol. 25, no. 13, pp. 2533–2538, 2004.
[43] S. Shadanbaz and G. J. Dias, “Calcium phosphate coatings on magnesium alloys for biomedical applications: A review,” *Acta Biomater.*, vol. 8, no. 1, pp. 20–30, 2012.
[44] T. J. Webster, A. A. Patel, M. N. Rahaman, and B. Sonny Bal, “Anti-infective and osteointegration properties of silicon nitride, poly(ether ether ketone), and titanium implants,” *Acta Biomater.*, vol. 8, no. 12, pp. 4447–4454, 2012.
[45] J. M. Toth, M. Wang, B. T. Estes, J. L. Scifert, H. B. Seim, and A. S. Turner, “Polyetheretherketone as a biomaterial for spinal applications,” *Biomaterials*, vol. 27, no. 3, pp. 324–334, 2006.
[46] D. L. P. Macuvele *et al.*, “Advances in ultra high molecular weight polyethylene/hydroxyapatite composites for biomedical applications: A brief review,” *Mater. Sci. Eng. C*, vol. 76, pp. 1248–1262, 2017.
[47] D. Firouzi *et al.*, “A new technique to improve the mechanical and biological performance of ultra high molecular weight polyethylene using a nylon coating,” *J. Mech. Behav. Biomed. Mater.*, vol. 32, pp. 198–209, 2014.
[48] R. B. Heimann, “Surface & Coatings Technology Structure , properties , and biomedical performance of osteoconductive bioceramic coatings,” *Surf. Coat. Technol.*, vol. 233, pp. 27–38, 2013.
[49] S. V. Dorozhkin, “Calcium orthophosphates in dentistry,” *J. Mater. Sci. Mater. Med.*, vol. 24, no. 6, pp. 1335–1363, 2013.
[50] G. Tripathi, Y. Sugiura, A. Kareiva, E. Garskaite, K. Tsuru, and K. Ishikawa, “Feasibility evaluation of low-crystallinity β-tricalcium phosphate blocks as a bone substitute fabricated by a dissolution–precipitation reaction from α-tricalcium phosphate blocks,” *Journal of Biomaterials Applications*, vol. 33, no. 2. pp. 259–270, 2018.
[51] W. Gotz and S. Papageorgiou, “Molecular, Cellular and Pharmaceutical Aspects of Synthetic Hydroxyapatite Bone Substitutes for

Oral and Maxillofacial Grafting," *Curr. Pharm. Biotechnol.*, vol. 18, no. 1, pp. 95–106, 2016.
[52] K. Kudoh *et al.*, "Maxillary Sinus Floor Augmentation Using Low-Crystalline Carbonate Apatite Granules With Simultaneous Implant Installation: First-in-Human Clinical Trial," *J. Oral Maxillofac. Surg.*, vol. 77, no. 5, p. 985.e1-985.e11, 2019.
[53] S. V. Dorozhkin, "Nanodimensional and nanocrystalline apatites and other calcium orthophosphates in biomedical engineering, biology and medicine," *Materials (Basel).*, vol. 2, no. 4, pp. 1975–2045, 2009.
[54] A. M. Yousefi, H. Oudadesse, R. Akbarzadeh, E. Wers, and A. Lucas-Girot, "Physical and biological characteristics of nanohydroxyapatite and bioactive glasses used for bone tissue engineering," *Nanotechnol. Rev.*, vol. 3, no. 6, pp. 527–552, 2014.
[55] A. J. Salinas and M. Vallet-Regí, "Bioactive ceramics: from bone grafts to tissue engineering," *RSC Adv.*, vol. 3, no. 28, p. 11116, 2013.
[56] L. C. Gerhardt and A. R. Boccaccini, "Bioactive glass and glass-ceramic scaffolds for bone tissue engineering," *Materials (Basel).*, vol. 3, no. 7, pp. 3867–3910, 2010.
[57] G. Kaur, O. P. Pandey, K. Singh, D. Homa, B. Scott, and G. Pickrell, "A review of bioactive glasses: Their structure, properties, fabrication and apatite formation," *J. Biomed. Mater. Res. - Part A*, vol. 102, no. 1, pp. 254–274, 2014.
[58] J. Diao *et al.*, "3D-Plotted Beta-Tricalcium Phosphate Scaffolds with Smaller Pore Sizes Improve In Vivo Bone Regeneration and Biomechanical Properties in a Critical-Sized Calvarial Defect Rat Model," *Adv. Healthc. Mater.*, vol. 7, no. 17, pp. 1–9, 2018.
[59] M. Seyedmajidi, S. Haghanifar, K. Hajian-Tilaki, and S. Seyedmajidi, "Histopathological, histomorphometrical, and radiological evaluations of hydroxyapatite/bioactive glass and fluorapatite/bioactive glass nanocomposite foams as cell scaffolds in rat tibia: an in vivo study," *Biomed. Mater.*, vol. 13, no. 2, p. 025015, Jan. 2018.
[60] M. Li *et al.*, "An overview of graphene-based hydroxyapatite composites for orthopedic applications," *Bioact. Mater.*, vol. 3, no. 1, pp. 1–18, 2018.
[61] M. Furkó, K. Balázsi, and C. Balázsi, "Comparative study on preparation and characterization of bioactive coatings for biomedical applications - A review on recent patents and literature," *Rev. Adv. Mater. Sci.*, vol. 48, no. 1, pp. 25–51, 2017.

[62] Y. Weng *et al.*, “A promising orthopedic implant material with enhanced osteogenic and antibacterial activity: Al 2 O 3 -coated aluminum alloy,” *Appl. Surf. Sci.*, vol. 457, pp. 1025–1034, 2018.
[63] B. M. Hidalgo-Robatto *et al.*, “Fluor‑carbonated hydroxyapatite coatings by pulsed laser deposition to promote cell viability and antibacterial properties,” *Surf. Coatings Technol.*, vol. 349, pp. 736–744, Sep. 2018.
[64] G. Graziani, M. Boi, and M. Bianchi, “A review on ionic substitutions in hydroxyapatite thin films: Towards complete biomimetism,” *Coatings*, vol. 8, no. 8, 2018.
[65] A. Madhan Kumar *et al.*, “PEDOT/FHA nanocomposite coatings on newly developed Ti-Nb-Zr implants: Biocompatibility and surface protection against corrosion and bacterial infections,” *Mater. Sci. Eng. C*, vol. 98, no. December 2018, pp. 482–495, 2019.
[66] P. Phatai, C. M. Futalan, S. Utara, P. Khemthong, and S. Kamonwannasit, “Structural characterization of cerium-doped hydroxyapatite nanoparticles synthesized by an ultrasonic-assisted sol-gel technique,” *Results Phys.*, vol. 10, no. August, pp. 956–963, 2018.
[67] C. C. Negrila, M. V. Predoi, S. L. Iconaru, and D. Predoi, “Development of zinc-doped hydroxyapatite by sol-gel method for medical applications,” *Molecules*, vol. 23, no. 11, pp. 1–15, 2018.
[68] O. Kaygili, S. Keser, N. Bulut, and T. Ates, “Characterization of Mg-containing hydroxyapatites synthesized by combustion method,” *Phys. B Condens. Matter*, vol. 537, no. 3, pp. 63–67, 2018.
[69] S. Lakshmanaperumal and C. Mahendran, “Structural, dielectric, cytocompatibility, and in vitro bioactivity studies of yttrium and strontium co-substituted nano-hydroxyapatite by sol–gel method,” *J. Sol-Gel Sci. Technol.*, vol. 88, no. 2, pp. 296–308, 2018.
[70] L. Sundarabharathi, M. Chinnaswamy, D. Ponnamma, H. Parangusan, and M. A. A. Al-Maadeed, “Investigation of antimicrobial properties and in-vitro bioactivity of Ce3+-Sr2+dual-substituted nano hydroxyapatites,” *J. Am. Ceram. Soc.*, vol. 102, no. 1, pp. 144–157, 2019.
[71] S. Basu, A. Ghosh, A. Barui, and B. Basu, “Epithelial cell functionality on electroconductive Fe/Sr co-doped biphasic calcium phosphate,” *J. Biomater. Appl.*, vol. 33, no. 8, pp. 1035–1052, 2019.
[72] R. G. Tilkin, J. G. Mahy, N. Régibeau, C. Grandfils, and S. D. Lambert, “Optimization of Synthesis Parameters for the Production of Biphasic Calcium Phosphate Ceramics via Wet Precipitation and Sol-Gel Process,” *ChemistrySelect*, vol. 4, no. 21, pp. 6634–6641, 2019.

[73] N. A. Nawawi, I. Sopyan, S. Ramesh, and Afzeri, "Phase behaviour of manganese-doped biphasic calcium phosphate ceramics synthesized via sol-gel method," *Asia-Pacific J. Chem. Eng.*, vol. 6, no. 6, pp. 823–831, Nov. 2011.
[74] M. S. Bahniuk, H. Pirayesh, H. D. Singh, J. A. Nychka, and L. D. Unsworth, "Bioactive glass 45S5 powders: Effect of synthesis route and resultant surface chemistry and crystallinity on protein adsorption from human plasma," *Biointerphases*, vol. 7, no. 1–4, pp. 1–15, 2012.
[75] F. Foroutan, J. V. Jokerst, S. S. Gambhir, O. Vermesh, H. W. Kim, and J. C. Knowles, "Sol-gel synthesis and electrospraying of biodegradable (P2O5)55-(CaO)30-(Na2O)15glass nanospheres as a transient contrast agent for ultrasound stem cell imaging," *ACS Nano*, vol. 9, no. 2, pp. 1868–1877, 2015.
[76] K. Kaur *et al.*, "Magnesium and silver doped CaO–Na2O–SiO2–P2O5 bioceramic nanoparticles as implant materials," *Ceram. Int.*, vol. 42, no. 11, pp. 12651–12662, 2016.
[77] N. S. Dessou *et al.*, "Influence of strontium for calcium substitution on the glass–ceramic network and biomimetic behavior in the ternary system SiO2–CaO–MgO," *J. Mater. Sci.*, vol. 52, no. 15, pp. 8871–8885, 2017.
[78] W. Wang and K. W. K. Yeung, "Bone grafts and biomaterials substitutes for bone defect repair: A review," *Bioact. Mater.*, vol. 2, no. 4, pp. 224–247, 2017.
[79] A. M. F. S. Mohamed, "An overview of bone cells and their regulating factors of differentiation," *Malaysian J. Med. Sci.*, vol. 15, no. 1, pp. 4–12, 2008.
[80] S. Zhao, W. Dong, Q. Jiang, F. He, X. Wang, and G. Yang, "Effects of zinc-substituted nano-hydroxyapatite coatings on bone integration with implant surfaces," *J. Zhejiang Univ. Sci. B*, vol. 14, no. 6, pp. 518–525, 2013.
[81] S. V. Dorozhkin, "Calcium orthophosphate deposits: Preparation, properties and biomedical applications," *Mater. Sci. Eng. C*, vol. 55, pp. 272–326, 2015.
[82] E. Novitskaya *et al.*, "Recent advances on the measurement and calculation of the elastic moduli of cortical and trabecular bone: A review," *Theor. Appl. Mech.*, vol. 38, no. 3, pp. 209–297, 2011.
[83] S. Lei, M. C. Frank, D. D. Anderson, and T. D. Brown, "A method to represent heterogeneous materials for rapid prototyping: The Matryoshka approach," *Rapid Prototyp. J.*, vol. 20, no. 5, pp. 390–402, 2014.

[84] Y. N. Yeni, C. U. Brown, and T. L. Norman, “Influence of bone composition and apparent density on fracture toughness of the human femur and tibia,” *Bone*, vol. 22, no. 1, pp. 79–84, 1998.
[85] M. J. Mirzaali *et al.*, “Mechanical properties of cortical bone and their relationships with age, gender, composition and microindentation properties in the elderly,” *Bone*, vol. 93, pp. 196–211, 2016.
[86] J. T. B. Ratnayake, M. Mucalo, and G. J. Dias, “Substituted hydroxyapatites for bone regeneration: A review of current trends,” *J. Biomed. Mater. Res. - Part B Appl. Biomater.*, vol. 105, no. 5, pp. 1285–1299, 2017.
[87] M. Malakauskaite-Petruleviciene, “Sol-gel synthesis and characterization of calcium hydroxyapatite thin films on different substrates,” *Vilnius Univ. Vilnius, Lith.*, vol. 134 p., 2016.
[88] J. Kolmas, E. Groszyk, and D. Kwiatkowska-Rózycka, “Substituted hydroxyapatites with antibacterial properties,” *Biomed Res. Int.*, vol. 2014, 2014.
[89] O. Lukáts, P. Bujtár, G. K. Sándor, and J. Barabás, “Porous hydroxyapatite and aluminium-oxide ceramic orbital implant evaluation using CBCT scanning: A method for in vivo porous structure evaluation and monitoring,” *Int. J. Biomater.*, vol. 2012, 2012.
[90] K. Ishikawa and A. Kareiva, “Sol–gel synthesis of calcium phosphate-based coatings – A review,” *Chemija*, vol. 31, no. 1, pp. 25–41, Feb. 2020.
[91] R. Z. Legeros, S. Lin, R. Rohanizadeh, D. Mijares, and J. P. Legeros, “Biphasic calcium phosphate bioceramics: Preparation, properties and applications,” *J. Mater. Sci. Mater. Med.*, vol. 14, no. 3, pp. 201–209, 2003.
[92] K. Madhumathi, Y. Rubaiya, M. Doble, R. Venkateswari, and T. S. S. Kumar, “Dual-Drug-Loaded Calcium Phosphate Nanocarriers — in Vitro and in Vivo Studies,” pp. 1066–1077, 2018.
[93] C. Duan, J. Wang, S. Zhou, B. Feng, X. Lu, and J. Weng, “Study on phase transformation and controllable synthesis of calcium phosphate using a sol-gel approach,” *J. Sol-Gel Sci. Technol.*, vol. 63, no. 1, pp. 126–134, 2012.
[94] F. Peng, D. Wang, D. Zhang, H. Cao, and X. Liu, “The prospect of layered double hydroxide as bone implants: A study of mechanical properties, cytocompatibility and antibacterial activity,” *Appl. Clay Sci.*, vol. 165, no. August, pp. 179–187, 2018.
[95] S. Bose, G. Fielding, S. Tarafder, and A. Bandyopadhyay, “Understanding of dopant-induced osteogenesis and angiogenesis in calcium phosphate ceramics,” *Trends Biotechnol.*, vol. 31, no. 10, pp. 594–605, 2013.

[96] A. Moghanian, S. Firoozi, M. Tahriri, and A. Sedghi, “A comparative study on the in vitro formation of hydroxyapatite, cytotoxicity and antibacterial activity of 58S bioactive glass substituted by Li and Sr,” *Mater. Sci. Eng. C*, vol. 91, pp. 349–360, 2018.

[97] Z. Wang, Y. Shen, and M. Haapasalo, “Dental materials with antibiofilm properties,” *Dent. Mater.*, vol. 30, no. 2, pp. e1–e16, 2014.

[98] K. S. Oh *et al.*, “Cytotoxicity and antimicrobial effect of Ag doped hydroxyapatite,” *Key Eng. Mater.*, vol. 264–268, no. III, pp. 2107–2110, 2004.

[99] P. Verma and S. K. Maheshwari, “Applications of Silver nanoparticles in diverse sectors,” *Int. J. Nano Dimens.*, vol. 0, no. 0, pp. 18–36, 2018.

[100] P. Li *et al.*, “Mechanical characteristics, in vitro degradation, cytotoxicity, and antibacterial evaluation of Zn-4.0Ag alloy as a biodegradable material,” *Int. J. Mol. Sci.*, vol. 19, no. 3, 2018.

[101] I. Grigoraviciute-Puroniene, Z. Stankeviciute, K. Ishikawa, and A. Kareiva, “Formation of calcium hydroxyapatite with high concentration of homogeneously distributed silver,” *Microporous Mesoporous Mater.*, vol. 293, no. October, p. 109806, 2020.

[102] O. Livitska *et al.*, “Copper(II), zinc(II) and copper(II)/zinc(II)-containing carbonate-substituted hydroxyapatite: Synthesis, characterization and thermal behaviour,” *Materwiss. Werksttech.*, vol. 47, no. 2–3, pp. 85–91, 2016.

[103] M. Othmani, H. Bachoua, Y. Ghandour, A. Aissa, and M. Debbabi, “Synthesis, characterization and catalytic properties of copper-substituted hydroxyapatite nanocrystals,” *Mater. Res. Bull.*, vol. 97, pp. 560–566, 2018.

[104] H. Kim, S. Mondal, S. Bharathiraja, P. Manivasagan, M. S. Moorthy, and J. Oh, “Optimized Zn-doped hydroxyapatite/doxorubicin bioceramics system for efficient drug delivery and tissue engineering application,” *Ceram. Int.*, vol. 44, no. 6, pp. 6062–6071, 2018.

[105] S. Tautkus, K. Ishikawa, R. Ramanauskas, and A. Kareiva, “Zinc and chromium co-doped calcium hydroxyapatite: Sol-gel synthesis, characterization, behaviour in simulated body fluid and phase transformations,” *J. Solid State Chem.*, vol. 284, no. November 2019, p. 121202, 2020.

[106] Z. Feng, Y. Liao, and M. Ye, “Synthesis and structure of cerium-substituted hydroxyapatite,” vol. 6, pp. 417–421, 2005.

[107] A. Yasukawa, K. Gotoh, H. Tanaka, and K. Kandori, "Preparation and structure of calcium hydroxyapatite substituted with light rare earth ions," *Colloids Surfaces A Physicochem. Eng. Asp.*, vol. 393, pp. 53–59, 2012.
[108] A. J. Nathanael, D. Mangalaraj, S. I. Hong, and Y. Masuda, "Synthesis and in-depth analysis of highly ordered yttrium doped hydroxyapatite nanorods prepared by hydrothermal method and its mechanical analysis," *Mater. Charact.*, vol. 62, no. 12, pp. 1109–1115, 2011.
[109] X. Wei, C. Fu, K. Savino, and M. Z. Yates, "Fully dense yttrium-substituted hydroxyapatite coatings with aligned crystal domains," *Cryst. Growth Des.*, vol. 12, no. 1, pp. 217–223, 2012.
[110] K. Kandori and M. Mitsui, "Synthesis and characterization of Ti(IV)-substituted calcium hydroxyapatite particles by forced hydrolysis of Ca(OH)2-Na5P3O10-TiCl4 mixed solution," *Colloid Polym. Sci.*, vol. 292, no. 11, pp. 2849–2856, 2014.
[111] T. Furuzono, M. Okazaki, Y. Azuma, M. Iwasaki, Y. Kogai, and Y. Sawa, "Newly Developed Biocompatible Material: Dispersible Titanium-Doped Hydroxyapatite Nanoparticles Suitable for Antibacterial Coating on Intravascular Catheters," *Contrib. Nephrol.*, vol. 189, pp. 144–152, 2016.
[112] E. György *et al.*, "Biocompatible Mn2+-doped carbonated hydroxyapatite thin films grown by pulsed laser deposition," *J. Biomed. Mater. Res. - Part A*, vol. 71, no. 2, pp. 353–358, 2004.
[113] B. Bracci, P. Torricelli, S. Panzavolta, E. Boanini, R. Giardino, and A. Bigi, "Effect of Mg2+, Sr2+, and Mn2+ on the chemico-physical and in vitro biological properties of calcium phosphate biomimetic coatings," *J. Inorg. Biochem.*, vol. 103, no. 12, pp. 1666–1674, 2009.
[114] N. Neves *et al.*, "Strontium-rich injectable hybrid system for bone regeneration," *Mater. Sci. Eng. C*, vol. 59, pp. 818–827, 2016.
[115] K. A. GROSS, C. S. CHAI, G. S. K. KANNANGARA, B. BEN-NISSAN, and L. HANLEY, "Thin hydroxyapatite coatings via sol–gel synthesis," *J. Mater. Sci. Mater. Med.*, vol. 9, no. 12, pp. 839–843, Dec. 1998.
[116] Y. MASUDA, K. MATUBARA, and S. SAKKA, "Synthesis of Hydroxyapatite from Metal Alkoxides through Sot-Gel Technique," *J. Ceram. Soc. Japan*, vol. 98, no. 1143, pp. 1255–1266, 1990.
[117] J. Ballarre, I. Manjubala, W. H. Schreiner, J. C. Orellano, P. Fratzl, and S. Ceré, "Improving the osteointegration and bone-implant interface by incorporation of bioactive particles in sol-gel coatings of stainless steel implants," *Acta Biomater.*, vol. 6, no. 4, pp. 1601–1609, 2010.
[118] J. Ballarre *et al.*, "Morphologic and nanomechanical characterization of bone tissue growth around bioactive sol-gel coatings containing

wollastonite particles applied on stainless steel implants," *Mater. Sci. Eng. C*, vol. 31, no. 3, pp. 545–552, 2011.

[119] R. Rojaee, M. Fathi, and K. Raeissi, "Electrophoretic deposition of nanostructured hydroxyapatite coating on AZ91 magnesium alloy implants with different surface treatments," *Appl. Surf. Sci.*, vol. 285, no. PARTB, pp. 664–673, 2013.

[120] C. García, S. Ceré, and A. Durán, "Bioactive coatings prepared by sol-gel on stainless steel 316L," *J. Non. Cryst. Solids*, vol. 348, pp. 218–224, 2004.

[121] G. G. Valle, P. Hammer, S. H. Pulcinelli, and C. V. Santilli, "Transparent and conductive ZnO:Al thin films prepared by sol-gel dip-coating," *J. Eur. Ceram. Soc.*, vol. 24, no. 6, pp. 1009–1013, 2004.

[122] B. Zhang, C. T. Kwok, F. T. Cheng, and H. C. Man, "Fabrication of nano-structured HA/CNT coatings on Ti6Al4V by electrophoretic deposition for biomedical applications," *J. Nanosci. Nanotechnol.*, vol. 11, no. 12, pp. 10740–10745, 2011.

[123] T. Fu, Y. G. Shen, Z. Alajmi, S. Y. Yang, J. M. Sun, and H. M. Zhang, "Sol-gel preparation and properties of Ag-TiO2 films on surface roughened Ti-6Al-4V alloy," *Mater. Sci. Technol. (United Kingdom)*, vol. 31, no. 4, pp. 501–505, 2015.

[124] M. Lilja, U. Butt, Z. Shen, and D. Bjöörn, "Nucleation and growth of hydroxyapatite on arc-deposited TiO 2 surfaces studied by quartz crystal microbalance with dissipation," *Appl. Surf. Sci.*, vol. 284, pp. 1–6, 2013.

[125] Y. Li *et al.*, "The effect of strontium-substituted hydroxyapatite coating on implant fixation in ovariectomized rats," *Biomaterials*, vol. 31, no. 34, pp. 9006–9014, 2010.

[126] J. Ballarre, D. A. López, W. H. Schreiner, A. Durán, and S. M. Ceré, "Protective hybrid sol-gel coatings containing bioactive particles on surgical grade stainless steel: Surface characterization," *Appl. Surf. Sci.*, vol. 253, no. 17, pp. 7260–7264, 2007.

[127] M. I. Coşkun, I. H. Karahan, and Y. Yücel, "Optimized electrodeposition concentrations for hydroxyapatite coatings on CoCrMo biomedical alloys by computational techniques," *Electrochim. Acta*, vol. 150, pp. 46–54, 2014.

[128] D. T. M. Thanh *et al.*, "Controlling the electrodeposition, morphology and structure of hydroxyapatite coating on 316L stainless steel," *Mater. Sci. Eng. C*, vol. 33, no. 4, pp. 2037–2045, 2013.

[129] S. Ban and S. Maruno, “Effect of temperature on electrochemical deposition of calcium phosphate coatings in a simulated body fluid,” *Biomaterials*, vol. 16, no. 13, pp. 977–981, 1995.
[130] Y. Cai, S. Zhang, X. Zeng, Y. Wang, M. Qian, and W. Weng, “Improvement of bioactivity with magnesium and fluorine ions incorporated hydroxyapatite coatings via sol-gel deposition on Ti6Al4V alloys,” *Thin Solid Films*, vol. 517, no. 17, pp. 5347–5351, 2009.
[131] R. Rojaee, M. Fathi, and K. Raeissi, “Comparing nanostructured hydroxyapatite coating on AZ91 alloy samples via sol-gel and electrophoretic deposition for biomedical applications,” *IEEE Trans. Nanobioscience*, vol. 13, no. 4, pp. 409–414, 2014.
[132] A. Tahmasbi Rad, M. Solati-Hashjin, N. A. A. Osman, and S. Faghihi, “Improved bio-physical performance of hydroxyapatite coatings obtained by electrophoretic deposition at dynamic voltage,” *Ceram. Int.*, vol. 40, no. 8 PART B, pp. 12681–12691, 2014.
[133] C. T. Kwok, P. K. Wong, F. T. Cheng, and H. C. Man, “Characterization and corrosion behavior of hydroxyapatite coatings on Ti6Al4V fabricated by electrophoretic deposition,” *Appl. Surf. Sci.*, vol. 255, no. 13–14, pp. 6736–6744, 2009.
[134] F. Batmanghelich and M. Ghorbani, “Effect of pH and carbon nanotube content on the corrosion behavior of electrophoretically deposited chitosan-hydroxyapatite-carbon nanotube composite coatings,” *Ceram. Int.*, vol. 39, no. 5, pp. 5393–5402, 2013.
[135] T. M. G. Chu, S. J. Hollister, J. W. Halloran, S. E. Feinberg, and D. G. Orton, “Manufacturing and characterization of 3-D hydroxyapatite bone tissue engineering scaffolds,” *Ann. N. Y. Acad. Sci.*, vol. 961, pp. 114–117, 2002.
[136] M. H. Fathi, M. Salehi, A. Saatchi, V. Mortazavi, and S. B. Moosavi, “In vitro corrosion behavior of bioceramic, metallic, and bioceramic-metallic coated stainless steel dental implants,” *Dent. Mater.*, vol. 19, no. 3, pp. 188–198, 2003.
[137] C. W. Yang, T. M. Lee, T. S. Lui, and E. Chang, “A comparison of the microstructural feature and bonding strength of plasma-sprayed hydroxyapatite coatings with hydrothermal and vacuum post-heat treatment,” *Mater. Trans.*, vol. 46, no. 3, pp. 709–715, 2005.
[138] Y. Yang, K. H. Kim, and J. L. Ong, “A review on calcium phosphate coatings produced using a sputtering process - An alternative to plasma spraying,” *Biomaterials*, vol. 26, no. 3, pp. 327–337, 2005.

[139] P. Berube, Y. Yang, D. L. Carnes, R. E. Stover, E. J. Boland, and J. L. Ong, “The Effect of Sputtered Calcium Phosphate Coatings of Different Crystallinity on Osteoblast Differentiation,” *J. Periodontol.*, vol. 76, no. 10, pp. 1697–1709, 2005.
[140] J. A. Toque, M. K. Herliansyah, M. Hamdi, A. Ide-Ektessabi, and I. Sopyan, “Adhesion failure behavior of sputtered calcium phosphate thin film coatings evaluated using microscratch testing,” *J. Mech. Behav. Biomed. Mater.*, vol. 3, no. 4, pp. 324–330, 2010.
[141] J. Li, H. Liao, and L. Hermansson, “Sintering of partially-stabilized zirconia and partially-stabilized zirconia-hydroxyapatite composites by hot isostatic pressing and pressureless sintering,” *Biomaterials*, vol. 17, no. 18, pp. 1787–1790, 1996.
[142] T. Onoki and T. Hashida, “New method for hydroxyapatite coating of titanium by the hydrothermal hot isostatic pressing technique,” *Surf. Coatings Technol.*, vol. 200, no. 24, pp. 6801–6807, 2006.
[143] J. M. Fernández-Pradas, L. Clèries, P. Serra, G. Sardin, and J. L. Morenza, “Evolution of the deposition rate during pulsed laser deposition of hydroxyapatite coatings and its relation with target morphology,” *Appl. Phys. A Mater. Sci. Process.*, vol. 72, no. 5, pp. 613–618, 2001.
[144] L. Clèries, J. M. Fernández-Pradas, and J. L. Morenza, “Bone growth on and resorption of calcium phosphate coatings obtained by pulsed laser deposition,” *J. Biomed. Mater. Res.*, vol. 49, no. 1, pp. 43–52, 2000.
[145] A. Bigi *et al.*, “Nanocrystalline hydroxyapatite coatings on titanium: A new fast biomimetic method,” *Biomaterials*, vol. 26, no. 19, pp. 4085–4089, 2005.
[146] R. A. Surmenev, “A review of plasma-assisted methods for calcium phosphate-based coatings fabrication,” *Surf. Coatings Technol.*, vol. 206, no. 8–9, pp. 2035–2056, 2012.
[147] P. Usinskas, Z. Stankeviciute, G. Niaura, J. Maminskas, G. Juodzbalys, and A. Kareiva, “Sol–gel processing of calcium hydroxyapatite thin films on silicon nitride (Si3N4) substrate,” *J. Sol-Gel Sci. Technol.*, vol. 83, no. 2, pp. 268–274, 2017.
[148] Ž. Stankevičiute, M. Malakauskaite, A. Beganskiene, and A. Kareiva, “Sol-gel synthesis of calcium phosphate coatings on Ti substrate using dip-coating technique,” *Chemija*, vol. 24, no. 4, pp. 288–295, 2013.
[149] S. A. Pauline and N. Rajendran, “Biomimetic novel nanoporous niobium oxide coating for orthopaedic applications,” *Appl. Surf. Sci.*, vol. 290, pp. 448–457, 2014.

[150] I. A. Karampas and C. G. Kontoyannis, “Characterization of calcium phosphates mixtures,” *Vib. Spectrosc.*, vol. 64, pp. 126–133, 2013.
[151] G. Niaura, A. K. Gaigalas, and V. L. Vilker, “Surface-enhanced Raman spectroscopy of phosphate anions: Adsorption on silver, gold, and copper electrodes,” *J. Phys. Chem. B*, vol. 101, no. 45, pp. 9250–9262, 1997.
[152] A. F. Khan, M. Awais, A. S. Khan, S. Tabassum, A. A. Chaudhry, and I. U. Rehman, “Raman spectroscopy of natural bone and synthetic apatites,” *Appl. Spectrosc. Rev.*, vol. 48, no. 4, pp. 329–355, 2013.
[153] A. M. Sofronia, R. Baies, E. M. Anghel, C. A. Marinescu, and S. Tanasescu, “Thermal and structural characterization of synthetic and natural nanocrystalline hydroxyapatite,” *Mater. Sci. Eng. C*, vol. 43, pp. 153–163, 2014.
[154] J. A. Norton, “Carcinoembryonic antigen: New applications for an old marker,” *Ann. Surg.*, vol. 213, no. 2, pp. 95–97, 1991.
[155] G. Ulian, G. Valdré, M. Corno, and P. Ugliengo, “The vibrational features of hydroxylapatite and type A carbonated apatite: A first principle contribution,” *Am. Mineral.*, vol. 98, no. 4, pp. 752–759, 2013.
[156] S. Saber-Samandari, K. Alamara, S. Saber-Samandari, and K. A. Gross, “Micro-Raman spectroscopy shows how the coating process affects the characteristics of hydroxylapatite,” *Acta Biomater.*, vol. 9, no. 12, pp. 9538–9546, 2013.
[157] R. Bosco, M. Iafisco, J. Van Den Beucken, S. Leeuwenburgh, and J. Jansen, “Adsorption of alendronate onto biomimetic apatite nanocrystals to develop drug carrier coating for bone implants,” *Key Eng. Mater.*, vol. 529–530, no. 1, pp. 475–479, 2013.
[158] A. Venuta, J. Wolfram, H. Shen, and M. Ferrari, “Post-nano strategies for drug delivery: multistage porous silicon microvectors,” *J. Mater. Chem. B*, vol. 5, no. 2, pp. 207–219, 2017.
[159] M. Malakauskaite-Petruleviciene, Z. Stankeviciute, G. Niaura, A. Prichodko, and A. Kareiva, “Synthesis and characterization of sol-gel derived calcium hydroxyapatite thin films spin-coated on silicon substrate,” *Ceram. Int.*, vol. 41, no. 6, pp. 7421–7428, 2015.
[160] M. Sitarz, M. Rokita, and K. Bułat, “Spectrochimica Acta Part A : Molecular and Biomolecular Spectroscopy,” vol. 79, pp. 722–727, 2011.
[161] U. Posset, E. Löcklin, R. Thull, and W. Kiefer, “Vibrational spectroscopic study of tetracalcium phosphate in pure polycrystalline form and as a constituent of a self-setting bone cement,” *J. Biomed. Mater. Res.*, vol. 40, no. 4, pp. 640–645, 1998.

[162] I. Rehman and W. Bonfield, “Characterization of hydroxyapatite and carbonated apatite by photo acoustic FTIR spectroscopy,” *J. Mater. Sci. Mater. Med.*, vol. 8, no. 1, pp. 1–4, 1997.
[163] M. Frasnelli *et al.*, “Synthesis and characterization of strontium-substituted hydroxyapatite nanoparticles for bone regeneration,” *Mater. Sci. Eng. C*, vol. 71, pp. 653–662, 2017.

SANTRAUKA

1. ĮVADAS

Sintetinės medžiagos, naudojamos kurti implantus, dažniausiai būna biologiškai inertiškos, o jų fizikinės savybės skiriasi nuo natūralaus kaulo. Tai prailgina implanto įsisavinimo laiką. Dėl fizinių savybių nesuderinamumo, nuolaužų kaupimosi ar kitų priežasčių implantai per laiką būna atmetami, ir pacientui atliekama pakartotina operacija. Senstant populiacijai šių procedūrų reikės vis daugiau.

Kalcio hidroksiapatitas (($Ca_{10}(PO_4)_6(OH)_2$, CHAp) yra viena pagrindinių natūralaus kaulo sudedamųjų dalių. Implantų dengimas sintetiniu kalcio hidroksiapatitu, sukuriant tarpinį sluoksnį tarp implanto ir kaulo, yra logiškas kelias sprendžiant anksčiau įvardintas problemas. Tai leistų greitesnį implanto įsisavinimą ir fizinių savybių suderinamumą.

Plazmos purškimas yra vienintelis patvirtintas Maisto ir vaistų administracijos JAV (FDA) biomedicininių prietaisų dengimo būdų. Nepaisant to jis turi savų trūkumų – dėl naudojamos aukštos temperatūros proceso valdymas yra sudėtingas. Sunku gauti homogeniškas, gerai sukibančias su padėklu, norimo sluoksnio storio dangas. Taip pat kyla problemų dengiant sudėtingų formų objektus. Dėl šių priežasčių susidomėjimas naujų medžiagų, tinkamų implantams, dangų gamybos ir dengimo būdais yra nuolat augantis.

Šios disertacijos tikslas yra kalcio hidroksiapatito plonų sluoksnių tikslinis dizainas ant skirtingų padėklų. Dangų gavimas ant modifikuotų paviršių ir skirtingų padėklų yra šio darbo išskirtinumas ir naujumas. Šiam tikslui pasiekti iškelti šie uždaviniai:

1. Modifikuoti titano (Ti) padėklo paviršių ir ant jo zolių-gelių metodu gauti porėtas bei hidrofilines kalcio hidroksiapatito dangas.
2. Susintetinti ir apibūdinti kalcio hidroksiapatito dangas and silicio nitrido (Si_3N_4) padėklo.
3. Sukurti greitesnį kalcio hidrosiapatito plonų sluoksnių gavimo būdą.

2. EKSPERIMENTO METODIKA

Eksperimento metodikos skyrius yra sudarytas iš dviejų poskyrių ir yra skirtas aprašyti atliko darbo eksperimentinius ypatumus. Visa metodika yra detaliai išdėstyta disertacijos antrajame skyriuje. Pirmame poskyryje yra išvardintos cheminės medžiagos, naudotos sintezei. Antrajame poskyryje yra išdėstyta visa eksperimento metodika, zolių-gelių sintezės metodika, padėklų paruošimas ir susintetintų medžiagų sudėties, morfologijos bei kitų savybių tyrimams naudota įranga.

3. REZULTATAI IR JŲ APTARIMAS

3.1 Porėto ir hidrofilinio kalcio hidroksiapatito dangos gavimas ant modifikuoto titano padėklo zolių–gelių metodu

Ca-Ti-O pirmtako gelių termogravimetrinės analizės rezultatai pateikti 1pav. Matome tris masės netekties sritis: ties 50–250 °C, 250–430 °C ir 430–650 °C. Pirmoji sritis (maždaug 15%) priskiriama adsorbuoto ir struktūrinio vandens pasišalinimui. Antrojoje srityje (maždaug 45%) masė mažėja dėl organinių medžiagų terminio skilimo (etilenglikolis, PVA, citratai). Paskutiniame etape suskyla likusios organinės medžiagos. Masės netekties virš 650 °C nepastebėta. Ca-Ti-O pirmtakų gelių terminis skilimas nepriklauso nuo to, ar sintezės metu naudojamas kalcio acetatas, ar kalcio hidroksidas.

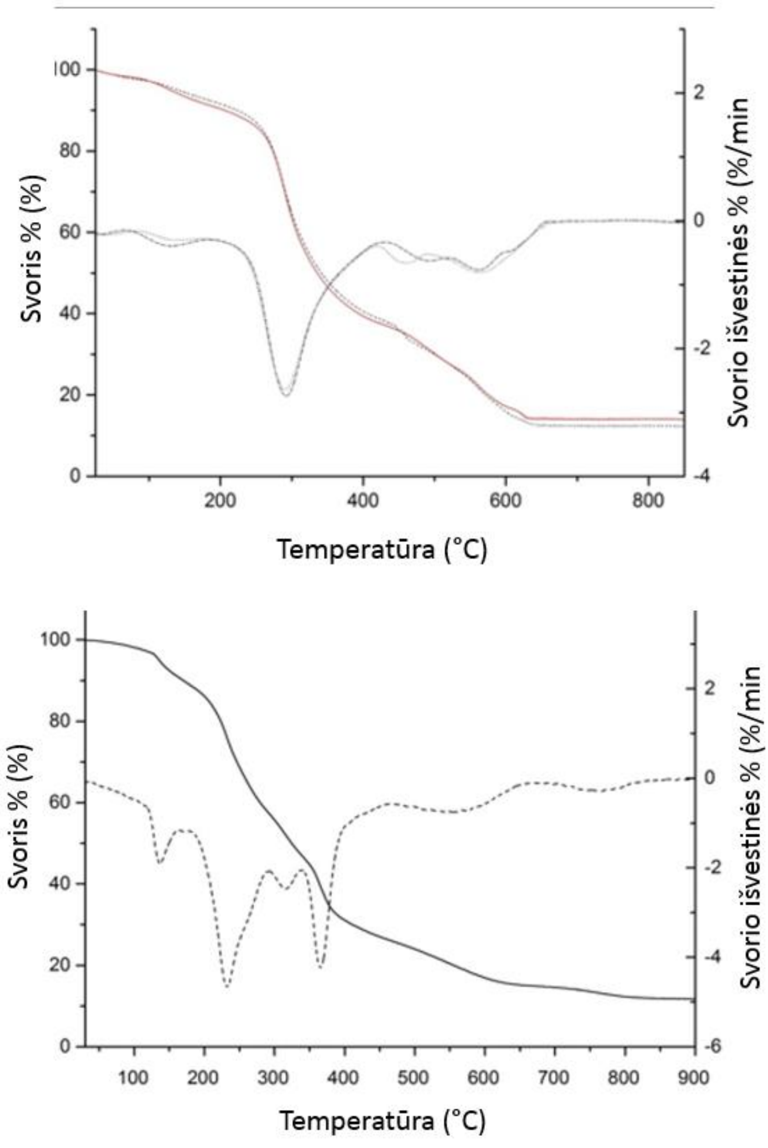

1 pav. Ca-Ti-O pirmtakų gelių, susintetintų naudojant kalcio acetatą (taškinė linija) ir kalcio hidroksidą (ištisinė linija) (viršuje), ir Ca-P-O pirmtakų gelių (apačioje) TG/DTA kreivės.

Ca-P-O pirmtako gelio termogravimetrinėje kreivėje matoma masės netektis (apie 15%) temperatūrų intervale 160–200 °C dėl drėgmės pasišalinimo, o pagrindinis gelio skilimas (apie 65%) yra stebimas iki 650 °C.

2 pav. pavaizduotos CHAp dangų, gautų ant Ti padėklų, kurie, prieš dengimą įmerkimo būdu, buvo iškaitinti, rentgeno spindulių difraktogramos. Padėklų kaitinimas buvo atliktas norint sukurti titano oksido sluoksnį, kuris neleistų oksido sluoksniui susidaryti formuojant CHAp dangas.

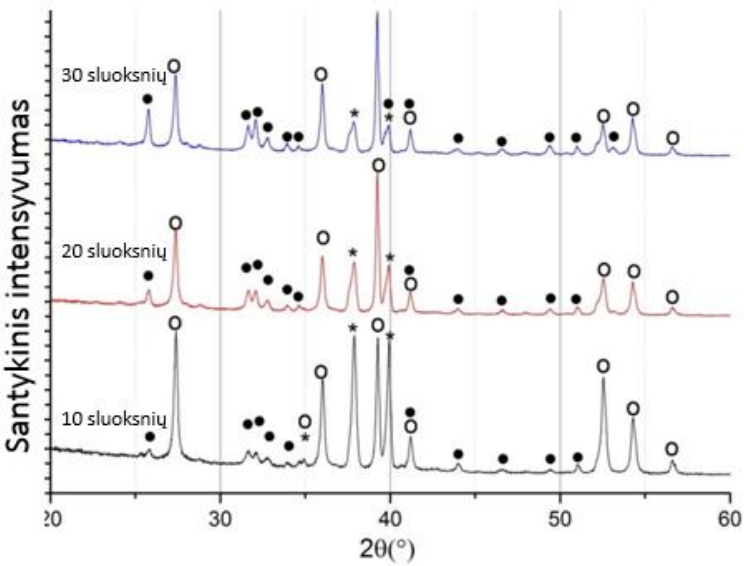

2 pav. CHAp dangų, gautų ant iškaitinto Ti (650 °C, 5 h ore), Rentgeno spindulių difraktogramos. Difrakcinės smailės: • - ($Ca_{10}(PO_4)_6(OH)_2$ (PDF: 74-0566); o – TiO_2 (PDF: 73-2224); * - Ti (PDF: 44-1294).

Smailių, priskiriamų CHAp fazei, intensyvumas didėja didėjant sluoksnių skaičiui. O smailių, priskiriamų TiO_2, intensyvumai mažėja. Galima daryti išvadą, kad TiO_2 susidarymas yra slopinamas dėl pradinio padėklo modifikavimo – kaitinimo 650 °C 5 val. ore prieš dengiant CHAp. Titano oksido difrakcijos smailių intensyvumas didėjant CHAp sluoksnių skaičiui lieka nepakitęs.

3 pav. pavaizduota CHAp dangų rentgeno spindulių difraktogramos, gautos ant nuvalyto titano padėklo, jo nekaitinant prieš dengimą. Šiuo atveju, CHAp difrakcinės smailės atsiranda jau po 10 sluoksnių. Jų intensyvumas didėja didėjant sluoksnių skaičiui. Ti priskiriamos difrakcijos smailių intensyvumas mažėja, tačiau TiO_2 fazės difrakcinių smailių intensyvumai didėja. Tai liudija tolimesnį titano oksido susidarymą. Šie rezultatai patvirtina, kad dengiant titaną CHAp sluoksniais, Ti iškaitinimo procedūra stabdo tolimesnį titano oksido sluoksnio augimą.

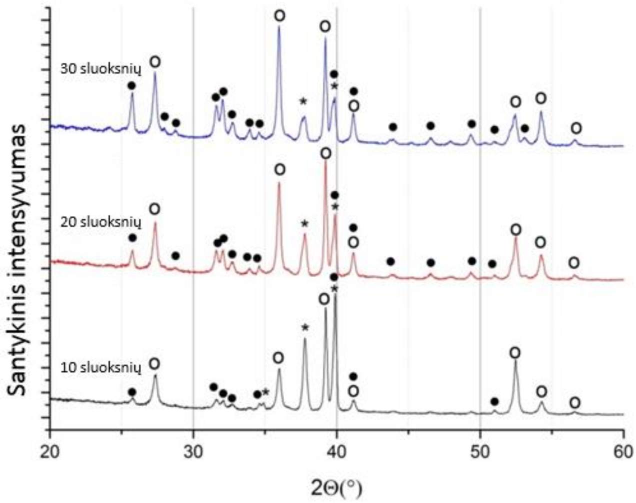

3 pav. CHAp sluoksnių, gautų ant Ti padėklo, Rentgeno spindulių difraktogramos. Difrakcinės smailės: • - ($Ca_{10}(PO_4)_6(OH)_2$ (PDF: 74-0566); o – TiO_2 (PDF: 73-2224); * - Ti (PDF: 44-1294).

4 ir 5 pav. atvaizduota CHAp dangų, gautų and Ti padėklo, padengto 10 sluoksnių $CaTiO_3$ (pasluoksnis) (kalcio acetatas buvo naudotas Ca šaltiniu).

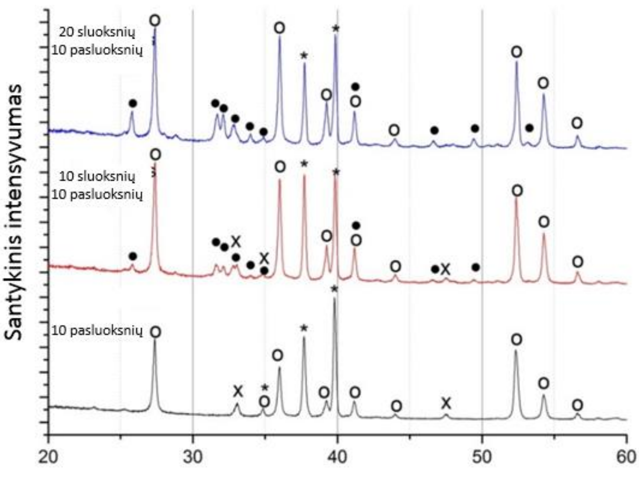

4 pav. CHAp dangų, gautų ant Ti (be pradinio iškaitinimo) padėklų su $CaTiO_3$ pasluoksniu (kalcio acetatas kaip Ca šaltinis), rentgeno spindulių difraktogramos. Difrakcijos smailės: • - ($Ca_{10}(PO_4)_6(OH)_2$ (PDF: 74-0566); o – TiO_2 (PDF: 73-2224); * - Ti (PDF: 44-1294); x – $CaTiO_3$ (PDF: 22-0153).

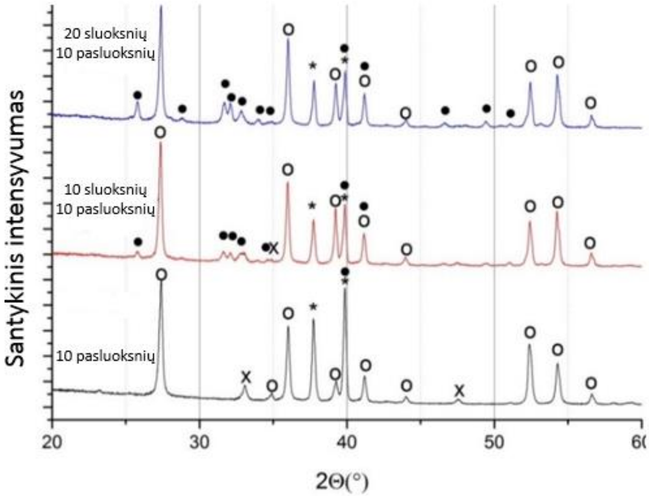

5 pav. CHAp dangų, gautų ant Ti (kaitinto 650 °C 5 h ore) padėklų su $CaTiO_3$ pasluoksniu (kalcio acetatas kaip Ca šaltinis), rentgeno spindulių difraktogramos. Difrakcijos smailės: • - ($Ca_{10}(PO_4)_6(OH)_2$ (PDF: 74-0566); o – TiO_2 (PDF: 73-2224); * - Ti (PDF: 44-1294); x – $CaTiO_3$ (PDF: 22-0153).

Galima pastebėti, kad $CaTiO_3$ priskiriamos smailės yra matomos po 10 dengimo ciklų, tačiau kartu pastebimas yra TiO_2 būdingos smailės. CHAp susidarymas taip pat matomas jau po 10 pamerkimo ir iškaitinimo procedūrų. Po papildomų 10 ciklų, CHAp priskiriamų smailių intensyvumas didėja, tačiau $CaTiO_3$ charakteringų smailių daugiau nebepastebime. Galima teigti, kad $CaTiO_3$ pasluoksnis buvo padengtas CHAp. TiO_2 priskiriamų smailių intensyvumas, kai buvo naudotas neiškaitintas padėklas, irgi didėja. Galima teigti, kad kalcio titanato pasluoksnis titano oksido susidarymo nesustabdo (4 pav.). Tačiau, kai Ti padėklas prieš dengiant kalcio titanato pasluoksnį buvo iškaitintas, buvo gauti kitokie rezultatai. Titano oksido smailių intensyvumas išliko nepakitęs iki 20 dengimo ciklų (5 pav.).

Toks pat eksperimentas buvo atliktas $CaTiO_3$ pasluoksnio gamybai ant Ti padėklo Ca šaltiniu naudojant kalcio hidroksidą. Iš gautų CHAp dangų, dengtų ant kalcio titanato pasluoksnio (ant iškaitinto arba tik nuvalyto Ti padėklo), rentgeno spindulių difraktogramų matoma, kad CHAp susidarymas yra analogiškas, t. y. nepriklauso nuo Ca šaltiniu naudotos medžiagos (6 ir 7 pav.).

Dangų morfologijos ypatumai yra pavaizduoti SEM nuotraukose (8 pav.). Vizualiai skirtumo tarp dangų, gautų ant iškaitinto ar neiškaitino padėklo nesimato. Tačiau didėjant sluoksnių skaičiui didėja paviršiaus porėtumas. 9 pav. pavaizduotos $CaTiO_3$ pasluoksnio, naudojant kalcio acetatą arba kalcio hidroksidą, ir ant pasluoksnio dengto CHAp, SEM nuotraukos. Kalcio titanato morfologija gerokai skiriasi nuo CHAp dangų. $CaTiO_3$ paviršius ant iškaitinto Ti yra sudarytas iš 2-3 µm dydžio salelių, kurios sudarytos iš sferinių nanodalelių. Ši morfologija pasikeičia po 10 dengimo ciklų – pradedamas matyti porėtas CHAp paviršius. Po dar 10 sluoksnių CHAp paviršiaus morfologija išlieka beveik tokia pati.

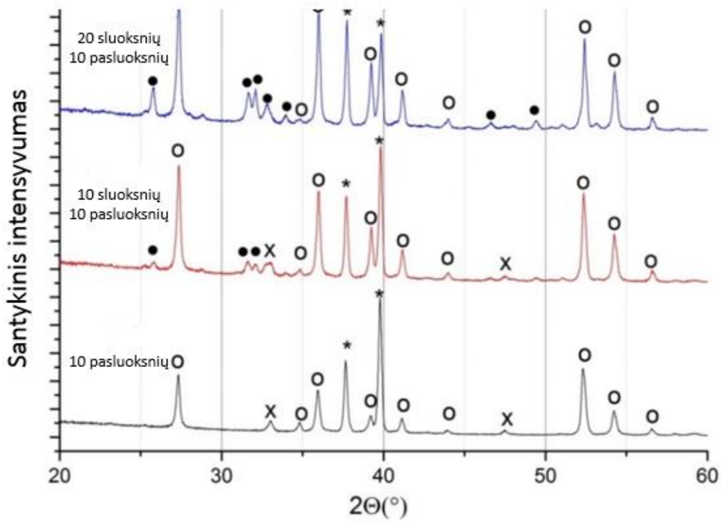

6 pav. CHAp dangų, gautų ant Ti (be pradinio iškaitinimo) su $CaTiO_3$ pasluoksniu (gauto iš kalcio hidroksido), rentgeno spindulių difraktogramos. Difrakcijos smailės: • - ($Ca_{10}(PO_4)_6(OH)_2$ (PDF: 74-0566); o – TiO_2 (PDF: 73-2224); * - Ti (PDF: 44-1294); x – $CaTiO_3$ (PDF: 22-0153).

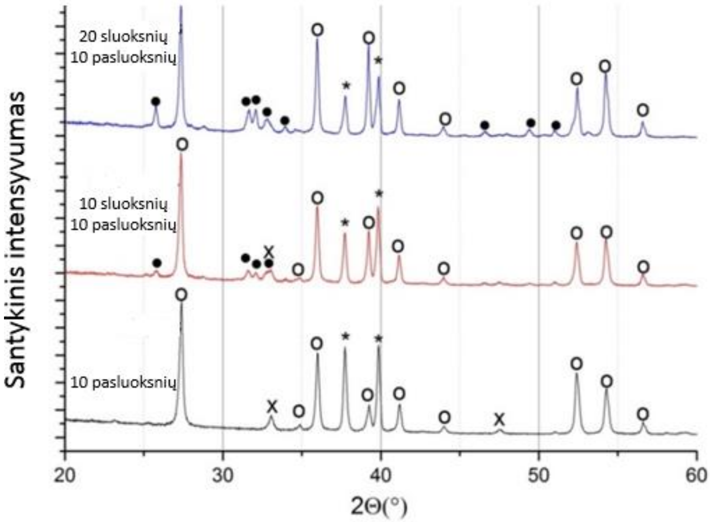

7 pav. CHAp dangų, gautų ant Ti padėklo (iškaitinto) su $CaTiO_3$ pasluoksniu (gauto iš kalcio hidroksido), rentgeno spindulių difraktograma. Difrakcijos smailės:
• - CHAP ($Ca_{10}(PO_4)_6(OH)_2$ (PDF: 74-0566); o – TiO_2 (PDF: 73-2224);
* - Ti (PDF: 44-1294); x – $CaTiO_3$ (PDF: 22-0153).

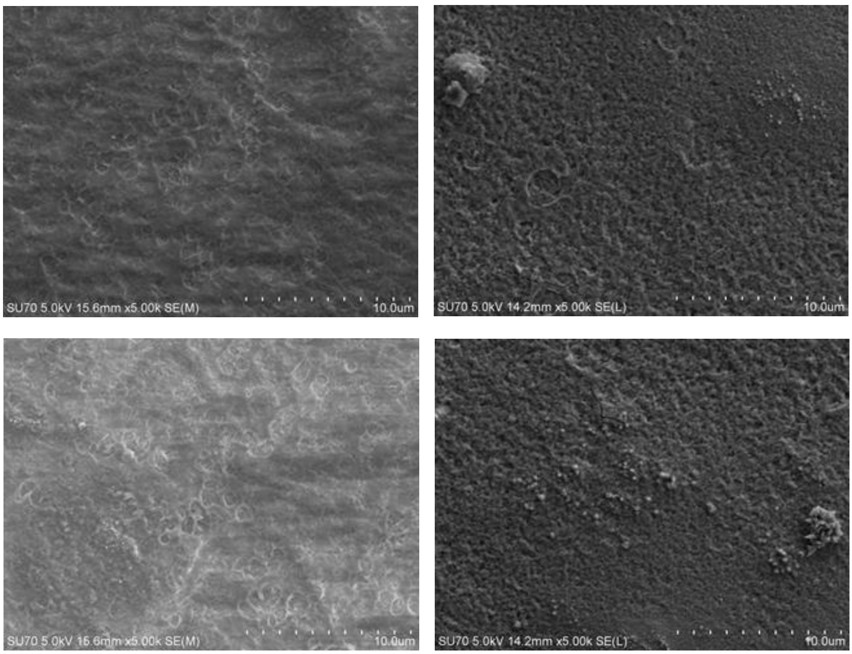

8 pav. CHAp dangų, gautų ant iškaitinto Ti (viršuje) ir neiškaitinto Ti (apačioje) padėklų, SEM nuotraukos: 10 sluoksnių (kairėje) ir 30 sluoksnių (dešinėje).

10 pav. pavaizduotos analogiškos CHAp gauto su $CaTiO_3$ pasluoksniu ant neiškaitinto Ti, SEM nuotraukos. CHAp dangos akivaizdžiai yra lygesnės ir labiau porėtos. Mikrostruktūra yra labai panaši į CHAp dangos, gautos ant neiškaitinto Ti ir be kalcio titanato pasluoksnio.

Dangų drėkinimo savybės buvo tiriamos matuojant kontaktinį kampą. Rezultatai apibendrinti 1 lentelėje. Įdomu pastebėti, kad hidrofobinės savybės nepriklauso nuo CHAp sluoksnių skaičiaus iki 20 sluoksnio. Mėginių ant iškaitinto ar neiškaitinto padėklų, su pasluoksniu arba be jo, kontaktinis kampas yra maždaug 70 ^{o}. Tačiau padidinus sluoksnių skaičių iki 30, kontaktinis kampas sumažėja nuo iki 49-59 ^{o}.

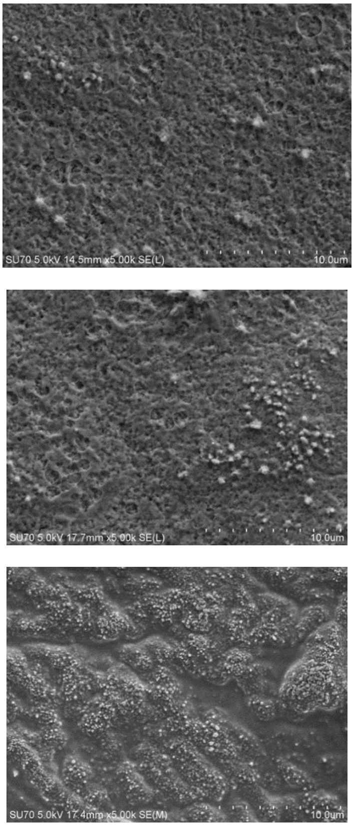

9 pav. $CaTiO_3$ dangos ant iškaitinto Ti padėklo (apačioje) ir CHAp dangų ant šio pasluoksnio (10 sluoksnių (viduryje) ir 20 sluoksnių (viršuje)), SEM nuotraukos.

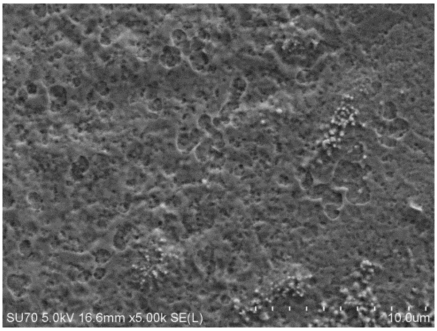

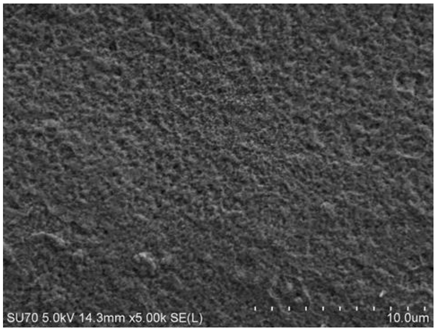

10 pav. $CaTiO_3$ dangos ant neiškaitinto Ti padėklo (kairėje) ir CHAp dangos ant šio pasluoksnio (20 sluoksnių), SEM nuotraukos.

1 lentelė. Kontaktinio kampo matavimo rezultatai (CA – kontaktinis kampas, SD – standartinis nuokrypis).

Sluoksnių skaičius ant modifikuoto padėklo	CA be pasluoksnio	CA su $CaTiO_3$ pasluoksniu iš $Ca(Ac)_2$	CA su $CaTiO_3$ pasluoksniu iš $Ca(OH)_2$
10	75,96±1,22	62,90±1,88	83,44±0,41
20	76,42±2,54	76,18±5,87	71,57±6,14
30	66,22±8,05	72,50±1,53	80,55±3,84
Sluoksnių skaičius ant nemodifikuoto padėklo			
10	68,93±3,17	67,24±0,85	71,96±1,00
20	49,42±0,67	58,53±5,46	51,36±3,15
30	52,07±1,46	53,35±5,59	51,26±2,18

3.2 Kalcio hidroksiapatito plonų sluoksnių ant silicio nitrido (Si_3N_4) padėklo sintezė zolių–gelių metodu

CHAp dangų be ir su pasluoksniu, gautų ant silicio nitrido padėklo, difraktogramos yra pavaizduotos 11 pav. CHAp fazės susidarymas pastebimas jau po 10 dengimo ciklų. Difrakcijos smailių intensyvumas didėja didinant sluoksnių skaičių.

CHAp ir kalcio titanato dangų SEM nuotraukos yra pavaizduotos 12 ir 13 pav. Matoma, kad kalcio titanato ir kalcio hidroksiapatito 10 sluoksnių dangų morfologijos skiriasi. $CaTiO_3$ pasluoksnio paviršius (13 pav.) yra lygus, o CHAp paviršius yra sudarytas iš salelių. Visais atvejais dangose susidaro įtrūkimai, kurie ryškėja didėjant sluoksnių skaičiui. Dangų trūkinėjimą greičiausiai sukėlė terminio plėtimosi tarp dangos bei padėklo nesuderinamumas. Kuo storesnis sluoksnio storis, tuo danga tampa mažiau atspari plėtimuisi ir susitraukimui. Šio eksperimento atveju mėginiai buvo paliekami ataušti krosnyje. Tiksliau kontroliuojant temperatūrą greičiausiai būtų galima gauti vientisas dangas. SEM tyrimais nustatyta, kad dangos po 30 dengimo ciklų storis buvo maždaug 2 μm.

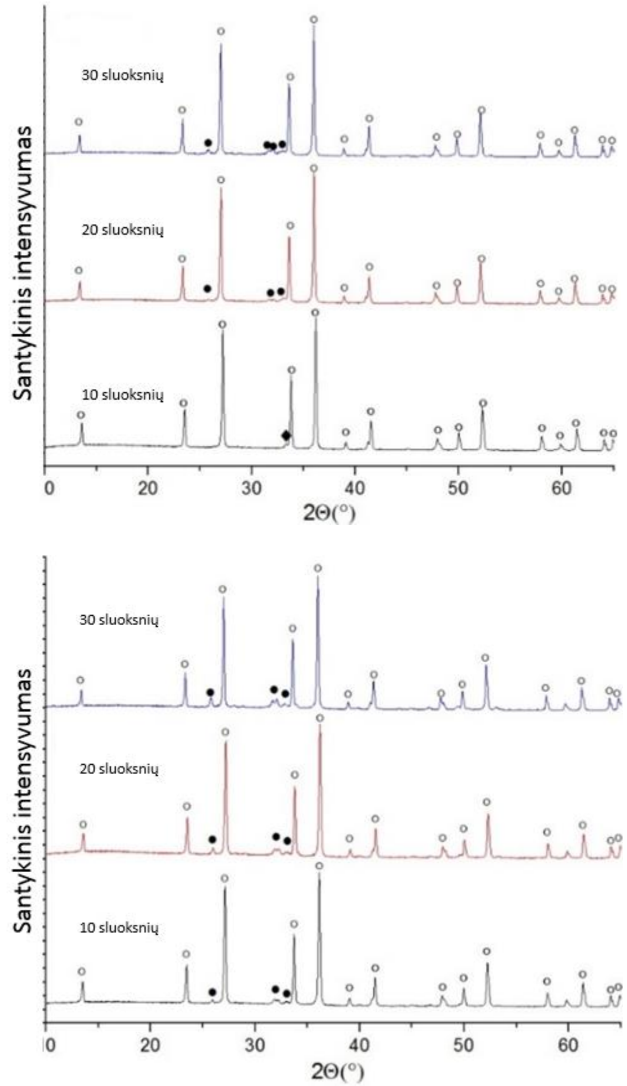

11 pav. CHAp dangų, gautų ant silicio nitrido, rentgeno spindulių difraktogramos: be pasluoksnio (viršuje) ir su pasluoksniu (apačioje). Difrakcijos smailės: • - $(Ca_{10}(PO_4)_6(OH)_2$ (PDF: 74-0566); o – Si_3N_4; ♦ - $CaTiO_3$.

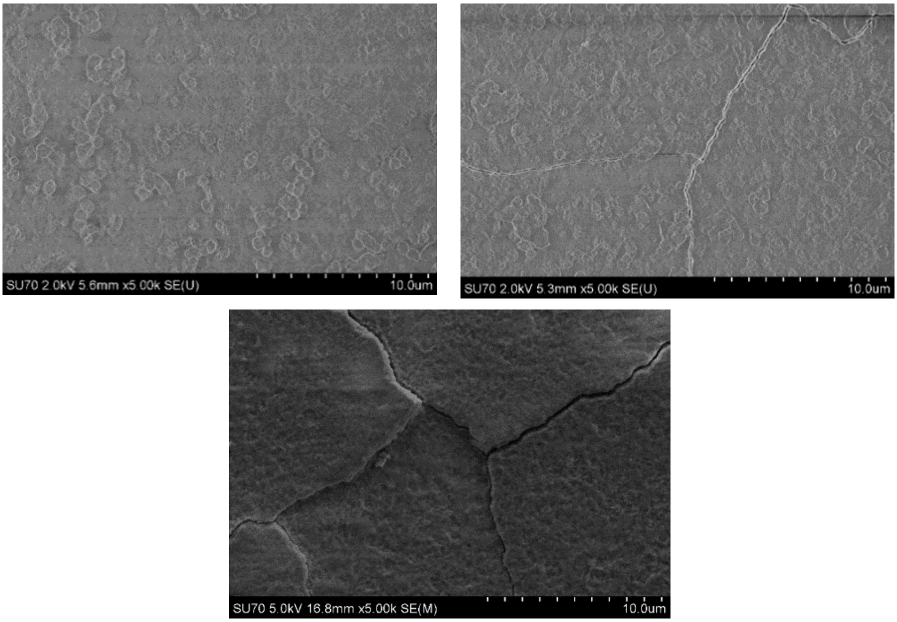

12 pav. CHAp dangų ant silicio nitrido be pasluoksnio SEM nuotraukos: 10 (kairė), 20 (dešinė) ir 30 (apačioje) sluoksnių.

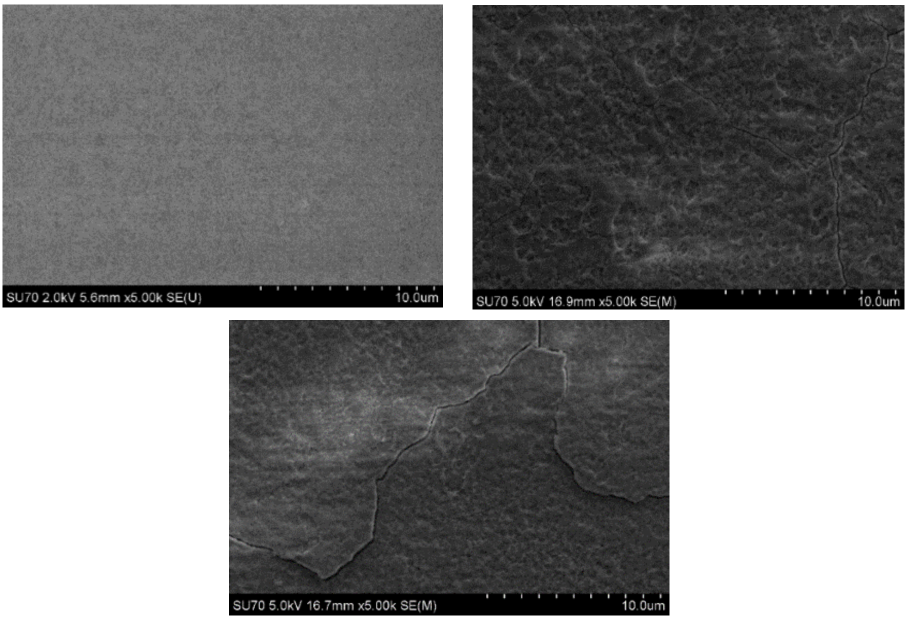

13 pav. $CaTiO_3$ pasluoksnio ant silicio nitrido (kairė) ir CHAp dangų ant pasluoksnio (10 (dešinė) ir 20 (apačioje) sluoksnių) SEM nuotraukos.

SEM rezultatus patvirtino ir atominės jėgos mikroskopijos matavimų duomenys (14 pav.).

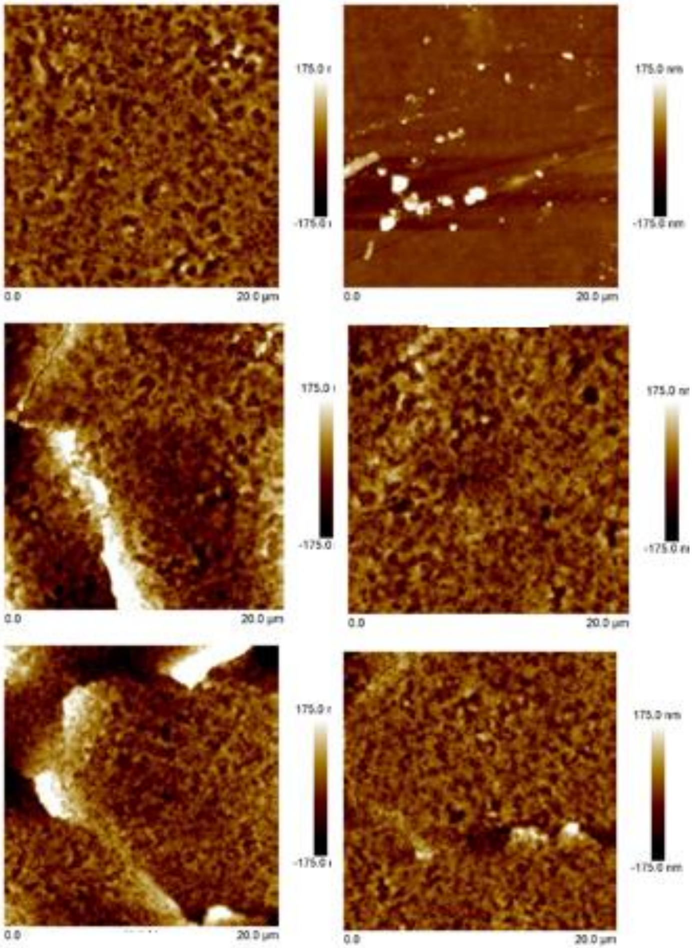

14 pav. CHAp dangų (kairėje) ir CHAp dangų ant pasluoksnio (dešinėje) AFM nuotraukos: 10, 20 ir 30 sluoksnių (nuo viršaus į apačią).

Kaip matome iš AFM nuotraukų, po 20 ir 30 sluoksnių pastebimi įtrūkimai. Taip pat galima teigti, kad CHAp dangos yra porėtos.

15 pav. pavaizduotas CHAp dangos, gautos po 30 dengimo ciklų ant silicio nitrido padėklo, Ramano spektras.

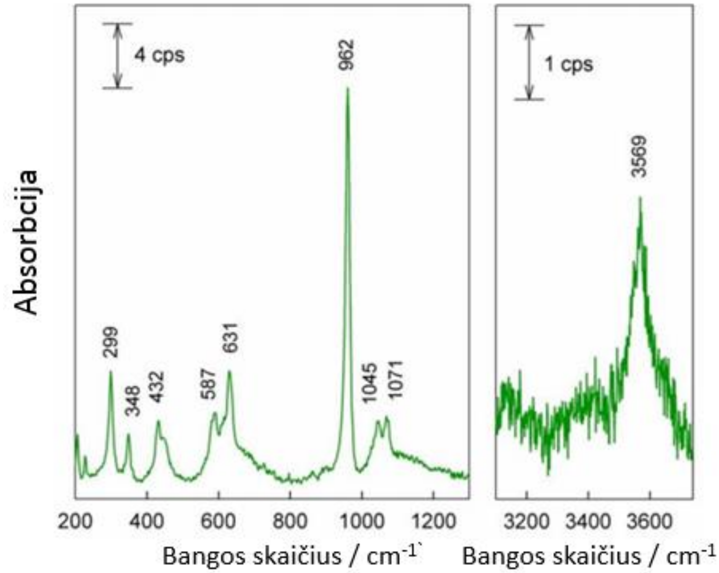

15 pav. CHAp dangos, gautos po 30 dengimo ciklų ant silicio nitrido padėklo, Ramano spektras 200–1300 ir 3100–3700 cm^{-1} spektro srityse. Sužadinimo bangos ilgis - 442 nm (0.8 mW).

Intensyviausia juosta ties 962 cm^{-1} priskiriama PO_4^{3-} grupei. Jos padėtis leidžia teigti, kad junginys yra stechiometrinis hidroksiapatitas, kuriame Ca ir P molinis santykis yra 1,667.

Norint nustatyti mėginių drėkinimo savybes buvo matuotas kontaktinis kampas. Rezultatai pateikti 2 lentelėje.

2 lentelė. Kontaktinio kampo matavimų rezultatai CHAp dangoms (n = 3).

CHAp sluoksnių skaičius	Be pasluoksnio	$CaTiO_3$ pasluoksnis iš $Ca(Ac)_2$
10	97,2±0,1	93,1±3,5
20	100,3±3,5	94,1±0,6
30	93,4±1,0	92,2±1,3

CHAp mėginių, susintetintų su kalcio titanato pasluoksniu ir mėginių be pasluoksnio, išmatuotos kontaktinio kampo vertės yra gana artimos. Dangų su 10, 20 ir 30 sluoksniais nustatytas kontaktinis kampas kito nuo 92 iki 100°. Reikia pastebėti, kad kontaktinis kampas nežymiai sumažėja, kai sluoksnių skaičius yra 30. To priežastimi gali būti labiau įtrūkusių dangų susidarymas.

Šio tyrimo metu nustatyta, kad zolių-gelių metodas puikiai tinka kalcio hidroksiapatito dangoms ant silicio nitrido gauti. Ši sintezės metodologija leidžia kontroliuoti dangų fazinį grynumą ir morfologines savybes.

3.3 Pagreitintas kalcio hidroksiapatito plonų sluoksnių gavimas ant silicio padėklo zolių–gelių metodu

CHAp dangų, gautų ant silicio padėklo pagreitintos procedūros keliu, rentgeno spindulių difraktogramos yra pavaizduotos 16 pav. Akivaizdu, kad CHAp fazė formuojasi jau po 1 dengimo ciklo (5 pamerkimai).

Gautų dangų SEM nuotraukos pateiktos 17 pav. Matyti, kad susidaro homogeniškas, lygus CHAp dangų paviršius su mažomis granulėmis jau po vieno dengimo ciklo. Padidinus dengimo ciklų skaičių, paviršius tampa šiurkštesnis, susidarant didesnėmis granulėmis ir keliais įtrūkimais.

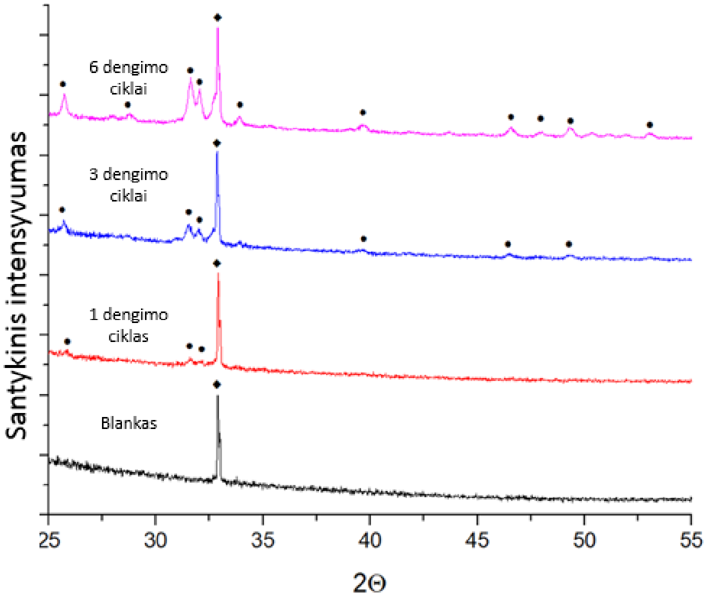

16 pav. CHAp dangų, gautų ant silicio padėklo pagreitintu būdu, rentgeno spindulių difraktogramos. Difrakcinės smailės: • - ($Ca_{10}(PO_4)6(OH)_2$ (PDF: 74-0566); ♦ - Si.

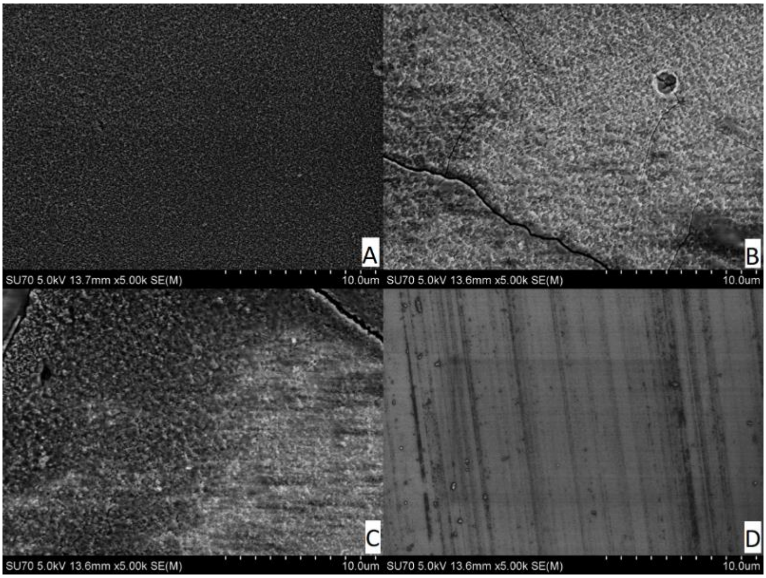

17 pav. CHAp dangų, gautų ant silicio padėklo, SEM nuotraukos.
Dengimo ciklų skaičius: 1 (A), 3 (B) 6 (C) ir 0 (D).

Tai gali būti dėl terminio plėtimosi tarp dangos ir padėklo nesuderinamumo. Po 6 dengimo ciklų susidaro didžiausio granulės.

SEM rezultatai sutampa su kontaktinio kampo matavimo rezultatais. Po pradinio dengimo kontaktinis kampas padidėjo nuo 67° (padėklas) iki 85°. Daugėjant sluoksnių skaičiui, kontaktinis kampas mažėjo dėl įtrūkimų susidarymo ir paviršiaus porėtumo didėjimo.

CHAp dangų ant silicio padėklo FTIR spektrai pateikti 18 pav.

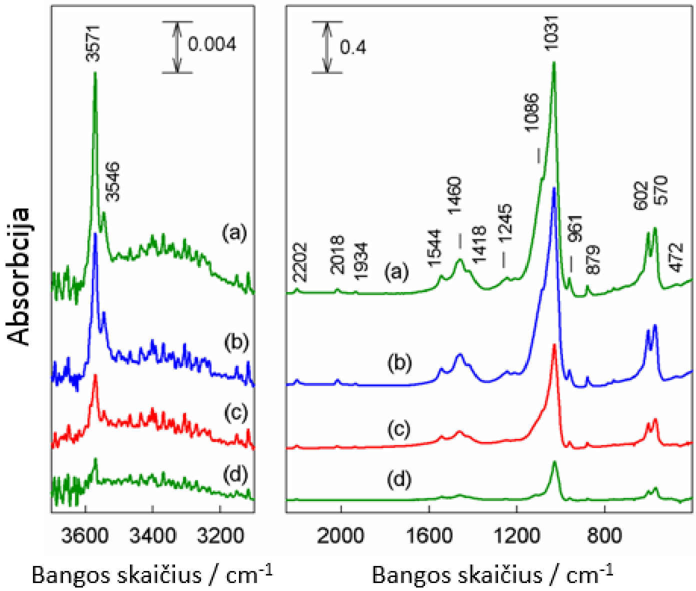

18 pav. CHAp dangų ant silicio padėklo FTIR spektrai: (a) 6 ciklai, (b) 5 ciklai; (c) 3 ciklai ir (d) 1 ciklas.

Nustatyta, kad laisvas PO_4^{3-} jonas priklauso tetrahedrinei (T_d) simetrijai. Absorbcijos juostų priskyrimas virpesiams yra pateiktas 3 lentelėje. PO_4^{3-} smailių padėtys sutampa su charakteringomis padėtimis, būdingomis hidroksiapatito struktūrai.

Aukštų dažnių srityje ties 3571 cm^{-1} stebima smaila O-H virpesių absorbcijos juosta. Šis rezultatas patvirtina, jog hidroksiapatito kristalinėje gardelėje yra hidroksidas. Santykinis karbonato jonų kiekis buvo nustatytas integruoto intensyvumo analizės metodu $A(CO_3^{2-})/A(PO_4^{3-})$ (3 lentelė). Iš jos galima matyti, kad santykinis karbonato kiekis šiek tiek mažėja didėjant sluoksnių skaičiui. Santykinis hidroksido jonų kiekis išlieka toks pat visuose tirtuose mėginiuose. Svarbu paminėti, kad hidroksiapatito struktūra išlieka visuomet, nepriklausomai nuo dangos ant Si padėklo storio.

3 lentelė. CHAp dangų ant Si padėklo FTIR absorbcijos juostos.

Molekulinė grupė	6 ciklai	5 ciklai	3 ciklai	1 ciklai	Moda
ν_1 (A_1), PO_4^{3-}	961,3 m	961,2 m	959,8 m	958,8 m	961,3 m
ν_2 (E), PO_4^{3-}	473 vw	473 vw	n.o.	n.o.	473 vw
ν_3 (F_2), PO_4^{3-}	1031,2 vs 1086 sh	1030,6 vs 1085 sh	1029,0 vs 1084 sh	1028,1 vs n.o.	1031,2 vs 1086 sh
ν_4 (F_2), PO_4^{3-}	570,4 s 601,8 s	570,8 s 602,2 s	569,2 s 601,1 s	567,8 s 600,6 s	570,4 s 601,8 s
$\nu_{as}(CO_3)$, CO_3^{2-}	1418 m, sh 1459,8 m 1544,3 m	1419 m, sh 1460,4 m 1543,9 m	1422 m, sh 1460,3 m 1543,1 m	1420 m, sh 1459,0 m 1541,1 m	1418 m, sh 1459,8 m 1544,3 m
$\gamma(CO_3)$, CO_3^{2-}	879,4 m	879,4 m	879,6 m	879,5 m	879,4 m
virštoniai/ kombinuoti režimai, PO_4^{3-}, HPO_4^{2-}	1933,9 w 2017,5 w 2202,2 w	1934,2 w 2017,0 w 2202,0 w	1935,9 w 2018,2 w 2202,7 w	1936,7 w 2017,0 m 2202,3 m	1933,9 w 2017,5 w 2202,2 w
ν(OH) OH^-	3545,6 vw 3570.8 w	3545,1 vw 3570,4 w	3544,7 vw 3570,3 w	n.o. 3570,0 w	3545,6 vw 3570,8 w
ν_1 (A_1), PO_4^{3-}	961,3 m	961,2 m	959,8 m	958,8 m	961,3 m

Santrumpos: n.o. – nestebėta; ν – išsitempimas; ν_{as} – asimetrinis išsitempimas; γ – neplokštuminė deformacija; vs – labai stipri; s – stipri; m – vidutinė; w – silpna; vw – labai silpna; sh –petys.

IŠVADOS

1. Pirmą kartą zolių-gelių metodu buvo gautos kalcio hidroksiapatito ($Ca_{10}(PO_4)_6(OH)_2$; CHAp) dangos ant titano padėklo, prieš dengimą iškaitinus titano paviršių ir/ar susintetinus kalcio titanato pasluoksnį. Ca-Ti-O pirmtako gelio termogravimetrinės analizės rezultatai parodė, kad pradine kalcio medžiaga gali būti naudojami kalcio acetatas ir kalcio hidroksidas. Ca-P-O pirmtako gelio, panašiai kaip ir Ca-Ti-O gelio, pagrindinė masės netekimo sritis stebėta ties 650 °C, kada netenkama apie 65% masės.
2. Nustatyta, kad CHAp fazei priskiriamų rentgeno spindulių difrakcinių atspindžių intensyvumas didėja didėjant sluoksnių skaičiui. TiO_2 fazės susidarymas, kuri mažina CHAp adheziją, gali būti nuslopintas Ti padėklą iškaitinant 650 °C temperatūroje, 5 h ore prieš dengiant dangas. Be to,

titano oksidui priskiriamų atspindžių intensyvumas išlieka nepakitęs dengiant dangas ant iškaitinto Ti su kalcio titanato pasluoksniu.

3. Pademonstruota, kad Ti padėklo paviršiaus modifikavimas neturėjo įtakos CHAp plonų dangų morfologijai. Didinant sluoksnių skaičių pastebėta, kad dangos tampa porėtesnės. Kontaktinio kampo matavimai parodė, kad susidaro hidrofilinės CHAp dangos, ir kad didinant sluoksnių skaičių nuo 20 iki 30, kontaktinis kampas mažėja nuo ~70 ^{o} iki 49,4-58,5^{o}.
4. Pirmą kartą kalcio hidroksiapatito dangos buvo susintetintos ant silicio nitrido padėklo substrato. CHAp dangos and silicio nitrido su kalcio titanato pasluoksniu ir be jo buvo gautos zolių-gelių metodu. Iš rentgeno spindulių difrakcinės analizės rezultatų nustatyta, kad CHAp formuojasi nepriklausomai, ar pasluoksnis yra, ar jo nėra, mėginius iškaitinant 5 h 650 °C temperatūroje. Reikia pastebėti, kad mėginiuose su $CaTiO_3$ pasluoksniu CHAp susidarė mažiau.
5. Iš SEM ir AFM nuotraukų nustatytos CHAp dangų morfologinės savybės. Pastebėta, kad jos priklauso nuo sluoksnių skaičiaus. Dengiant tiesiai ant silicio nitrido padėklo (be pasluoksnio), po 20 sluoksnių pastebėtos susidarančios salelės. Mėginiuose su kalcio titanato pasluoksniu pastebėta, kad salelės yra labiau sukibusios. Po 30 sluoksnių abiem atvejais mėginių paviršius pasidaro porėtas ir sutrūkinėjęs, paviršiuje salelės nebesusidaro.
6. Ramano spektroskopijos duomenys įrodė, kad dangos ant silicio nitrido pasižymi kalcio hidroksiapatito molekuline struktūra. Oksihidroksiapatito $Ca_{10}(PO_4)_6(OH)_{2-2x}O_x$ susidarymo nepastebėta. Žemo hidrofobiškumo dangų nustatytas kontaktinis kampas po 10, 20 ir 30 dengimo ciklų buvo tarp 92–100°.
7. Kalcio hidroksiapatito ploni sluoksniai buvo susintetinti iš Ca-P-O zolio-gelio ant silicio padėklo įmerkimo būdu, naudojant pagreitintą technologiją. CHAp dangos gautos 4 kartus greičiau nei įprastine procedūra.
8. CHAp fazės susidarymas po mėginių iškaitinimo 5 h ore 650 °C temperatūroje buvo patvirtintas rentgeno spindulių difrakcinės analizės duomenimis. CHAp paviršiaus SEM nuotraukos parodė, kad paviršius yra lygus ir homogeniškas, su mažomis granulėmis. Dalelių dydis (~100-200 nm) nepriklausė nuo dengimo skaičiaus.
9. Spektroskopiniai duomenys taip pat patvirtino tvarkingos CHAp kristalinės struktūros susidarymą dangose. SEM rezultatai sutapo su kontaktinio kampo matavimo rezultatais. Kontaktinis kampas padidėjo nuo 67° iki 85°. Tačiau toliau didinant sluoksnių skaičių, kontaktinis kampas dėl padidėjusio paviršiaus porėtumo ir įtrūkimų atsiradimo mažėjo.

ACKNOWLEDGEMENTS

This research work would not have been possible without the contribution and support from my colleagues, family and friends.

First of all, I would like to thank my supervisor Dr. Živilė Stankevičiūtė for her guidance, motivation and belief in this work. I would also like to thank academic consultant Prof. Habil. Dr. Aivaras Kareiva for providing a push when it was needed the most, consultations, guidance and contributing to this work.

I am also extremely grateful for my co-authors – Gediminas Niaura, Justinas Ceponkus, Julius Maminskas and others for their help in their field of expertise.

I would like to thank all my colleagues from the Faculty of Chemistry – Vilnius University for the time I have spend with you and for the most interesting discussions we had.

Lastly, I would like to thank my family for the patience and support during this time.

LIST OF PUBLICATIONS

1. P. Usinskas, Z. Stankeviciute, A. Beganskiene and A. Kareiva. Sol-gel derived porous and hydrophilic calcium hydroxyapatite coating on modified titanium substrate. *Surf. Coat. Technol.*, 307 (2016) 935-940.

2. P. Usinskas, Z. Stankeviciute, G. Niaura, G. Juodzbalys and A. Kareiva. Sol-gel processing of calcium hydroxyapatite thin films on silicon nitride (Si_3N_4) substrate. *J. Sol-Gel Sci. Technol.*, **83** (2017) 268-274.

3. P. Usinskas, Z. Stankeviciute, G. Niaura, J. Ceponkus and A. Kareiva, A novel approach for accelerated fabrication of calcium hydroxyapatite thin films. *Mater. Sci.-Medziagotyra* **25** (2019) 365-368.

Paper I

Sol-gel derived porous and hydrophilic calcium hydroxyapatite coating on modified titanium substrate

P. Usinskas, Z. Stankeviciute, A. Beganskiene and A. Kareiva.

Surf. Coat. Technol., 307 (2016) 935-940

https://doi.org/10.1016/j.surfcoat.2016.10.032

Surface & Coatings Technology 307 (2016) 935–940

Contents lists available at ScienceDirect

Surface & Coatings Technology

journal homepage: www.elsevier.com/locate/surfcoat

Sol-gel derived porous and hydrophilic calcium hydroxyapatite coating on modified titanium substrate

Pranas Usinskas *, Zivile Stankeviciute, Aldona Beganskiene, Aivaras Kareiva

Faculty of Chemistry, Vilnius University, Naugarduko 24, LT-03225 Vilnius, Lithuania

A R T I C L E   I N F O

Article history:
Received 15 June 2016
Revised 10 October 2016
Accepted in revised form 11 October 2016
Available online 12 October 2016

Keywords:
Hydroxyapatite
Titanium
Sublayers
Thin films
Sol-gel processing
Dip-coating

A B S T R A C T

Hydroxyapatite ($Ca_{10}(PO_4)_6(OH)_2$; HAp) coatings on titanium substrate were prepared by a sol-gel method combined with dip-coating technique. The influence of Ti substrate modification on the formation of HAp coatings was also investigated. To achieve a better quality of HAp coatings, Ti substrates were modified by adding a calcium titanate ($CaTiO_3$) sublayer or additional preheating at 650 °C. The thermal behavior of Ca-P-O and Ca-Ti-O precursor gels was investigated by thermogravimetric (TG-DTG) measurements. X-ray diffraction (XRD) analysis was employed to characterize the phase composition of synthesized coatings. Scanning electron microscopy (SEM) was used to study the morphological features of $CaTiO_3$ sublayers and HAp coatings surfaces. Contact angle (CA) measurements were used to evaluate the hydrophilic/hydrophobic properties of the end products.

1. Introduction

The demand for implants to improve human life quality keeps rising, as the bones lose their physical properties over time. Titanium is almost a perfect material for orthopedic and dental applications, because it is non-toxic, has great corrosion resistance, good mechanical and antibacterial properties [1–5]. Main drawbacks are weak titanium osteoconductivity and mechanical mismatch between bone and the implant [6,7]. This means, that after 10–25 years implants may fail and need to be replaced requiring an arduous, painful, and expensive revision surgery [8]. Coating titanium with osteoconductive biomaterials is one of various surface modification methods used to improve the mechanical, chemical and biological properties of titanium and its alloys for biomedical applications [1,4,9]. Hydroxyapatite ($Ca_{10}(PO_4)_6(OH)_2$; HAp) is a promising bioceramic material for this application, because it is similar to the inorganic part of the bones and teeth [10–13]. To increase osteoconductivity and serving time of the implant, the HAp coating must have particular properties. These include thickness, crystallinity, microstructure, surface roughness, porosity, Ca/P ratio and phase composition [14]. There is an agreement, that the purity of HAp in implant coatings must be as high as possible, the Ca/P ratio – 1.67, it must have good adhesion to the substrate and chemical stability [15]. Coating density and porosity are two conflicting requirements, as porosity is essential for the cell in-growth and coating density should be high for superior adhesion. Crystallinity is another factor to be taken into consideration, as to large extent it controls in vivo coating dissolution [16–19]. All these properties and also implant shape and its surface texture are variables to achieve coating with optimum properties.

The HAp thin films have been synthesized using many preparation methods including electrochemical deposition, biomimetic coating, hot isostatic pressing, pulsed laser deposition, sputter coating, dynamic mixing, ion beam sputtering, sol–gel deposition, thermal spraying, and combinations of these processes [4,18]. Although, plasma spray technique is the only method approved by the US Food and Drug Administration for biomedical applications and gained commercial success [20,21], the method has several disadvantages. First of all, it needs costly equipment. Moreover, plasma spraying may lead to phase and structural inhomogeneity, which result in resorption differences from area to area. Also, high temperatures cause HAp degradation to secondary phases like α-tricalcium phosphate, β-tricalcium phosphate, tetracalcium phosphate and oxyhydroxyapatite [18,21,22]. Finally, particles suffer rapid cooling, once deposited on the substrate and this may lead to formation of amorphous calcium phosphate (ACP), poor adhesion and cracking which may cause implant failure [20,23,24].

Sol-gel processing is a low cost and simple method, which allows achieving molecular - level mixing of the HAp precursors [21]. Much better chemical homogeneity of the HAp as compared to solid-state reactions could be achieved. Besides, milder conditions are applied and this leads to better structural integrity and less defects [24,25]. This also prevents metal substrates from mechanical degradation or phase transition as the coating process is carried out generally at ambient temperature [7,13,22,26]. The annealing of HAp coatings at elevated

* Corresponding author.
E-mail address: pranas_usinskas@yahoo.com (P. Usinskas).

http://dx.doi.org/10.1016/j.surfcoat.2016.10.032
0257-8972/

temperatures causes oxidation of Ti with formation of TiO_2. Although on the other hand titanium dioxide shows antibacterial properties [27], formation of this auxiliary phase may lead to cracking of HAp coatings. On the other hand, it improves the adhesion of HAp to the substrate and improves bioactivity [5,21,28,29]. In this contribution the HAp coatings on Ti substrate were prepared by sol-gel method using dip-coating technique. The aim of this study is to achieve HAp coatings on Ti with good adhesion, high porosity and correct phase composition by modifying its surface by adding a calcium titanate sublayer and/or pre-heating the substrate at elevated temperatures before the coating procedure. The effect of modification of Ti substrate on the formation of TiO_2 during annealing was investigated with the purpose to improve the adhesion of the HAp coating to the titanium.

2. Materials and methods

To deposit calcium titanate sublayers by a sol-gel route, citric acid (≥99.5%; Fluka) was dissolved in distilled water and mixed with titanium (IV) isopropoxide (TiIPro, 97%; Alfa Aesar). The solution was stirred at 90 °C until the titanium isopropoxide was completely dissolved. In the next step, either calcium acetate monohydrate $Ca(CH_3COO)_2 \cdot H_2O$ (99.9%; Fluka) or calcium hydroxide $Ca(OH)_2$ (≥95%, Roth) as the Ca source were added to the above solution. Therefore, two separate solutions were prepared. Next, 1,2-ethandiol (99.0%; Alfa Aesar) was added to the both solutions under stirring for 1 h at room temperature. Finally, these solutions were mixed with poly(vinyl alcohol) (PVA 70000, 99.5%; Aldrich) dissolved in distilled water.

To prepare thin HAp films, calcium acetate monohydrate was used as starting material. To the aqueous solution of $Ca(CH_3COO)_2$ the 1,2-ethandiol was added. The obtained mixture was stirred for 30 min at 65 °C. Then ethylenediaminetetraacetic acid (EDTA; 99.0%; Alfa Aesar) was added, and after 15 min triethanolamine (TEA; 99.0%; Merck) was slowly added as a complexing agent. The solution was stirred for the next 10 h. Then diluted orthophosphoric acid (H_3PO_4 85%; Reachem) was added (Ca/P ratio was 1.67). Finally, this solution was mixed with PVA dissolved in distilled water.

These solutions were used to synthesize calcium titanate sublayers and calcium hydroxyapatite thin films on Ti substrate using dip-coating technique. Additionally, in some experiments the Ti substrates were heat-treated at 650 °C for 5 h, after reaching this temperature with a heating rate of 1 °C/min. Before coating, all substrates were cleaned in an ultrasonic bath with acetone, ethanol and distilled water sequentially. The dip-coated samples were also annealed at 650 °C for 5 h using the same heating rate of 1 °C/min. Fig. 1 shows the schematical view of sol-gel preparation of calcium titanate sublayers and calcium hydroxyapatite thin films on Ti substrate. The coating and annealing procedures were repeated 10, 20 and 30 times.

The formation of coatings on Ti substrate was performed using a dip-coater (KSV Dip Coater D). Thermogravimetric analysis of precursor gels was performed using Perkin Elmer Pyris 1 TGA instrument. The synthesis products were analyzed by X-ray diffraction (XRD, Rigaku MiniFlex II) analysis, scanning electron microscopy (SEM, Hitachi SU 70) and contact angle measurements (KSV Instrument CAM 100).

3. Results and discussion

The results of thermogravimetric (TG) analysis of synthesized Ca-Ti-O precursor gels are presented in Fig. 2. Three weight loss mechanisms in the temperature ranges of 50–250 °C, 250–430 °C and 430–650 °C can be distinguished in the TG curves. In the first step, the weight loss (approximately 15%) is associated with evaporation of the adsorbed and structural water. In the second stage the main decomposition of the gel occurs (45%) due to thermal degradation of organic parts (ethylene glycol, PVA, citrates) present in the gels. Finally, pyrolysis of the remaining constituents (about 20%) of the gels between 430 and 650 °C takes place. No further weight loss could be observed above 650 °C.

Interestingly, the TG curves Ca-Ti-O precursor gels obtained using calcium acetate and calcium hydroxide as starting material are almost identical. The TG/DTA curves of the Ca-P-O precursor gel are shown in Fig. 2. Again, in the first mass loss stage (about 15%) in the temperature range of 160–200 °C evaporation of moisture from the gel takes place. The main decomposition of the gel with the mass loss of about 65% could be observed up to 650 °C, similarly to the Ca-Ti-O gel.

Fig. 3 represents XRD patterns of HAp coatings fabricated on the Ti substrate which was heat-treated before dip-coating procedure. The pre-heating of Ti substrate was performed to create an initial titanium oxide layer that would prevent further development of oxide layer during the formation of the coatings.

The intensity of reflections attributable to the HAp phase increases with increasing number of coating layers. Consequently, the intensity of the diffraction peaks related to the Ti substrate monotonically decreases. Evidently, the formation of TiO_2 is suspended by the initial pre-heating process of substrate at 650 °C for 5 h in air. The intensity of characteristic diffraction peaks of titanium oxide remains unchanged upon increasing the number of dip-coating and annealing procedures.

For example, Fig. 4 represents XRD patterns of HAp coatings obtained directly on cleaned titanium substrate without preliminary heating at elevated temperatures. In this case, the HAp diffraction peaks are visible already after 10 coating procedures. Their intensity monotonically increases with increasing number of layers up to 30 layers. Again, the intensity of diffraction peak attributable to Ti decreased with increasing number of HAp layers. However, the intensity of the peaks associated with TiO_2 phase evidently increases, indicating the continuous growth

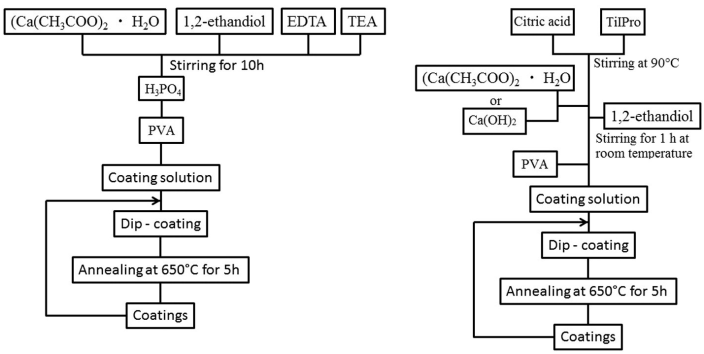

Fig. 1. A schematical diagrams of sol-gel preparation of calcium titanate sublayers (at left) and calcium hydroxyapatite thin films (at right) on Ti substrate.

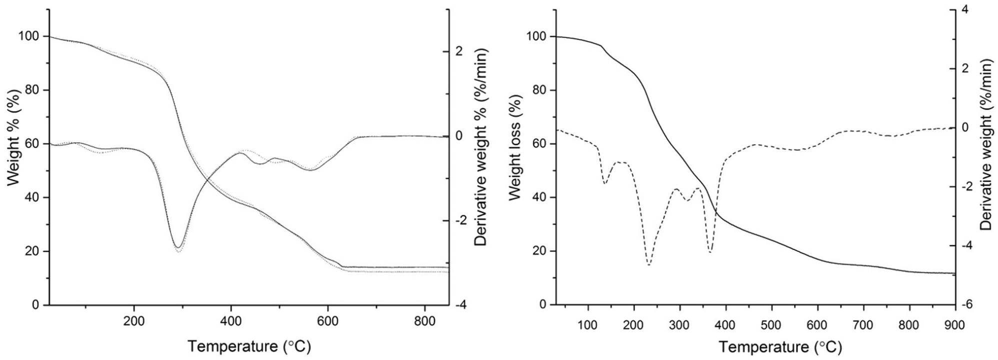

Fig. 2. TG/DTA curves of Ca-Ti-O precursor gels obtained using calcium acetate (dotted line) and calcium hydroxide (solid line) as starting material (left) and TG/DTA curves of Ca-P-O precursor gels (right).

of titanium oxide. These results confirm the effect of pre-annealing procedure of Ti substrate to prevent further development of titanium oxide layer during fabrication of the HAp coatings.

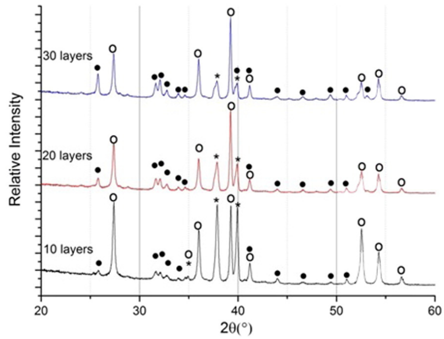

Fig. 3. XRD patterns of HAp films on the pre-heated at 650 °C for 5 h in air. Diffraction peaks: • - $Ca_{10}(PO_4)_6(OH)_2$ (PDF: 74-0566); o – TiO_2 (PDF: 73-2224); * - Ti (PDF: 44-1294).

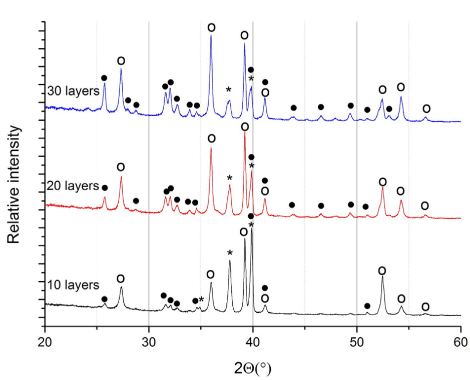

Fig. 4. XRD patterns of HAp films on Ti substrate. Diffraction peaks: • - $Ca_{10}(PO_4)_6(OH)_2$ (PDF: 74-0566); o – TiO_2 (PDF: 73-2224); * - Ti (PDF: 44-1294).

Figs. 5 and 6 represent XRD patterns of HAp coatings obtained on the Ti substrates prepared with 10 sublayers of $CaTiO_3$ (calcium acetate was used as Ca source). As evident, the peaks attributable to $CaTiO_3$ are clearly visible after 10 coating cycles, however, along with $CaTiO_3$, TiO_2 is present at the Ti surface. The formation of HAp is visible after 10 dipping procedures. After additional 10 coating cycles, the intensity of HAp diffraction peaks evidently increased. The diffraction peaks attributable to $CaTiO_3$ are not visible anymore, as the sublayer of $CaTiO_3$ was fully covered by HAp. Moreover, it appears that TiO_2 is also forming in the sol-gel processing when the Ti substrate was not preheated before the formation of the $CaTiO_3$ sublayer (see Fig. 5). The intensity of TiO_2 reflections increases with each step of dipping in the HAp gel procedure. Thus, the initial formation of a sublayer of calcium titanate on the Ti substrate did not prevent the formation of titanium oxide.

The situation is different, when the Ti substrate was pre-heated before the formation of a calcium titanate sublayer. Apparently, the intensities of diffraction peaks of TiO_2 remain unchanged with increasing number of HAp layers up to 20 (see Fig. 6).

The same set of experiments was performed when calcium hydroxide was used as Ca source to form a $CaTiO_3$ sublayer on the Ti substrate. XRD patterns of HAp coatings obtained on sublayers of $CaTiO_3$ (calcium hydroxide was used as Ca source), which were fabricated on heat-

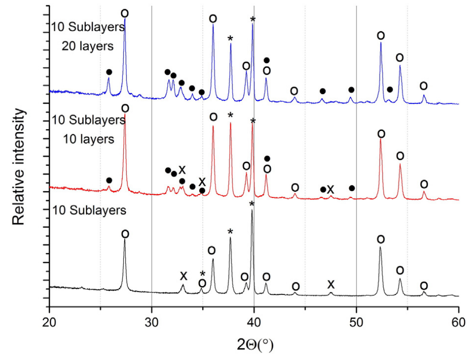

Fig. 5. XRD patterns of HAp films on Ti (without initial pre-heating) with $CaTiO_3$ sublayer (derived from calcium acetate) annealed at 650 °C for 5 h in air. Diffraction peaks are marked: • - $Ca_{10}(PO_4)_6(OH)_2$ (PDF: 74-0566); o – TiO_2 (PDF: 73-2224); * - Ti (PDF: 44-1294); x – $CaTiO_3$ (PDF: 22-0153).

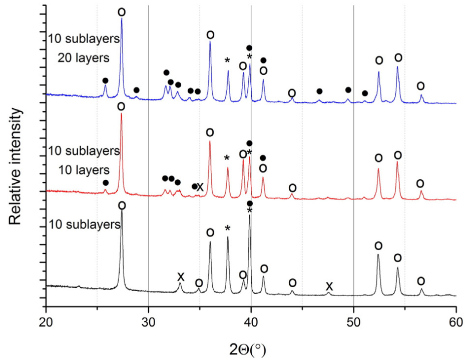

Fig. 6. XRD patterns of HAp films on Ti (initially pre-heated) with $CaTiO_3$ sublayer (derived from calcium acetate) annealed at 650 °C for 5 h in air. Diffraction peaks are marked: • - $Ca_{10}(PO_4)_6(OH)_2$ (PDF: 74-0566); o – TiO_2 (PDF: 73-2224); * - Ti (PDF: 44-1294); x – $CaTiO_3$ (PDF: 22-0153).

treated and just cleaned titanium substrate indicated that the formation of HAp proceeds independently on the nature of the calcium starting material. The intensity of reflections attributable to TiO_2 remains unchanged with increasing the number of HAp coatings on the heat-treated Ti substrate (with $CaTiO_3$ sublayer). However, the amount of TiO_2 increased monotonically when Ti without initial pre-heating was used.

The morphology of coatings was investigated using scanning electron microscopy (SEM). Fig. 7 shows the SEM micrographs of HAp obtained on as-prepared for coating and thermally processed Ti substrates. Obviously, the influence of pre-annealing of the substrate on the morphology of HAp thin films is negligible. However, the formation of a more porous surface with increasing number of layers is evident.

As mentioned before, the $CaTiO_3$ sublayer was synthesized using calcium acetate and calcium hydroxide, respectively as starting materials on both pre-heated and as-received Ti substrates. The SEM micrographs of the $CaTiO_3$ sublayer and Hap layer on $CaTiO_3$ sublayer obtained from calcium acetate on heat-treated Ti substrates are shown in Fig. 8. The main morphological features of calcium titanate are quite different compared to HAp.

The $CaTiO_3$ islands 2–3 μm in size composed of spherical nanoparticles have formed on the pre-heated Ti substrate. This type of surface morphology disappeared after dipping this substrate 10 times to the Ca-P-O sol-gel solution. Again, the formation of a porous HAp surface is observed. With increasing number of HAp layers, however, the surface morphology of thin films remains almost unchanged. The SEM micrographs of $CaTiO_3$ sublayer and HAp on $CaTiO_3$ sublayer obtained from calcium hydroxide on just cleaned Ti substrates are shown in Fig. 9. Apparently, after formation of the HAp films the surface became flatter and more porous. The microstructure of fabricated HAp is very similar to that observed for the HAp coating on Ti substrate without initial pre-heating and without additional $CaTiO_3$ sublayer.

To estimate the wettability of the coatings obtained, contact angle measurements (CAM) were performed. The results of these measurements are summarized in Table 1.

Interestingly, the hydrophobic properties are not dependent on a number of HAp layers up to 20. The contact angle of dip-coated samples on unheated and pre-heated Ti substrates with and without $CaTiO_3$ sublayers remains around 70°. However, increasing the number of HAp layers to 30, the contact angle decreased monotonically from ~70 down to 49.4–58.5°. This very interesting tendency could be related to the phase composition of the HAp films [30]. As evident from the XRD patterns, the crystallinity of HAp also increases significantly after obtaining 30 layers on the substrates. So, the decrease of hydrophobicity is associated with formation of HAp crystallites with hydrophilic OH groups. The surfaces remained hydrophilic after 30 immersing, withdrawal and annealing steps independent of the Ti surface pre-treatment conditions. The increased hydrophilicity of HAp-coated Ti enhances a wettability of the coatings. Consequently, such coatings can accelerate osteointegration, i. e. structural and functional connection between living bone and the surface of a load-bearing artificial implant [30].

4. Conclusion

This study reports on composition, microstructure and hydrophilic/hydrophobic properties of hydroxyapatite ($Ca_{10}(PO_4)_6(OH)_2$; HAp) coatings deposited from sol-gel precursors on Ti substrates. HAp coatings on Ti were achieved by modifying its surface by a calcium titanate sublayer and/or pre-heating the substrate at elevated temperatures before the coating procedure. The results of TG analysis of synthesized Ca-Ti-O precursor gels obtained using calcium acetate and calcium

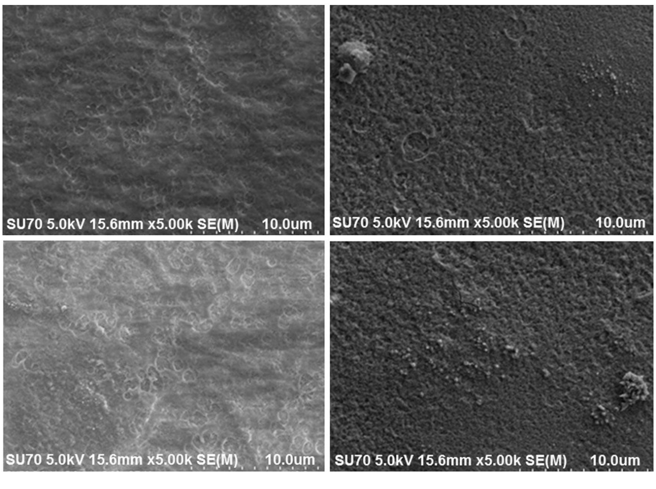

Fig. 7. SEM micrographs of HAp coatings obtained on Ti without initial pre-heating (bottom) and on initially pre-heated (top): 10 (left) and 30 layers (right).

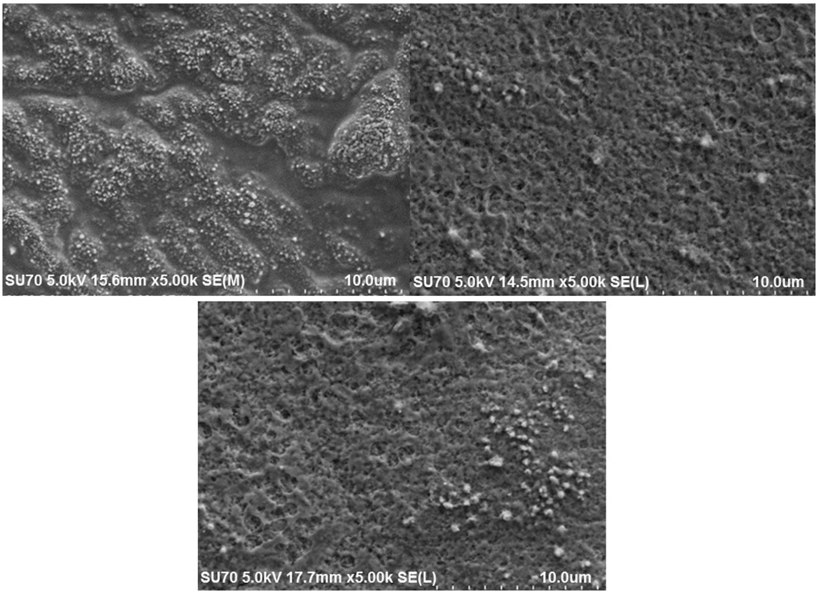

Fig. 8. SEM micrographs of $CaTiO_3$ obtained from calcium acetate on heat-treated Ti substrate (left) and HAp coatings prepared on $CaTiO_3$ sublayer: 10 layers (bottom) and 20 layers (right).

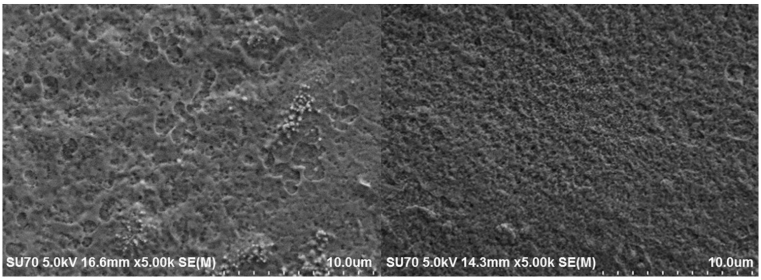

Fig. 9. SEM micrographs of $CaTiO_3$ obtained from calcium hydroxide on Ti substrate without initial pre-heating (left) and 20 layers of HAp coatings prepared on $CaTiO_3$ sublayer (right).

hydroxide as starting material were almost identical. The main decomposition of the Ca-P-O precursor gel with the mass loss of about 65% was observed up to 650 °C, similarly to the Ca-Ti-O gel. The intensity of reflections attributable to the HAp phase in the XRD patterns of fabricated films increased with increasing number of coating layers. The formation of TiO_2 phase which reduces adhesion of HAp films was arrested by initial pre-heating of the substrate at 650 °C for 5 h in air. Besides, the intensity of reflections attributable to TiO_2 remained unchanged with increasing the number of HAp coatings on the heat-treated Ti substrates with $CaTiO_3$ sublayer. Moreover, it was demonstrated that surface modification of Ti substrate did not have any influence on the morphology of the HAp thin films. However, the formation of more porous surface with increasing amount of layers was evident. Contact angle measurements showed that with increasing the number of HAp layers from 20 up to 30, the contact angle decreased monotonically from ~70 to 49.4–58.5°, indicating the formation of high quality of hydrophilic Hap coatings.

Table 1
Contact angle results determined for CHAp coatings (n = 3).

Amount of CHAp layers	Pre-heated substrates			Unheated substrates		
	Without sublayer	$CaTiO_3$ sublayer from $Ca(Ac)_2$	$CaTiO_3$ sublayer from $Ca(OH)_2$	Without sublayer	$CaTiO_3$ sublayer from $Ca(Ac)_2$	$CaTiO_3$ sublayer from $Ca(OH)_2$
10	76.0 ± 1.2	62.9 ± 1.9	83.4 ± 0.4	66.2 ± 2.5	72.5 ± 5.9	80.6 ± 6.1
20	76.4 ± 2.1	76.2 ± 1.5	71.6 ± 3.8	68.9 ± 3.2	67.2 ± 0.9	72.0 ± 1.0
30	49.4 ± 0.7	58.5 ± 5.5	51.4 ± 3.2	52.1 ± 1.5	53.4 ± 5.6	51.3 ± 2.2

Acknowledgments

This research was funded by a grant KALFOS (No. LJB-2/2015) from the Research Council of Lithuania.

References

[1] X. Liu, P.K. Chu, C. Ding, Surface modification of titanium, titanium alloys, and related materials for biomedical applications, Mater. Sci. Eng. R 47 (2004) 49–121.
[2] M. Geetha, A.K. Singh, R. Asokamani, A.K. Gogia, Ti based biomaterials, the ultimate choice for orthopaedic implants – a review, Prog. Mater. Sci. 54 (2009) 397–425.
[3] F.A. Shah, M. Trobos, P. Thomsen, A. Palmquist, Commercially pure titanium (cp-Ti) versus titanium alloy (Ti6Al4V) materials as bone anchored implants — is one truly better than the other? Mater. Sci. Eng. C. 62 (2016) 960–966.
[4] E. Mohseni, E. Zalnezhad, A.R. Bushroa, Comparative investigation on the adhesion of hydroxyapatite coating on Ti–6Al–4V implant: a review paper, Int. J. Adhes. Adhes. 48 (2014) 238–257.
[5] H.-W. Kim, Y.-H. Koh, L.-H. Li, S. Lee, H.-E. Kim, Hydroxyapatite coating on titanium substrate with titania buffer layer processed by sol–gel method, Biomaterials 25 (2004) 2533–2538.
[6] A. Barbas, A.S. Bonnet, P. Lipinski, R. Pesci, G. Dubois, Development and mechanical characterization of porous titanium bone substitutes, J. Mech. Behav. Biomed. Mater. 9 (2012) 34–44.
[7] M. Catauro, F. Bollino, F. Papale, Biocompatibility improvement of titanium implants by coating with hybrid materials synthesized by sol–gel technique, J. Biomed. Mater. Res. A 102 (2014) 4473–4479.
[8] E. Fournier, R. Devaney, M. Palmer, J. Kramer, R. El Khaja, M. Fonte, Superelastic orthopedic implant coatings, J. Mater. Eng. Perform. 23 (2014) 2464–2470.
[9] R. Bosco, E.R.U. Edreira, J.G.C. Wolke, S.C.G. Leeuwenburgh, J.J.J.P. van den Beucken, J.A. Jansen, Instructive coatings for biological guidance of bone implants, Surf. Coat. Technol. 233 (2013) 91–98.
[10] S.V. Dorozhkin, Calcium orthophosphate-containing biocomposites and hybrid biomaterials for biomedical applications, J. Funct. Biomater. 6 (2015) 708–832.
[11] L.-X. Yang, J.-J. Yin, L.-L. Wang, G.-X. Xing, P. Yin, Q.-W. Liu, Hydrothermal synthesis of hierarchical hydroxyapatite: preparation, growth mechanism and drug release property, Ceram. Int. 38 (2012) 495–502.
[12] S. Subramaniam, Y.-H. Fang, S. Sivasubramanian, F.-H. Lin, C.-p. Lin, Hydroxyapatite-calcium sulfate-hyaluronic acid composite encapsulated with collagenase as bone substitute for alveolar bone regeneration, Biomaterials 74 (2016) 99–108.
[13] S. Shadanbaz, G.J. Dias, Calcium phosphate coatings on magnesium alloys for biomedical applications: a review, Acta Mater. 8 (2012) 20–30.
[14] R.A. Surmenev, M.A. Surmeneva, A.A. Ivanova, Significance of calcium phosphate coatings for the enhancement of new bone osteogenesis – a review, Acta Mater. 10 (2014) 557–579.
[15] L. Sun, C.C. Berndt, K.A. Gross, A. Kucuk, Material fundamentals and clinical performance of plasma-sprayed hydroxyapatite coatings: a review, J. Biomed. Mater. Res. A 58 (2001) 570–592.
[16] Y.C. Tsui, C. Doyle, T.W. Clyne, Plasma sprayed hydroxyapatite coatings on titanium substrates part 1: mechanical properties and residual stress levels, Biomaterials 19 (1998) 2015–2029.
[17] M. Epple, R.A. Surmenev, Bioactive surfaces for hard tissue regeneration, RSC Adv. 3 (2013) 11057.
[18] M. Mittal, S.K. Nath, S. Prakash, Improvement in mechanical properties of plasma sprayed hydroxyapatite coatings by Al_2O_3 reinforcement, Mater. Sci. Eng. C. Mater. Biol. Appl. 33 (2013) 2838–2845.
[19] R.B. Heimann, Structure, properties, and biomedical performance of osteoconductive bioceramic coatings, Surf. Coat. Technol. 233 (2013) 27–38.
[20] K. Balani, Y. Chen, S.P. Harimkar, N.B. Dahotre, A. Agarwal, Tribological behavior of plasma-sprayed carbon nanotube-reinforced hydroxyapatite coating in physiological solution, Acta Mater. 3 (2007) 944–951.
[21] W. Xu, W. Hu, M. Li, C.e. Wen, Sol–gel derived hydroxyapatite/titania biocoatings on titanium substrate, Mater. Lett. 60 (2006) 1575–1578.
[22] C.J. Tredwin, G. Georgiou, H.-W. Kim, J.C. Knowles, Hydroxyapatite, fluor-hydroxyapatite and fluorapatite produced via the sol–gel method: bonding to titanium and scanning electron microscopy, Dent. Mater. J. 29 (2013) 521–529.
[23] D.M. Liu, T. Troczynski, W.J. Tseng, Water-based sol-gel synthesis of hydroxyapatite: process development, Biomaterials 22 (2001) 1721–1730.
[24] E. Milella, F. Cosentino, A. Licciulli, C. Massaro, Preparation and characterisation of titania/hydroxyapatite composite coatings obtained by sol–gel process, Biomaterials 22 (2001) 1425–1431.
[25] P.A. Ramires, A. Romito, F. Cosentino, E. Milella, The influence of titania/hydroxyapatite composite coatings on in vitro osteoblasts behaviour, Biomaterials 22 (2001) 1467–1474.
[26] M. Catauro, F. Bollino, F. Papale, Preparation, characterization, and biological properties of organic–inorganic nanocomposite coatings on titanium substrates prepared by sol–gel, J. Biomed. Mater. Res. A. 102 (2014) 392–399.
[27] X. Hu, K.G. Neoh, J. Zhang, E.-T. Kang, Bacterial and osteoblast behavior on titanium, cobalt–chromium alloy and stainless steel treated with alkali and heat: a comparative study for potential orthopedic applications, J. Colloid Interface Sci. 417 (2014) 410–419.
[28] N. Ohtsu, K. Sato, A. Yanagawa, K. Saito, Y. Imai, T. Kohgo, A. Yokoyama, K. Asami, T. Hanawa, CaTiO(3) coating on titanium for biomaterial application—optimum thickness and tissue response, J. Biomed. Mater. Res. A 82 (2007) 304–315.
[29] G. He, B. Guo, H. Wang, C. Liang, L. Ye, Y. Lin, X. Cai, Surface characterization and osteoblast response to a functionally graded hydroxyapatite/fluoro-hydroxyapatite/titanium oxide coating on titanium surface by sol–gel method, Cell Prolif. 47 (2014) 258–266.
[30] S.A. Pauline, N. Rajendran, Biomimetic novel nanoporous niobium oxide coating for orthopaedic applications, Appl. Surf. Sci. 290 (2014) 448–457.

Paper II

Sol-gel processing of calcium hydroxyapatite thin films on silicon nitride (Si3N4) substrate

P. Usinskas, Z. Stankeviciute, G. Niaura, G. Juodzbalys and A. Kareiva

J. Sol-Gel Sci. Technol., 83 (2017) 268-274

DOI: 10.1007/s10971-017-4431-y

J Sol-Gel Sci Technol
DOI 10.1007/s10971-017-4431-y

ORIGINAL PAPER: FUNCTIONAL COATINGS, THIN FILMS AND MEMBRANES (INCLUDING DEPOSITION TECHNIQUES)

Sol–gel processing of calcium hydroxyapatite thin films on silicon nitride (Si_3N_4) substrate

P. Usinskas[1] · Z. Stankeviciute[1] · G. Niaura[2] · J. Maminskas[3] · G. Juodzbalys[3] · A. Kareiva[4]

Received: 3 March 2017 / Accepted: 18 May 2017

Abstract Calcium hydroxyapatite ($Ca_{10}(PO_4)_6(OH)_2$, CHAp) films were obtained on silicon nitride (Si_3N_4) substrate by a sol–gel method using a dip-coating technique. In the sol–gel process, ethylendiamintetraacetic acid and 1,2-ethandiol, triethanolamine, and polyvinyl alcohol were used as complexing agents and gel network forming agents, respectively. Calcium acetate monohydrate was used as Ca source. The samples were annealed at 650 °C for 5 h in air after each dip-coating procedure which was repeated 10, 20, and 30 times. The coatings were characterized using X-ray diffraction, scanning electron microscopy, atomic force microscopy, Raman spectroscopy, and contact angle measurements. Monophasic CHAp layers on silicon nitride (Si_3N_4) substrate were fabricated and characterized for the first time to the best our knowledge.

Graphical Abstract

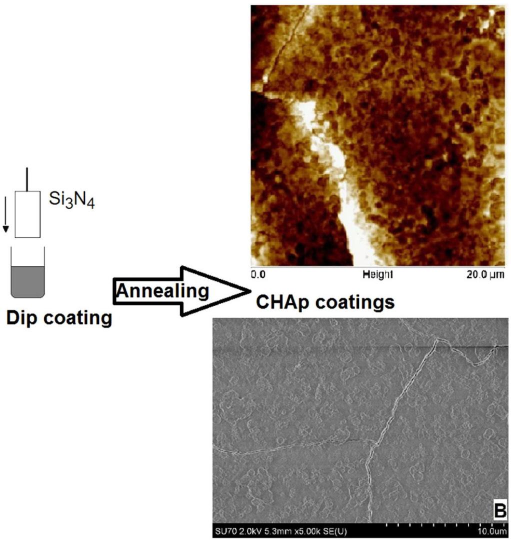

Keywords Calcium hydroxyapatite · Sol–gel processing · Dip-coating · Thin films · Si_3N_4 substrate

✉ P. Usinskas
pranas_usinskas@yahoo.com

[1] Department of Applied Chemistry, Vilnius University, Naugarduko 24, 03225 Vilnius, Lithuania

[2] Department of Organic Chemistry, Center for Physical Sciences and Technology, Sauletekio Ave. 3, 10257 Vilnius, Lithuania

[3] Department of Maxillofacial Surgery, Lithuanian University of Health Sciences, Kaunas, Lithuania

[4] Department of Inorganic Chemistry, Vilnius University, Naugarduko 24, 03225 Vilnius, Lithuania

1 Introduction

As the demand for bone implants keeps increasing [1], biomaterials research has focused on the improvement of implant design features in an attempt to accelerate bone healing at early implantation times [2, 3]. Materials used for

Published online: 27 May 2017

implantation could be divided to metals, ceramics, and plastics [4]. The metals and metal alloys are usually used to replace load-bearing bones with titanium being the most popular. Because of their chemical properties, the range of metals is narrowed to stainless steels, titanium and its alloys, tantalum, and cobalt–chromium-based alloys. As for dental applications, the metal-implants are preferable for patients up to today. However, the release of metal particles and ions can lead to osteolysis and allergies [5, 6]. Also, implant after a while loses stability due to mechanical differences between bone and metal. Moreover, if screws and plates are used to secure bone fractures, implant will have to be removed by a surgical procedure [3, 7–9]. High density polyethylene (PE) is also used for hip and knee replacement with predictable and durable results. It shows good properties of biocompatibility, good wear resistance, and chemical stability. Although, during the years PE implant wear particles give adverse biological effects like osteolysis (a painful inflammatory reaction) [4, 10].

Silicon nitride (Si_3N_4) is a non-oxide ceramic that was primary used for industrial applications like internal combustion and high-temperature gas turbines. After improvements were made in its synthesis, processing, and properties, Si_3N_4 is now one of the most extensively studied ceramics in history. It is used where extreme toughness, strength, low coefficient of friction, and low wear properties are required and these properties are ideal for the medical applications like bearing components of prosthetic hip and knee joints as it is biocompatible and have the ability to propagate human osteoblast cells in vitro [4, 9, 11, 12]. The fact, that silicon nitride dissolves in aqueous fluids propose that wear particles can dissolve in vivo, which may reduce possibility of infection and increase the serving time of the implant [13, 14].

To optimize bonding of implant material and tissue, surface modifications of the implant are being utilized like coating, surface etching, and blasting [2, 8, 14, 15]. Coatings of synthetic calcium hydroxyapatite (CHAp, $Ca_{10}(PO_4)_6(OH)_2$) are being extensively explored as it has been clinically applied on orthopedic and dental implants due to their excellent biocompatibility and osseointegration [16–20]. CHAp has chemical similarity to the mineral component of mammalian bones and teeth [6, 7, 21]. To achieve long-term implant stability and good osseointegration, CHAp coating should have particular properties like porosity, crystallinity, uniformity of coating thickness, surface roughness, phase purity, and good adhesion [2, 22, 23]. There is an agreement, that chemical purity must be as high as possible with Ca/P ratio of 1.67 and a trend to produce crystalline coatings [24]. Also, a good adhesion and no cracking is desired. Other desired properties may depend on the application as they may be conflicting. For example, the coating density and porosity are two conflicting requirements, as porosity is essential for the cell in-growth and coating density should be high for superior adhesion [25].

There are many techniques used for implant coating like plasma spraying, thermal spraying, pulsed laser ablation, dynamic mixing, electrophoretic deposition, biomimetic coating, ion-beam-assisted-deposition, hot isostatic pressing, and others [3, 22, 23]. Amongst all the techniques, plasma spraying is the most used, as it was approved by the Food and Drug Administration, USA for biomedical coatings. However, despite of the advantages of this technique, the coated hydroxyapatite shows poor mechanical properties [18, 22]. The dip-coating coating technique along with sol–gel processing is an inexpensive and fast technique that requires simple equipment. Besides, it allows to mass produce coatings on big substrates of irregular shapes. The parameters of coating can be controlled through the sol–gel concentration, withdrawal speed, and annealing temperature [8, 26]. Combination of sol–gel and dip-coating provides other potential advantages, such as a high purity and homogeneity and reduced thickness of coating. On the other hand, it has some limitations like brittleness of the coating and high annealing temperatures [8].

In this study, the dip-coated CHAp layers from sol–gel solution were fabricated for the first time to the best our knowledge on silicon nitride substrate. Considering the properties of substrate, such as high strength and fracture toughness, inherent phase stability, scratch resistance, low wear, biocompatibility, hydrophilic behavior, easier radiographic imaging and resistance to bacterial biofilm formation and the properties of CHAp coating like excellent biocompatibility and osseointegration should be interesting for orthopedic applications [27]. To obtain CHAp thin films on silicon nitride we used the same synthetic procedure as for Ti substrate [28]. Since many reports about the importance of sublayer to increase adhesion of CHAp coatings on Ti substrate are known, the CHAp coatings on silicon nitride substrates were prepared with or without calcium titanate sublayer. However, the special challenge to coat this material was that silicon nitride was never coated by CHAp coating. The samples were characterized by X-ray diffraction (XRD) analysis, scanning electron microscopy (SEM), atomic force microscopy (AFM), Raman spectroscopy and contact angle measurements (CAM).

2 Materials and methods

Materials and methods used for this experiment were similar to the previously reported [28]. For the deposition of calcium titanate sublayers by a sol–gel route, the citric acid (≥99.5%; Fluka) was dissolved in distilled water and mixed with titanium (IV) isopropoxide (TiIPro, 97%; Alfa Aesar).

The solution was stirred at 90 °C until the titanium isopropoxide was completely dissolved. In the next step, calcium acetate monohydrate $Ca(CH_3COO)_2{\cdot}H_2O$ (99.9%; Fluka) was added to the above solution as the Ca source. Next, 1,2-ethandiol (99.0%; Alfa Aesar) was added to the solution under stirring for 1 h at room temperature. Finally, the solution was mixed by ratio 5:3 with poly(vinyl alcohol) (PVA 70000, 99.5%; Aldrich) dissolved in distilled water. Molar ratios: 0.03 mol $Ca(CH_3COO)_2{\cdot}H_2O$, 2.22 mol$\cdot H_2O$, 0.036 mol 1,2-ethandiol, 0.033 mol ethylenediaminetetraacetic acid (EDTA), 0.113 triethanolamine (TEA), 0.018 mol $H_3(PO)_4$ and 0.00004 mol PVA 70,000, 5.39 mol H_2O.

To prepare CHAp films, calcium acetate monohydrate was used as starting material. To the aqueous solution of Ca $(CH_3COO)_2$ the 1,2-ethandiol was added. The obtained mixture was stirred for 30 min at 65 °C. Then EDTA (99.0%; Alfa Aesar) was added, and after 15 min TEA (99.0%; Merck) was slowly added as a complexing agent. The solution was stirred for the next 10 h. Then diluted orthophosphoric acid (H_3PO_4 85%; Reachem) was added (Ca/P ratio was 1.67). Finally, this solution was mixed by ratio 5:3 with PVA dissolved in distilled water. Molar ratios —0.003 mol $Ca(CH_3COO)_2{\cdot}H_2O$, 0.003 mol TiIPro, 0.009 mol citric acid, 2.22 mol H_2O and 0.00004 mol PVA 70,000, 5.39 mol H_2O.

The calcium titanate sublayers and CHAp thin films on silicon nitride substrate were obtained using dip-coating technique. Before the processing, all substrates were cleaned in an ultrasonic bath with acetone, ethanol, and distilled water sequentially. The dip-coated samples were annealed at 650 °C for 5 h, reaching this temperature with heating rate of 1 °C/min. The samples were left to cool to the room temperature within the furnace. Coating and annealing procedures were repeated 10, 20, and 30 times. The formation of coatings on silicon nitride substrate was performed using a dip-coater (KSV Dip Coater D). The dipping rate of substrate was 85 mm/min and lifting rate was 40 mm/min. The substrate was left in the gel solution for 20 s.

The synthesis products were analyzed by XRD (Rigaku MiniFlex II) analysis, SEM(Hitachi SU 70), AFM measurements (Veeco Bioscope 2 atomic force microscope) and CAM (KSV Instrument CAM 100). Raman spectra were recorded using inVia Raman (Renishaw, United Kingdom) spectrometer equipped with thermoelectrically cooled (−70 °C) CCD camera and microscope. Raman spectra were excited with 442 nm radiation from He–Cd laser. The 50×/0.75 NA objective lens and 2400 lines/mm grating were used to record the Raman spectra. The accumulation time was 400 s. To avoid damage of the sample, the laser power at the sample was restricted to 0.8 mW. The Raman frequencies were calibrated using the silicon standard according to the line at 520.7 cm^{-1} and air O_2 (1555.0 cm^{-1}) and N_2 (2330.1 cm^{-1}) bands. The high resolution Raman spectra were excited with 632.8 nm He–Ne laser (1 mW power at the sample) and dispersed with 2400 lines/mm grating. Spectral slit width near 1500 cm^{-1} determined by analysis of air O_2 band was 3.4 cm^{-1}. Parameters of the bands were determined by fitting the experimental spectra with Gaussian-Lorentzian shape components using GRAMS/A1 8.0 (Thermo Scientific) software.

3 Results

The results of XRD analysis of CHAp coatings are presented in Fig. 1. The XRD patterns of CHAp films on silicon nitride substrate without $CaTiO_3$ sublayer show the

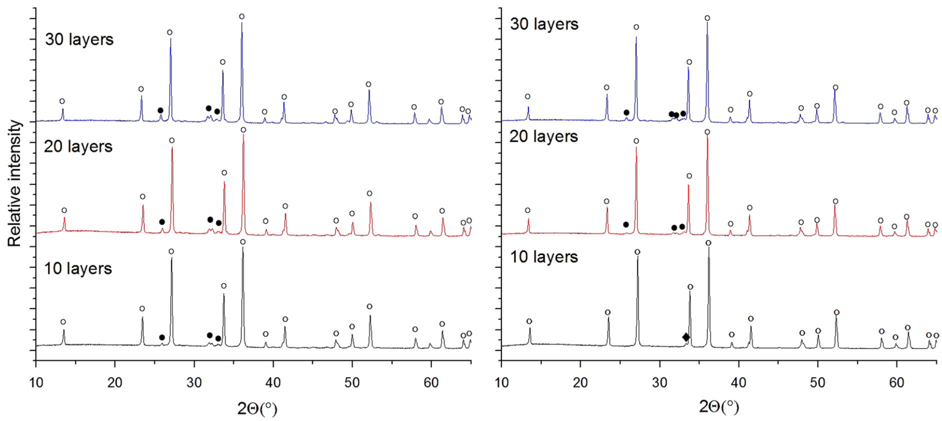

Fig. 1 XRD patterns of CHAp films (*left*) and CHAp films with $CaTiO_3$ sublayer (*right*) on silicon nitride substrate. Diffraction peaks: •—$(Ca_{10}(PO_4)_6(OH)_2$ (PDF: 74-0566); o—Si_3N_4; ♦—$CaTiO_3$

formation of CHAp phase already after ten coating procedures. The intensity of diffraction peaks attributable to the CHAp increases with increasing the number of coatings. Evidently, the $CaTiO_3$ sublayer formed on silicon nitride does not promote the formation of CHAp phase.

SEM micrographs of the CHAp coatings are presented in Figs. 2 and 3. Evidently, the morphology of ten layers of CHAp and $CaTiO_3$ on silicon nitride is different. The surface of $CaTiO_3$ sublayer (Fig. 3a) totally flat and smooth, whereas the formation of islands of CHAp (Fig. 2a) on the surface of substrate is clearly seen. In both cases (without and with sublayer) the surface morphology changes with increasing amount of CHAp layers. The island structure remains for the CHAp sample obtained after 20 coating procedures directly on the silicon nitride substrate. However, the good connectivity between CHAp grains is visible for the sample obtained on the substrate with calcium titanate sublayer. Besides, the cracks on the coatings have formed in both cases. The cracks become more visible for the CHAp coatings obtained after 30 dip-coating cycles. The differences of the surface morphology of thicker coatings disappeared, i.e., are not dependent on the sublayer structure. The both coatings are slightly cracked, having smoother surface without formation of islands. The cracking could have been caused by thermal expansion mismatch between the film and the susbtrate. As the films get more thicker they get more vulnerable to the expansion and contraction. As we left our samples to cool in furnace during procedure, this could potentially be avoided by controlled and slower cooling.

The coating thickness determined by SEM for the sample obtained after 30 dip-coating cycles was about 2 μm.

The results obtained by SEM are in a good agreement with those obtained by AFM measurements (Fig. 4). The edges of cracks are evident in the AFM images of CHAp coatings obtained after 20 and 30 dip-coating procedures. Moreover, the obtained CHAp coatings are porous. The coatings should be porous for the medical applications since the blood and related human fluids should have a possibility to circulate through the material. However, the pore size is not crucial feature.

Figure 5 shows Raman spectrum of 30-layer coating on Si_3N_4 substrate. The most intense band at 962 cm^{-1} belongs to ν_1 (A_1) symmetric stretching vibration of tetrahedral PO_4^{3-} group [29–31]. Peak position of this band indicates that studied compound is stoichiometric hydroxyapatite with molar Ca/P ratio of 1.667 [29, 32]. Lower intensity bands near at 587 and 631 cm^{-1} are associated with triple degenerate (F_2 symmetry) asymmetric bending modes ν_4 of phosphate group [30, 31]. The doubly degenerate (E symmetry) symmetric deformation vibrational modes ν_2 are visible near 432 cm^{-1}. Two bands located at 1045 and

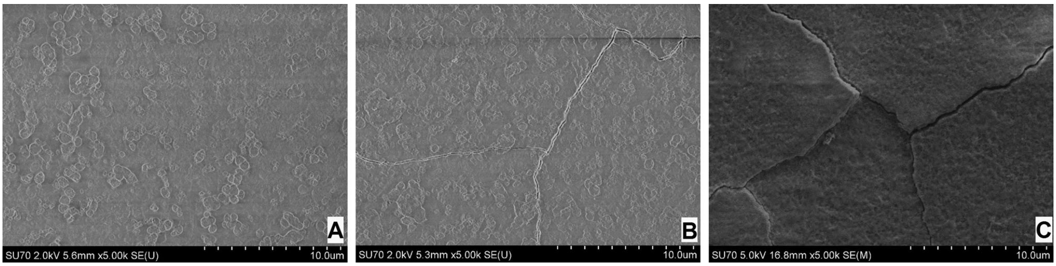

Fig. 2 SEM micrographs of CHAp coatings obtained on silicon nitride. Number of layers: 10 (**a**), 20 (**b**), and 30 (**c**)

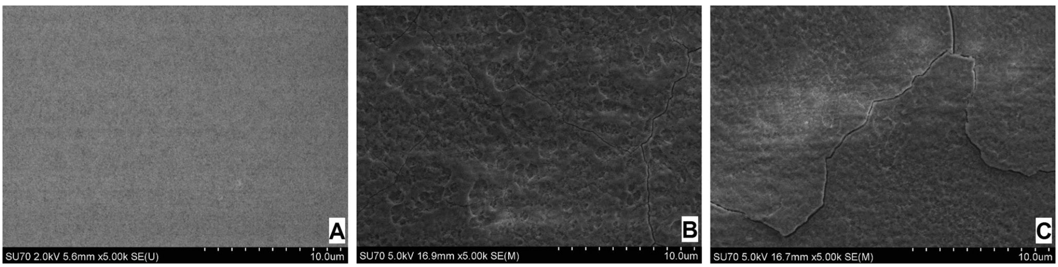

Fig. 3 SEM micrographs of coatings obtained on silicon nitride: 10 layers of $CaTiO_3$ sublayer (**a**), 20 (**b**) and 30 (**c**) layers of CHAp on top of $CaTiO_3$

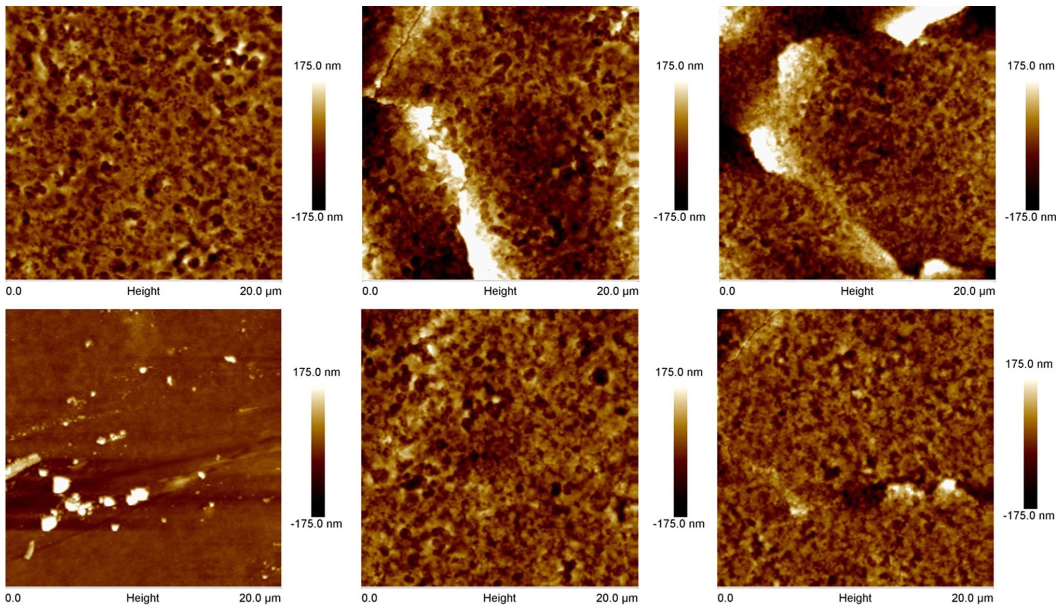

Fig. 4 AFM micrographs of CHAp films on silicon nitride (*top*) and on silicon nitride with sublayer (*bottom*): 10, 20, and 30 layers (from *left* to *right*)

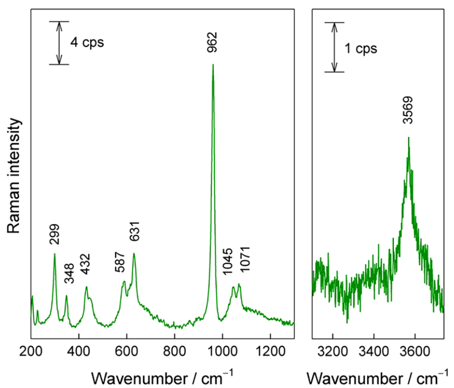

Fig. 5 Raman spectrum of sample containing 30 layers of Ca–P–O gel deposited on Si_3N_4 substrate in 200–1300 and 3100–3700 cm^{-1} spectral regions. Excitation wavelength is 442 nm (0.8 mW)

1071 cm^{-1} are assignable to triply degenerate (F_2) asymmetric stretching vibrational mode of phosphate group ν_3 [30, 31]. The low frequency bands (below 350 cm^{-1}) might be associated with translations of Ca^{2+}, PO_4^{3-}, and OH^- groups and vibrations of phosphate group [32, 33]. In the high frequency spectral region the relatively broad feature is visible at 3569 cm^{-1}. This band belongs to O–H stretching vibration of hydroxyl group and immediately confirms hydroxylation of the studied sample [32–35]. The width of the ν_1 band provides information on the degree of crystallinity of the studied compounds [32, 35]. For this purpose we recorded high resolution Raman spectra by using 632.8 nm excitation wavelength and 2400 lines/mm grating. The width of ν_1 band determined as full width at half maximum (FWHM) was found to be 11.5 cm^{-1}. Similar FWHM values were obtained for 10-layer (11.8 cm^{-1}) and 20-layer (11.7 cm^{-1}) deposited samples on Si_3N_4 substrate. Obtained FWHM values are relatively high comparing with well-ordered crystalline structure of hydroxyapatite (4–7 cm^{-1}) [32, 35]. The FWHM value of O–H stretching vibration was also relatively high (70.3 cm^{-1}), comparing with previously reported values for hydroxyapatite (6–12 cm^{-1}) [35]. Thus, presented Raman data indicate that studied samples possess hydroxyapatite molecular structure; although the long range arrangement is relatively disordered with dominant nanocrystalline-like form. Interestingly, during sol–gel preparation of CHAp thin films on silicon substrate, the formation of oxyhydroxyapatite $Ca_{10}(PO_4)_6(OH)_{2-2x}O_x$ instead of CHAp was observed [36]. However, this was not the case during fabrication of CHAp films on silicon nitride substrate.

To estimate wettability of the coatings obtained, the CAM using distilled water were performed. The results of these measurements are summarized in Table 1. No significant differences could be observed between the CHAp

Table 1 The results of contact angle measurements for CHAp coatings ($n = 3$)

Amount of CHAp layers	Without sublayer	With $CaTiO_3$ sublayer
10	97.2 ± 1.1	93.1 ± 3.5
20	100.3 ± 3.5	94.1 ± 0.6
30	93.4 ± 1.0	92.2 ± 1.3

coatings fabricated without and with $CaTiO_3$ sublayer. The contact angles determined for the synthesized specimens using 10, 20, and 30 immersion and withdrawal procedures were found to be in the range of 92–100°. The obtained results of CAMs show slight correlations between number of layers and contact angle values of CHAp surfaces. However, the contact angle slightly decreases for the CHAp films obtained after 30 coating procedures possibly due to the formation of cracks and higher porosity. As seen, with increasing number of layers up to 20, the hydrophobicity of surfaces increased. As compared with the results of the coatings on Ti substrate [28], the values of contact angle in this case are larger. This could be explained by the different nature of the substrates. Finally, the results presented in this study demonstrated that suggested sol–gel process is perfectly suitable for the synthesis of CHAp on the silicon nitride substrate allowing to control phase purity and morphological properties of CHAp. The obtained materials could be effectively used as multifunctional delivery systems for biotechnological applications [37, 38].

4 Conclusion

Calcium hydroxyapatite (CHAp, $Ca_{10}(PO_4)_6(OH)_2$) layers were fabricated from Ca–P–O sol–gel solution for the first time to the best our knowledge on silicon nitride (Si_3N_4) substrate. For comparison, the CHAp films were dip-coated also on a silicon nitride substrate modified with calcium titanate sublayer. From XRD results were observed that formation of CHAp as single phase occurs after annealing of coatings with or without calcium titanate sublayer in air atmosphere at 650 °C for 5 h. However, the amount of deposited CHAp was found to be lower in the presence of $CaTiO_3$ sublayer. According to SEM micrographs and AFM images, the morphological features of CHAp coatings were dependent on number of layers of the end product. The formation of islands was observed for the CHAp sample obtained after 20 coating procedures directly on the silicon nitride substrate. However, the good connectivity between CHAp grains was determined for the sample obtained on the substrate with calcium titanate sublayer. The both CHAp coatings obtained after 30 dip-coating cycles were slightly cracked and porous, having smoother surface without formation of islands. The Raman data indicated that studied samples possess hydroxyapatite molecular structure and no formation of oxyhydroxyapatite $Ca_{10}(PO_4)_6(OH)_{2-2x}O_x$ on silicon nitride was observed. The contact angles determined for the synthesized specimens using 10, 20, and 30 immersion and withdrawal procedures were found to be in the range of 92–100° showing low level of hydrophobicity.

Acknowledgements This research was funded by a grant KALFOS (No. LJB-2/2015) from the Research Council of Lithuania.

Compliance with ethical standards

Conflict of interest The authors declare that they have no competing interests.

References

1. Wu S, Liu X, Yeung KWK, Liu C, Yang X (2014) Biomimetic porous scaffolds for bone tissue engineering. Mater Sci Eng R-Rep 80:1–36
2. Surmenev RA, Surmeneva MA, Ivanova AA (2014) Significance of calcium phosphate coatings for the enhancement of new bone osteogenesis—a review. Acta Biomater 10:557–579
3. Asri RIM, Harun WSW, Hassan MA, Ghani SAC, Buyong Z (2016) A review of hydroxyapatite-based coating techniques: sol–gel and electrochemical depositions on biocompatible metals. J Mech Behav Biomed Mater 57:95–108
4. Bal BS, Rahaman MN (2012) Orthopedic applications of silicon nitride ceramics. Acta Biomater 8:2889–2898
5. Kohal RJ, Bächle M, Att W, Chaar S, Altmann B, Renz A, Butz F (2013) Osteoblast and bone tissue response to surface modified zirconia and titanium implant materials. Dent Mater 29:763–776
6. Arifin A, Sulong AB, Muhamad N, Syarif J, Ramli MI (2014) Material processing of hydroxyapatite and titanium alloy (HA/Ti) composite as implant materials using powder metallurgy: a review. Mater Des 55:165–175
7. Dorozhkin SV (2014) Calcium orthophosphate coatings on magnesium and its biodegradable alloys. Acta Biomater 10:2919–2934
8. Catauro M, Papale F, Bollino F (2015) Characterization and biological properties of TiO2/PCL hybrid layers prepared via sol–gel dip coating for surface modification of titanium implants. J Non-Cryst Solids 415:9–15
9. Catauro M, Bollino F, Papale F, Ferrara C, Mustarelli P (2015) Silica–polyethylene glycol hybrids synthesized by sol–gel: biocompatibility improvement of titanium implants by coating. Mater Sci Eng C 55:118–125
10. Firouzi D, Youssef A, Amer M, Srouji R, Amleh A, Foucher DA, Bougherara H (2014) A new technique to improve the mechanical and biological performance of ultra high molecular weight polyethylene using a nylon coating. J Mech Behav Biomed Mater 32:198–209
11. Mazzocchi M, Bellosi A (2008) On the possibility of silicon nitride as a ceramic for structural orthopaedic implants. Part I: processing, microstructure, mechanical properties, cytotoxicity. J Mater Sci Mater Med 19:2881–2887
12. Webster TJ, Patel AA, Rahaman MN, Sonny Bal B (2012) Anti-infective and osteointegration properties of silicon nitride, poly

(ether ether ketone), and titanium implants. Acta Biomater 8:4447–4454

13. Pettersson M, Tkachenko S, Schmidt S, Berlind T, Jacobson S, Hultman L, Engqvist H, Persson C (2013) Mechanical and tribological behavior of silicon nitride and silicon carbon nitride coatings for total joint replacements. J Mech Behav Biomed Mater 25:41–47
14. Pettersson M, Berlind T, Schmidt S, Jacobson S, Hultman L, Persson C, Engqvist H (2013) Structure and composition of silicon nitride and silicon carbon nitride coatings for joint replacements. Surf Coat Technol 235:827–834
15. Baptista R, Gadelha D, Bandeira M, Arteiro D, Delgago MI, Ferro AC, Guedes M (2016) Characterization of titanium–hydroxyapatite biocomposites processed by dip coating. Bull Mater Sci 39:263–272
16. Metoki N, Leifenberg-Kuznits L, Kopelovich W, Burstein L, Gozin M, Eliaz N (2014) Hydroxyapatite coatings electrodeposited at near-physiological conditions. Mater Lett 119:24–27
17. Frajkorová F, Molero E, Montero P, Gomez-Guillen MC, Sanchez-Herencia AJ, Ferrari B (2016) Biodegradable bi-layered coatings shaped by dipping of Ti films followed by the EPD of gelatin/hydroxyapatite composites. J Eur Ceram Soc 36:343–355
18. Fielding GA, Roy M, Bandyopadhyay A, Bose S (2012) Antibacterial and biological characteristics of silver containing and strontium doped plasma sprayed hydroxyapatite coatings. Acta Biomater 8:3144–3152
19. Rojaee R, Fathi M, Raeissi K (2013) Electrophoretic deposition of nanostructured hydroxyapatite coating on AZ91 magnesium alloy implants with different surface treatments. Appl Surf Sci 285:664–673
20. Kang M-H, Jung H-D, Kim S-W, Lee S-M, Kim H-E, Estrin Y, Koh Y-H (2013) Production and bio-corrosion resistance of porous magnesium with hydroxyapatite coating for biomedical applications. Mater Lett 108:122–124
21. Bosco R, Edreira ERU, Wolke JGC, Leeuwenburgh SCG, van den Beucken JJJP, Jansen JA (2013) Instructive coatings for biological guidance of bone implants. Surf Coat Technol 233:91–98
22. Mohseni E, Zalnezhad E, Bushroa AR (2014) Comparative investigation on the adhesion of hydroxyapatite coating on Ti–6Al–4V implant: a review paper. Int J Adhes Adhes 48:238–257
23. Gopi D, Ramya S, Rajeswari D, Kavitha L (2013) Corrosion protection performance of porous strontium hydroxyapatite coating on polypyrrole coated 316L stainless steel. Colloids Surf B 107:130–136
24. Sun L, Berndt CC, Gross KA, Kucuk A (2001) Material fundamentals and clinical performance of plasma-sprayed hydroxyapatite coatings: a review. J Biomed Mater Res 58:570–592
25. Heimann RB (2013) Structure, properties, and biomedical performance of osteoconductive bioceramic coatings. Surf Coat Technol 233:27–38
26. Thongsuriwong K, Amornpitoksuk P, Suwanboon S (2013) Structure, morphology, photocatalytic and antibacterial activities of ZnO thin films prepared by sol–gel dip-coating method. Adv Powder Technol 24:275–280
27. Bock R, McEntire B, Bal BS, Rahaman M, Boffelli M, Pezzotti G (2015) Surface modulation of silicon nitride ceramics for orthopaedic applications. Acta Biomater 26:318–330
28. Usinskas P, Stankeviciute Z, Beganskiene A, Kareiva A (2016) Sol–gel derived porous and hydrophilic calcium hydroxyapatite coating on modified titanium substrate. Surf Coat Technol 307:935–940
29. Karampas IA, Kontoyannis CG (2013) Characterization of calcium phosphates mixtures. Vibr Spectrosc 64:126–133
30. Khan AF, Awais M, Khan AS, Tabassum S, Chaudhry AA, Rehman I (2013) Raman spectroscopy of natural bone and synthetic apatites. Appl Spectrosc Rev 48:329–355
31. Niaura G, Gaigalas AK, Vilker VL (1997) Surface-enhanced Raman spectroscopy of phosphate anions: adsorption on silver, gold, and copper electrodes. J Phys Chem B 101:9250–9262
32. Sofronia AM, Baies R, Anghel EM, Marinescu CA, Tanasescu S (2014) Thermal and structural characterization of synthetic and natural nanocrystalline hydroxyapatite. Mater Sci Eng C 43:153–163
33. Markovic M, Fowler BO, Tung MS (2004) Preparation and comprehensive characterization of a calcium hydroxyapatite reference material. J Res Natl Inst Stand Technol 109:553–568
34. Ulian G, Valdrè G, Corno M, Ugliengo P (2013) The vibrational features of hydroxyapatite and type A carbonated apatite: a first principle contribution. Am Mineral 98:752–759
35. Saber-Samandari S, Alamara K, Saber-Samandari S, Gross KA (2013) Micro-Raman spectroscopy shows the coating process affects the characteristics of hydroxylapatite. Acta Biomater 9:9538–9546
36. Malakauskaite-Petruleviciene M, Stankeviciute Z, Niaura G, Garskaite E, Beganskiene A, Kareiva A (2016) Characterization of sol–gel processing of calcium phosphate thin films on silicon substrate by FTIR spectroscopy. Vibr Spectrosc 85:16–21
37. Bosco R, Iafisco M, van den Beucken J, Leeuwenburgh SCG, Jansen JA (2013) Adsorption of alendronate onto biomimetic apatite nanocrystals to develop drug carrier coating for bone implants. Key Eng Mater 529–530:475–479
38. Venuta A, Wolfram J, Shen H, Ferrari M (2017) Post-nano strategies for drug delivery: multistage porous silicon microvectors. J Mater Chem B 5:207–219

Paper III

A novel approach for accelerated fabrication of calcium hydroxyapatite thin films

P. Usinskas, Z. Stankeviciute, G. Niaura, J. Ceponkus and A. Kareiva.

Sci.-Medziagotyra 25 (2019) 365-368.

DOI: https://doi.org/10.5755/j01.ms.25.4.21251

ISSN 1392–1320 MATERIALS SCIENCE (MEDŽIAGOTYRA). Vol. 25, No. 4. 2019

A Novel Approach for Accelerated Fabrication of Calcium Hydroxyapatite Thin Films

Pranas USINSKAS [1] *, Živilė STANKEVIČIŪTĖ [1], Gediminas NIAURA [2], Justinas ČEPONKUS [2], Aivaras KAREIVA [1]

[1] *Institute of Chemistry, Vilnius University, Naugarduko 24, LT-03225, Vilnius, Lithuania*
[2] *Institute of Chemical Physics, Vilnius University, Sauletekio Ave. 9-3, LT-10222, Vilnius, Lithuania*

crossref http://dx.doi.org/10.5755/j01.ms.25.4.21251

Received 16 July 2018; accepted 22 October 2018

In this study we demonstrate, that sol–gel route is suitable to quicker obtain calcium hydroxyapatite ($Ca_{10}(PO_4)_6(OH)_2$, CHAp) coatings on crystalline Si substrate by modified dip-coating technique. The substrate was dip-coated by precursor and dried for 10 minutes at 200 °C with following cooling using the heating block for 110 min and annealing at 650 °C. Ethylendiamintetraacetic acid and 1,2-ethandiol, and triethanolamine and polyvinyl alcohol were used as complexing agents and as gel network forming agents, respectively. The obtained coatings were characterized by X-ray diffraction (XRD) analysis, scanning electron microscopy (SEM), FTIR spectroscopy and contact angle measurements (CAM).

Keywords: hydroxyapatite, sol–gel, dip–coating, thin film.

1. INTRODUCTION

Engineering of biomaterials is a growing field that focuses on the development of materials to replace or augment human tissues [1]. Orthopedic and dental implants are medical devices manufactured to replace a missing joint or bone or to support a damaged bone [2]. The medical implants are mainly fabricated using stainless steel and titanium alloys [1, 3]. As the metal implants should stay in the human body for a long time, they should not have drawbacks like corrosion or dissolution and toxic ion release.

Many different techniques are being used to synthesize Calcium Hydroxyapatite (CHAp) coatings on the substrate [4]. Plasma spraying is the only one approved by the Food and Drug Administration (FDA) [5]. This method is being criticized because of its expensive equipment, use of high temperatures, which may cause degradation on CHAp and difficulty in controlling coating quality and adhesion [6]. Dip-coating, combined with sol-gel processing in an inexpensive and simple process, that can be carried out with simple equipment. This method allows to mass produce coating on various size and shape substrates and the parameters can be controlled through sol-gel concentration, withdrawal speed and annealing temperatures. Also, high purity and homogeneity can be achieved. On the other hand, annealing temperatures are usually high and coating is brittle [7–9].

In this study we combined dip-coating with sol-gel processing to produce quicker CHAp films on silica substrate. Drying step was introduced into dip-coating process that made this process less time consuming.

2. EXPERIMENTAL DETAILS

To prepare CHAp films, calcium acetate monohydrate was used as calcium source. To the aqueous solution of $Ca(CH_3COO)_2$ the 1,2-ethandiol was added. The obtained mixture was stirred for 30 min at 65 °C. Then ethylenediaminetetraacetic acid was added, and after 15 min triethanolamine (TEA) was slowly added. The solution was stirred for 10 h. Then diluted orthophosphoric acid was added (Ca/P ratio was 1.67). Finally, this solution was mixed by ratio 5:3 with PVA dissolved in distilled water [10, 11]. All crystalline Si substrates were cleaned in an ultrasonic bath with acetone, ethanol and distilled water sequentially. One dip-coating cycle consisted of dipping the substrate and retrieving it, drying for 10 min at 200 °C in dip-coater dryer and leaving for 110 min. The procedure was repeated 5 times. After that, samples were heated at 650 °C for 5 h using the heating rate of 1 °C/min. The samples were cooled to the room temperature within the furnace. The formation of coatings on silicon substrate was performed using a dip-coater (Holmarc HO-TH-02B). The dipping rate of substrate was 85 mm/min and lifting rate was 40 mm/min. The substrate was left in the gel solution for 20 s.

The coatings were characterized by X-ray diffraction (XRD, Rigaku MiniFlex II) analysis, scanning electron microscopy (SEM, Hitachi SU 70) and contact angle measurements (KSV Instrument CAM 100). FTIR spectra were recorded in transmission mode by using FTIR spectrometer ALPHA (Bruker, Inc.), equipped with a room temperature detector DLATGS. Spectra were acquired from 100 interferogram scans with 2 cm^{-1} resolution.

Blank Si substrate after 6 cycles (without coating) was used as a reference sample.

* Corresponding author. Tel.: +370-6-0100440;
E-mail address: *pranas_usinskas@yahoo.com* (P. Usinskas)

3. RESULTS AND DISCUSSION

The XRD results of CHAp coatings obtained by accelerated procedure are presented in Fig. 1. The XRD patterns of CHAp films on silica substrate show the formation of CHAp phase already after 1 coating cycle (5 dips).

SEM micrographs of the CHAp coatings are presented in Fig. 2. As seen, a smooth homogenous surface with small grains is obtained after 1 coating cycle. After 3 coating cycles, the surface is rougher, with bigger grains and few cracks. This might be caused by thermal expansion mismatch between the coating and the substrate. This more perfect microstructe could be obtained by controlling the cooling procedure. The final sample, obtained after 6 coating cycles contains the biggest grains due to the increased number of annealing procedures. The SEM results are in a good agreement with the results of contact angle measurements. After the initial coating, the contact angle increased from 67° (blank sample) to 85°. With the increasing number of coating cycles, the contact angle decreased due to the existence of cracks on the surface and higher porosity.

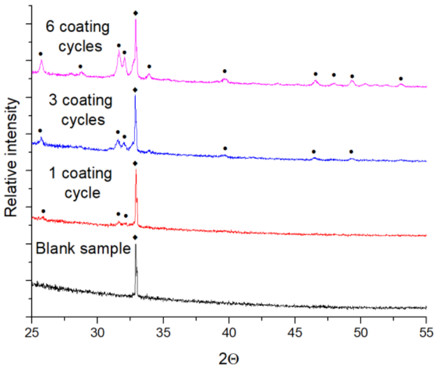

Fig. 1. XRD patterns of CHAp films on silica substrate. Diffraction peaks: • – $(Ca_{10}(PO_4)_6(OH)_2$ (PDF: 74-0566); ♦ – Si

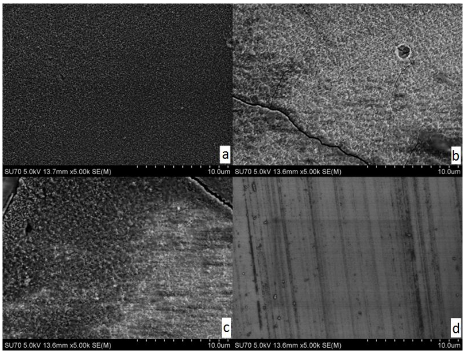

Fig. 2. SEM micrographs of CHAp coatings obtained on silica: a – 1, b – 3; c – 6 coating cycles; d – blank sample

Fourier transform infrared (FTIR) spectroscopy in transmission mode revealed that free PO_4^{3-} ion belongs to tetrahedral (T_d) symmetry and its vibrational spectrum consists from four modes; Raman-active totally symmetric stretching ν_1 (A_1), Raman-active double degenerate symmetric deformation ν_2 (E), both infrared- and Raman-active triply degenerate asymmetric stretching ν_3 (F_2), and both infrared- and Raman-active triply degenerate asymmetric deformation ν_4 (F_2) vibrational modes [12 – 15]. Fig. 3 compares FTIR spectra of different CHAp layers on Si substrate. Peak positions and assignments of the bands are listed in Table 1. Peak positions of the PO_4^{3-} coincide well with hydroxyapatite structure [16 – 18]. In the high frequency region, the sharp band due to O–H stretching vibrations of OH^- ion is visible at 3571 cm^{-1}; thus confirming presence of the hydroxyapatite crystal lattice. The width of ν(OH) band determined as full width at half maximum (FWHM) was found to be 15.5 cm^{-1} for 6 cycles sample. This value is slightly large comparing with previously reported values for crystalline hydroxyapatite (6 – 12 cm^{-1}) [19]; however, is considerable lower comparing with calcium hydroxyapatite film on Si_3N_4 substrate (70.3 cm^{-1}) [20].

The relative amount of carbonate ions was evaluated by analysis of integrated intensity ratios $A(CO_3^{2-})/A(PO_4^{3-})$ (Table 1). One can see that relative amount of carbonate slightly increases with decreasing number of deposited layers. The relative amount of hydroxyl ion remains similar for all studied samples. Importantly, the hydroxyapatite structure is preserved even for very thin (1 cycle – 5 dips) coating on Si, as clearly visible from the presence of ν(OH) peak near 3570 cm^{-1} (Fig. 3).

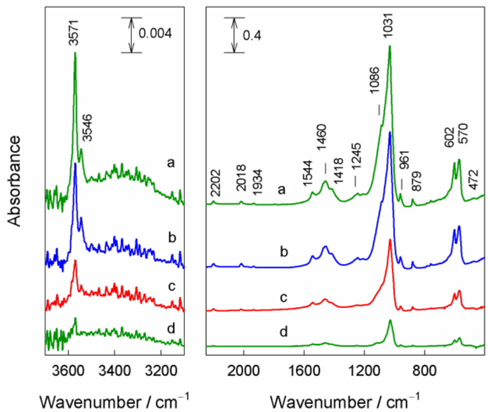

Fig. 3. FTIR absorbance spectra of annealed (650 °C, 5 h) CHAp films on Si substrate: a – 6 cycles, b – 5 cycles; c – 3 cycles; d – 1 cycle

4. CONCLUSIONS

Calcium hydroxyapatite (CHAp, $Ca_{10}(PO_4)_6(OH)_2$) thin layers were fabricated from Ca-P-O sol-gel solution on silicon (Si) substrate using improved dip-coating method. This suggested technique allowed to achieve desired results 4 times faster in comparison with previously suggested processing. XRD results confirmed the formation of CHAp as single phase after annealing of coatings in air atmosphere at 650 °C for 5 h.

Table 1. Infrared wavenumbers [cm^{-1}] of CHAp films on Si substrate

Mode, molecular group	6 cycles	5 cycles	3 cycles	1 cycle	Mode, molecular group
ν_1 (A_1), PO_4^{3-}	961.3 m	961.2 m	959.8 m	958.8 m	961.3 m
ν_2 (E), PO_4^{3-}	473 vw	473 vw	n.o.	n.o.	473 vw
ν_3 (F_2), PO_4^{3-}	1031.2 vs 1086 sh	1030.6 vs 1085 sh	1029.0 vs 1084 sh	1028.1 vs n.o.	1031.2 vs 1086 sh
ν_4 (F_2), PO_4^{3-}	570.4 s 601.8 s	570.8 s 602.2 s	569.2 s 601.1 s	567.8 s 600.6 s	570.4 s 601.8 s
$\nu_{as}(CO_3)$, CO_3^{2-}	1418 m, sh 1459.8 m 1544.3 m	1419 m, sh 1460.4 m 1543.9 m	1422 m, sh 1460.3 m 1543.1 m	1420 m, sh 1459.0 m 1541.1 m	1418 m, sh 1459.8 m 1544.3 m
$\gamma(CO_3)$, CO_3^{2-}	879.4 m	879.4 m	879.6 m	879.5 m	879.4 m
Overtones/combination modes, PO_4^{3-}, HPO_4^{2-}	1933,9 w 2017.5 w 2202.2 w	1934.2 w 2017.0 w 2202.0 w	1935.9 w 2018.2 w 2202.7 w	1936.7 w 2017.0 m 2202.3 m	1933,9 w 2017.5 w 2202.2 w
ν(OH) OH^-	3545.6 vw 3570.8 w	3545.1 vw 3570.4 w	3544.7 vw 3570.3 w	n.o. 3570.0 w	3545.6 vw 3570.8 w
ν_1 (A_1), PO_4^{3-}	961.3 m	961.2 m	959.8 m	958.8 m	961.3 m
Abbreviations: n.o. – not observed; ν – stretching; ν_{as} – asymmetric stretching; γ – out of plane deformation; vs – very strong; s – strong; m – middle; w – weak; vw – very weak; sh –shoulder.					

The spectroscopic data also indicated the presence of ordered crystalline structure of hydroxyapatite film. SEM micrographs of the CHAp surfaces revealed the formation of smooth and homogenous coatings with small grains. The SEM results were in a good agreement with the results of contact angle measurements.

Acknowledgments

This work was supported by a grant SEMAT (No. SEN-02/2016) of National Research Programme „Healthy ageing“ from the Research Council of Lithuania.

REFERENCES

1. **Paital, S.R., Dahotre, N.B.** Calcium Phosphate Coatings for Bio-implant Applications: Materials, Performance Factors, and Methodologies *Materials Science and Engineering: R: Reports* 66 2009: pp. 1 – 70. https://doi.org/10.1016/j.mser.2009.05.001
2. **Skwarek, E., Janusz, W., Sternik, D.** The Influence of the Hydroxyapatite Synthesis Method on the Electrochemical, Surface and Adsorption Properties of Hydroxyapatite *Adsorption Science & Technology* 35 (5 – 6) 2017: pp. 507 – 518. https://doi.org/10.1177/0263617417698966
3. **Geuli, O., Metoki, N., Eliaz, N., Mandler, D.** Electrochemically Driven Hydroxyapatite Nanoparticles Coating of Medical Implants *Advanced Functional Materials* 26 2016: pp. 8003 – 8010. https://doi.org/10.1002/adfm.201603575
4. **Huang, Y., Zhang, X., Zhao, R., Mao, H., Yan, Y., Pang, X.** Antibacterial Efficacy, Corrosion Resistance, and Cytotoxicity Studies of Copper-Substituted Carbonated Hydroxyapatite Coating on Titanium Substrate *Journal of Materials Science* 50 2015: pp. 1688 – 1700. http://dx.doi.org/10.1007/s10853-014-8730-1
5. **Mohseni, E., Zalnezhad, E., Bushroa, A.R.** Comparative Investigation on the Adhesion of Hydroxyapatite Coating on Ti–6Al–4V Implant: A Review Paper *International Journal of Adhesion and Adhesives* 48 2014: pp. 238 – 257. https://doi.org/10.1016/j.ijadhadh.2013.09.030
6. **Shamray, V.F., Sirotinkin, V.P., Smirnov, I.V., Kalita, V.I., Fedotov, A.Y., Barinov, S.M., Komlev, V.S.** Structure of the Hydroxyapatite Plasma-Sprayed Coatings Deposited on Pre-heated Titanium Substrates *Ceramics International* 43 2017: pp. 9105 – 9109. https://doi.org/10.1016/j.ceramint.2017.04.057
7. **Valle, G.G., Hammer, P., Pulcinelli, S.H., Santilli, C.V.** Transparent and Conductive Zno:Al Thin Films Prepared By Sol-Gel Dip-Coating *Journal of the European Ceramic Society* 24 2004: pp. 1009 – 1013. https://doi.org/10.1016/S0955-2219(03)00597-1
8. **Song, Y.W., Shan, D.Y., Han, E.H.** Electrodeposition of Hydroxyapatite Coating on AZ91D Magnesium Alloy gor Biomaterial Application *Materials Letters* 62 2008: pp. 3276 – 3279. https://doi.org/10.1016/j.matlet.2008.02.048
9. **Catauro, M., Papale, F., Bollino, F.** Characterization and Biological Properties of Tio_2/PCL Hybrid Layers Prepared Via Sol–Gel Dip Coating for Surface Modification of Titanium Implants *Journal of Non-Crystalline Solids* 415 2015: pp. 9 – 15. https://doi.org/10.1016/j.jnoncrysol.2014.12.008
10. **Usinskas, P., Stankeviciute, Z., Niaura, G., Maminskas, J., Juodzbalys, G., Kareiva, A.** Sol–gel Processing of Calcium Hydroxyapatite Thin Films on Silicon Nitride (Si_3N_4) Substrate *Journal of Sol-Gel Science and Technology* 83 2017: pp. 268 – 274. http://dx.doi.org/10.1007/s10971-017-4431-y
11. **Usinskas, P., Stankeviciute, Z., Beganskienė, A., Kareiva, A.** Sol-gel Derived Porous and Hydrophilic Calcium Hydroxyapatite Coating on Modified Titanium Substrate *Surface and Coatings Technology* 307 2016: pp. 935 – 940. https://doi.org/10.1016/j.surfcoat.2016.10.032
12. **Jastrzębski, W., Sitarz, M., Rokita, M., Bulat, K.** Infrared Spectroscopy of Different Phosphates Structures

Spectrochimica Acta Part A: Molecular and Biomolecular Spectroscopy 79 2011: pp. 722 – 727. https://doi.org/10.1016/j.saa.2010.08.044

13. **Nakamoto, K.** Infrared and Raman Spectra of Inorganic and Coordination Compounds, Part A: Theory and Applications in Inorganic Chemistry, Wiley 2008. https://doi.org/10.1002/0470027320.s4104
14. **Niaura, G., Gaigalas, A., Vilker, V.L.** Surface-Enhanced Raman Spectroscopy of Phosphate Anions: Adsorption on Silver, Gold, and Copper Electrodes *The Journal of Physical Chemistry B* 101 (45) 1997: pp. 9250 – 9262, 1997. https://doi.org/10.1021/jp970097k
15. **Posset, U., Löcklin, E., Thull, R., Kiefer, W.** Vibrational Spectroscopic Study of Tetracalcium Phosphate in Pure Crystalline Form and as a Constituent of a Self-Setting Bone Cement *Journal of Biomedical Materials Research* 40 (4) 1998: pp. 64 – 645. https://doi.org/10.1002/(SICI)1097-4636(19980615)40:4%3C640::AID-JBM16%3E3.0.CO;2-J
16. **Karampas, I.A., Kontoyannis, C.G.** Characterization of Calcium Phosphates Mixtures *Vibrational Spectroscopy* 64 2013: pp. 126 – 133. https://doi.org/10.1016/j.vibspec.2012.11.003
17. **Rehman, I., Bonfield, W.** Characterization of Hydroxyapatite and Carbonated Apatite by Photo Acoustic FTIR Spectroscopy *Journal of Materials Science: Materials in Medicine* 8 1997: pp. 1 – 4.
18. **Frasnelli, M., Cristofaro, F., Sglavo, V.M., Dirè, S., Callone, E., Ceccato, R., Bruni, G., Cornaglia, A.I., Visai, L.** Synthesis and Characterization of Strontium-Substituted Hydroxyapatite Nanoparticles for Bone Regeneration *Materials Science and Engineering: C* 71 2017: pp. 653 – 662. https://doi.org/10.1016/j.msec.2016.10.047
19. **Saber-Samandari, S., Alamara, K., Saber-Samandari, S., Gross, K.A.** Micro-Raman Spectroscopy Shows how the Coating Process Affects the Characteristics of Hydroxylapatite *Acta Biomaterialia* 9 2013: pp. 9538 – 9546. https://doi.org/10.1016/j.actbio.2013.08.021
20. **Arends, J., Davidson, C.L.** $HPO_4^{\ 2-}$ Content in Enamel and Artificial Carious Lesions *Calcified Tissue Research* 18 1975: pp. 65 – 79. http://doi.org/10.1007/BF02546227

Vilnius University Press
9 Saulėtekio Ave., Building III, LT-10222 Vilnius
Email: info@leidykla.vu.lt, www.leidykla.vu.lt
Print run copies 15